FREQUENCY TUNING CONCEPTS FOR PIEZOELECTRIC CANTILEVER BEAMS AND PLATES FOR ENERGY HARVESTING

by

David Charnegie

B.S. in Mechanical Engineering, University of Pittsburgh, 2005

Submitted to the Graduate Faculty of

the School of Engineering in partial fulfillment

of the requirements for the degree of

Master of Science

University of Pittsburgh

2007

UNIVERSITY OF PITTSBURGH

SCHOOL OF ENGINEERING

This thesis was presented

by

David Charnegie

It was defended on

May 10, 2007

and approved by

Dr. Jeffrey S. Vipperman, Associate Professor, Department of Mechanical Engineering and

Materials Science

Dr. Patrick Smolinski, Associate Professor, Department of Mechanical Engineering and

Materials Science

Thesis Advisor: Dr. William W. Clark, Professor, Department of Mechanical Engineering

and Materials Science

FREQUENCY TUNING CONCEPTS FOR PIEZOELECTRIC CANTILEVER BEAMS AND PLATES FOR ENERGY HARVESTING

David Charnegie, M.S.

University of Pittsburgh, 2007

A great deal of research has repeatedly demonstrated that piezoelectric energy harvesters hold the promise of providing an alternative power source that can enhance or replace conventional batteries and power wireless devices. Also, ambient vibrations have been the focus as a source due to the amount of energy available in them. By using energy harvesting devices to extract energy from their environments, the sensors that they power can be self-reliant and maintenance time and cost can be reduced. In order to harvest the most energy with the device, the beam's fundamental mode must be excited. However, this is not always possible due to manufacturing of the device or fluctuations in the vibration source. By being able to change the frequencies of the beam, the device can be more effective in harvesting energy. This work utilizes a shunt capacitor-tuning concept on a piezoelectric bimorph energy harvester. Design parameters are investigated and discussed to achieve the most tuning from the device. Static and dynamic beam and plate models are derived to predict natural frequencies and power and are later used to compare to experimental results. Results are presented for the tunability of a square cantilever bimorph. In addition, the amount of power able to be harvested from each layer of the bimorph is tested. Finally, several other tuning methods are discussed.

TABLE OF CONTENTS

LIST OF TABLES

LIST OF FIGURES

xiv

ACKNOWLEDGMENTS

1.0   INTRODUCTION

Technology is continuously becoming smaller and smaller. With these advancements, sensors and other electronics can be used in the most remote locations and transmit information wirelessly. However, although the devices are smaller, they still require power sources such as batteries, which can degrade and would have to be replaced. One possible solution is to use an energy harvesting device containing a piezoceramic to harvest energy from the environment of the sensor.

A great deal of research has repeatedly demonstrated that piezoelectric energy harvesters hold the promise of providing an alternative power source that can enhance or replace conventional batteries and power wireless devices. Also, ambient vibrations have been the focus as a source due to the amount of energy available in them. By using energy harvesting devices to extract energy from their environments, the sensors that they power can be self-reliant and maintenance time and cost can be reduced.

To maximize the amount of energy harvested from the source, generally a resonant mode of the harvester should match one of the dominant frequencies of the source. Due to inconsistencies in the fabrication of the harvester or variations in the source, frequency matching can be difficult to achieve. By being able to tune the device during fabrication or in real time during operation, a means to meet this criterion during operation of the device can be provided.

In this study both theoretical and experimental analysis will be done on a piezoelectric cantilever bimorph. A bimorph harvester contains a substrate material sandwiched between two piezoelectric layers and is shown in Figure 1.1.
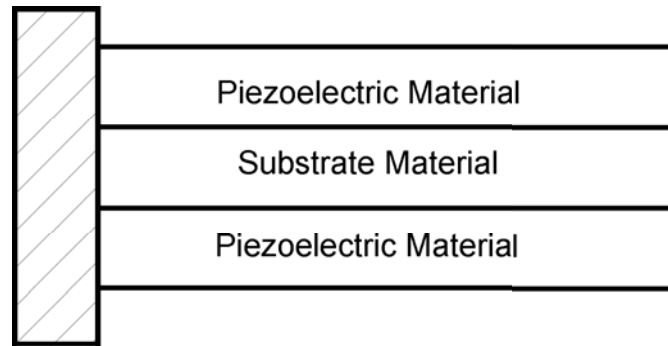
Figure 1.1. Bimorph Cantilever Energy Harvester

It has been shown that the stiffness of a piezoelectric element in parallel with a capacitive element is dependent on the impedance of the circuit. Thus, by shunting a piezoelectric layer with various capacitances, the stiffness of the beam and hence the natural frequency of the harvester can be varied. Much research has been done utilizing this concept in tuning resonators but little has been investigated pertaining to energy harvesting. The objective of this research is to investigate the tuning concept as it pertains to piezoelectric cantilever beams and plates and to study its effect on energy harvesting from a particular vibration source.

1.1   OUTLINE OF THESIS

The thesis is laid out in the following manner. Initially, background information on piezoelectricity is given, explaining terminology necessary to understand general piezoelectric

concepts. This is followed by a literature review that will cover previous advancements in energy harvesting and will take a look at other methods of tuning cantilever-type harvesting devices. A capacitive tuning concept will be presented and applied to a cantilever beam bimorph harvester as well as a plate. The general procedure for calculating the energy of the harvesters will be presented next. Testing and analysis of the tuning concept will be presented and discussed. Finally, some general conclusions will be presented and future work will be discussed.

The literature review has two main topics. The first reviews advances in energy harvesting and it's applications, which provides a basis for the need to continue research in the area and shows promise in developing power for wireless devices. The second section describes the capacitive tuning concept as it pertains to applications other than energy harvesting. The idea stems from original work dealing with using capacitors for structural damping as well as using it for tuning mechanical resonators. Other tuning concepts for harvesting devices will also be discussed.

As mentioned earlier, both cantilever beam and plate bimorphs will be analyzed. First, mode shapes and deflections will be calculated from a vibrational analysis of a continuous system. Using strain energy methods the theoretical amount of energy able to be harvested can be calculated. Next, a shunt capacitor concept will be applied to determine the amount of tuning available in each device as well as effects on energy harvesting.

Lastly, a test setup will be described as well as the fabrication process of the energy harvesters. The upper and lower tuning ranges of the harvesters will be determined along with the amount of energy able to be pulled from the device. The results will be compared with theoretical values.

2.0   PIEZOELECTRIC BACKGROUND INFORMATION

The brothers Pierre and Jacques Curie first demonstrated the piezoelectric effect in 1880. Piezo originates from the Greek word meaning 'to press' and electric refers to energy or voltage.   The Curie's showed that certain materials exhibited electrical polarization when a mechanical stress was applied.   In 1881, Lippmann mathematically proved that applying a voltage to a piezoelectric material induces strain in the material. The Curie brothers immediately obtained quantitative proof of this effect.   In their experiments, Quartz and Rochelle salt were able to produce a small amount of electrical energy, however it was very small and of little use. It was not until the LiTiBa ceramic was discovered that the piezoelectric performance was increased and able to be used in a practical manner in electromechanical devices.

2.1   PIEZOELECTRIC FUNDAMENTALS

A point group describes a material's lattice structure.   There are 20 point groups which lack a center of symmetry. This means that the material develops a dielectric polarization when subjected to a stress and is known as the piezoelectric effect. The piezoelectric effect is the reason piezoelectric materials can be used as both sensors and actuators. The direct piezoelectric effect describes the material's ability to produce a voltage when mechanically strained and is utilized in sensor applications. Common sensor applications taking advantage of this are found

in accelerometers and in pickups for acoustic guitars. The converse piezoelectric effect is a material's ability to transform an applied voltage into mechanical strain energy. This is commonly used in actuator applications such as creating ultrasonic waves used in medical imaging devices. Figure 2.1 shows both the direct and converse piezoelectric effect.
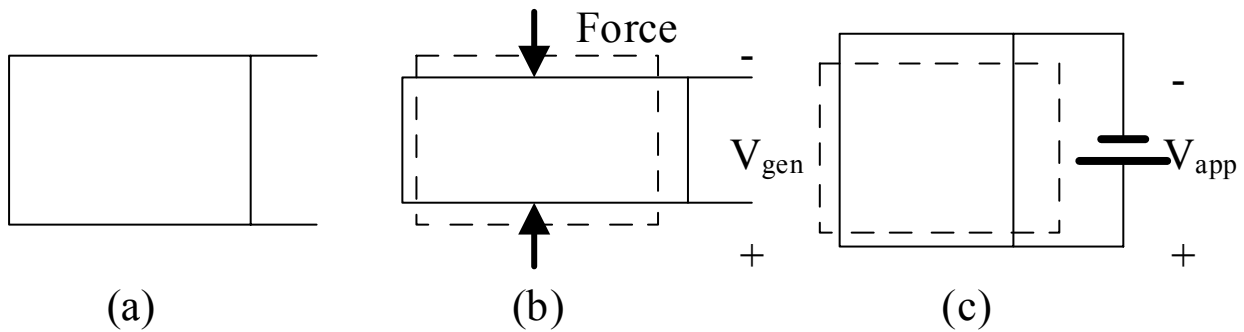
Figure 2.1. (a) Unstrained piezoelectric material. (b) direct piezoelectric effect. (c) converse piezoelectric effect.

Piezoelectric materials also belong to a group of materials known as ferroelectrics. Ferroelectrics have the characteristic of having locally random oriented electric dipoles throughout their material composition. When the material is heated above its Curie temperature, and an electric field is applied across the material, the electric dipoles align themselves relative to the applied electric field. When the material is cooled, the electric dipoles maintain their alignment. This process is known as poling. Once a ferroelectric material is poled, it will exhibit the piezoelectric effect. The poling of a ferroelectric material is shown in Figure 2.2.
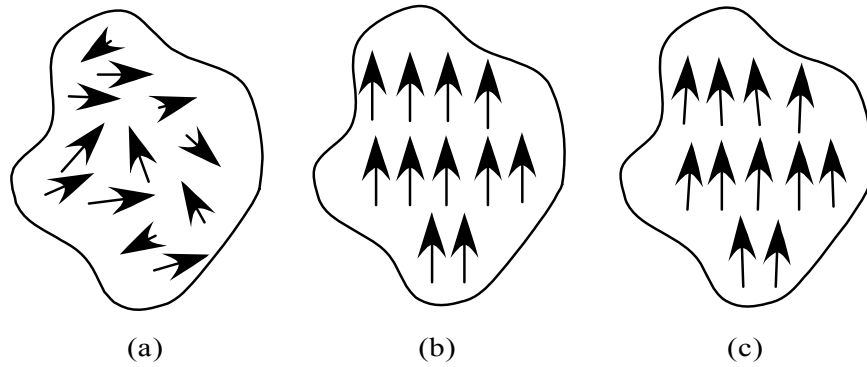
Figure 2.2. Poling process: (a) unpoled ferroelectric ceramic, (b) material heated above Curie temperature and voltage applied, (c) poled piezoelectric material

After the material has been poled, an electric field can be applied to the material to induce a stress (or a stress applied to create a voltage). Since the electric field can be applied on several surfaces in different directions there is a sign convention that is normally used when dealing with piezoelectric materials. The poling direction is always assigned the 3 direction. All other properties are based off of this direction. Properties are usually denoted as x_{ij}, where x is the property variable and i and j are subscripts that are common to denoting all piezoelectric properties. The first subscript shows the direction that charge is collected and the second subscript denotes the direction of stress. The direction of induced or applied stress is assigned relative to the poling direction. Therefore, if the stress is in the same direction as the poling direction, it will also be in the 3 direction. If the stress is perpendicular to the electric field it will be in the 1 direction. Figure 2.3 illustrates this sign convention. When the mechanical stress or strain is shear, the subscript 4, 5, and 6 are used for the second subscript.
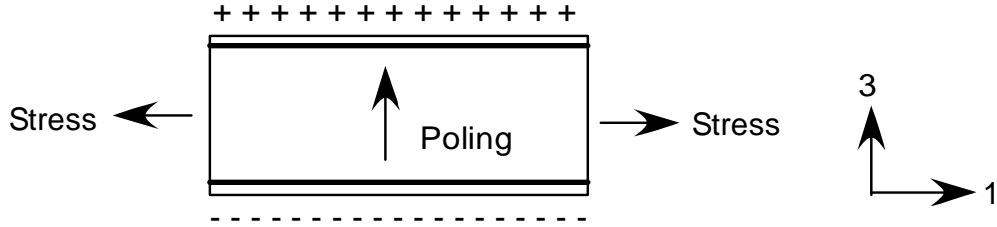
Figure 2.3. 31-direction: Charge collection in 3 direction and stress in 1 direction

An important relation for piezoelectric material is that between charge and stress, denoted as a constant *d*. The larger this constant is, the more energy can be generated from a certain applied stress. In this work a piezoelectric material, Lead Zirconate Titanate (PZT), a 4mm class crystal, has 5 piezoelectric (d or g) constants (d_{31}, d_{33}, d_{32}, d_{15}, and d_{24}). For this work, all other remaining constants are zero. The constant d_{31} is the same as d_{32} since 1 and 2 are both perpendicular to 3 and the material is isotropic in the 1-2 plane. Also, d_{15} is the same as d_{24} due to the isotropic nature of the material. Therefore, there are technically only 3 piezoelectric constants. The d_{31} constant is the smallest among the three constants. The d_{33} constant is approximately twice as large as the d_{31} constant and d_{15} is approximately five times as large. Although the d_{33} and d_{15} are larger than the d_{31}, they are harder to realize in a real structure. The 33 and 15 directions are shown in Figure 2.4.
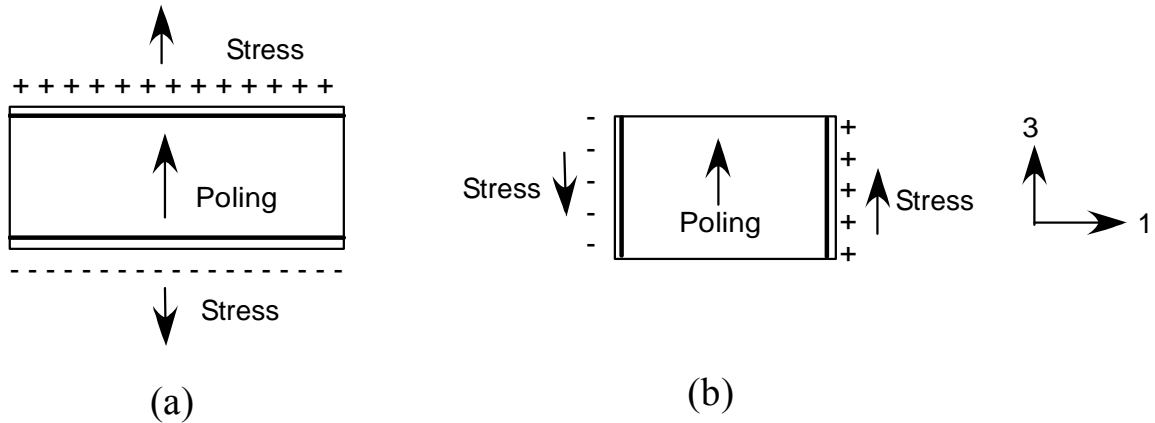
Figure 2.4. (a) 33 direction: Charge collection and stress in 3 direction (b) 15 direction: Charge collection in 1 direction and shear stress in 5 direction (which is 1-3 plane shear stress)

2.2   TYPES OF PIEZOELECTRIC ACTUATORS / SENSORS

This section will briefly review several common configurations of piezoelectric actuators or sensors that utilize the different poling configurations. For each case a description and example is given.

2.2.1   Piezoelectric stack devices

Currently, one of the most common devices operating in the 33 direction is the stack actuator. Piezoelectric devices generally cannot create large deformations. Also, it takes a relatively large electric field to produce a large strain. This fact, along with the material being extremely brittle makes it difficult to use as an actuation device. However, if a large number of thin piezoelectric plates are glued together and wired in parallel, a large strain, or deflection, can be produced with a small electric field. This is known as a piezoelectric stack actuator. The device can also operate as an energy harvester if a force is applied in the same direction as poling. However,

8

energy can only be generated if the force is applied longitudinally so the structure would not be very good to use in vibration applications where bending is usually used as a stress inducer. Also, the volume of piezoelectric stack actuators is usually large. Both a piezoelectric stack actuator and energy harvester are shown in Figure 2.5.

(a)

(b)
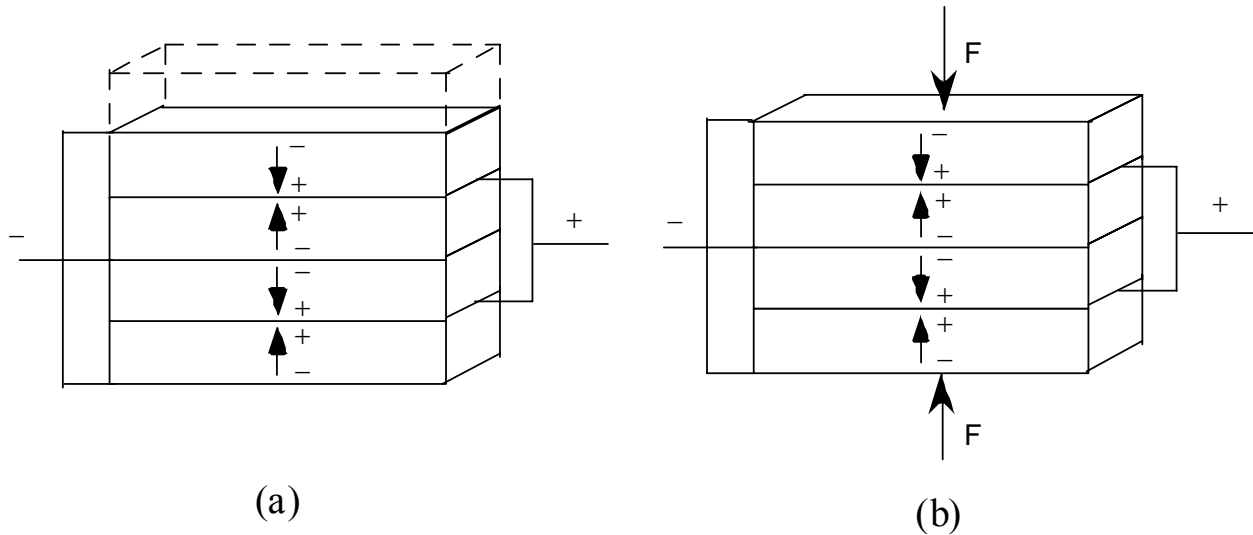
Figure 2.5. Piezoelectric Stack Actuator and Generator. (a) Actuator device (b) Energy Harvester

2.2.2 Piezoelectric cantilever bender devices

The cantilever beam is another piezoelectric device commonly used as an actuator or generator. The cantilever is able to create relatively large deflections and take up less space than its stack counterpart. As an energy harvester, cantilever beams work well in vibration applications because high stress is induced with very little force as compared to a stack.

Since piezoelectric materials are brittle, it is common to have multiple layers in piezoelectric cantilever devices. A piezoelectric layer is used to actuate or produce energy and a non-piezoelectric layer is used to add stiffness as well as make the device more durable. When

the beam has only a piezoelectric layer attached to a substrate layer, the device is known as a unimorph. When a substrate material is sandwiched between two piezoelectric materials, the device is known as a bimorph. A piezoelectric unimorph and bimorph is shown in Figure 2.6.
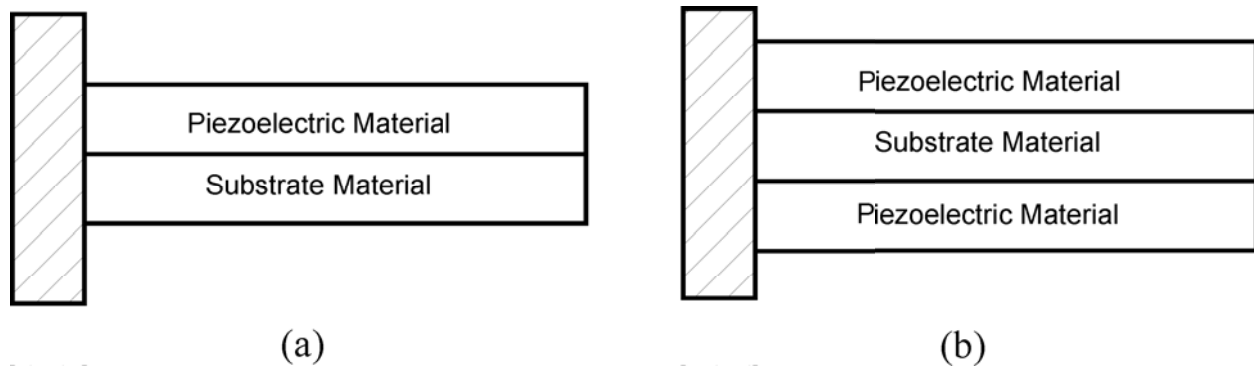
Figure 2.6. Piezoelectric Cantilever Benders. (a) unimorph (b) bimorph

The operation of cantilever benders is relatively simple. If one layer is in compression, the other layer is in tension. The stress in one layer affects the stress in the other layer. For example, in a piezoelectric unimorph when an electric field is applied to the piezoelectric layer, the piezoelectric layer expands or contracts where as the non-piezoelectric material is not affected by the electric field. This causes the bender to bend. The opposite also occurs when the beam undergoes bending from an applied force from an external vibration source. This bending causes a charge to be generated between the electrodes of the piezoelectric layer. In this situation, energy can be harvested from the electrodes.

Different from a piezoelectric stack device, a cantilever beam can be manufactured to operate in either 31 or 33 modes. Since the stress in a cantilever beam is always in the longitudinal direction, it is just a matter of configuring the electrodes on the piezoelectric material to manipulate the poling direction within the material. If the electrodes fully cover the

piezoelectric material, the electric field will always be in the direction normal to the electrodes and hence be perpendicular to the stress in the bender. This can be seen in Figure 2.7.
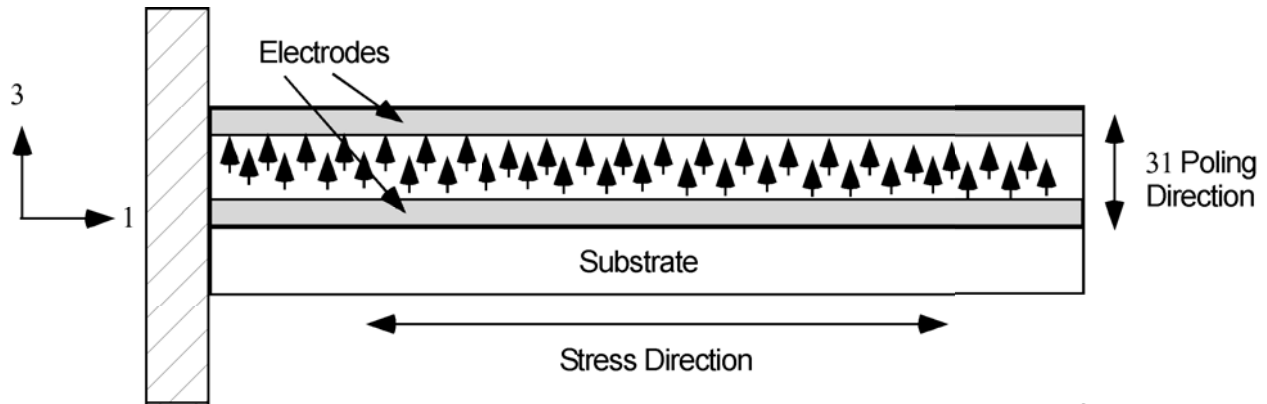
Figure 2.7. 31 Piezoelectric Cantilever Bender

It is very difficult to pole piezoelectric material in the direction of the beam length and hence create a 33 poling direction along the entire length of the beam, since the electrodes would have to be on the ends of the beam. In order to create a large enough electric field, the voltage required would be too high. Also, the electrodes would have to be at the ends. However, if electrodes are spaced out on one surface, the material can be poled so that the electric field is generated between the electrodes as seen in Figure 2.8. This is known as having interdigitated electrodes. This method cannot generate a precise 33 direction due to non-uniform poling directions. Also, the poling field might not reach the whole depth of the material. These issues can be neglected for proper electrode size and spacing. It is also assumed the 33 direction exists everywhere except directly below the electrodes.
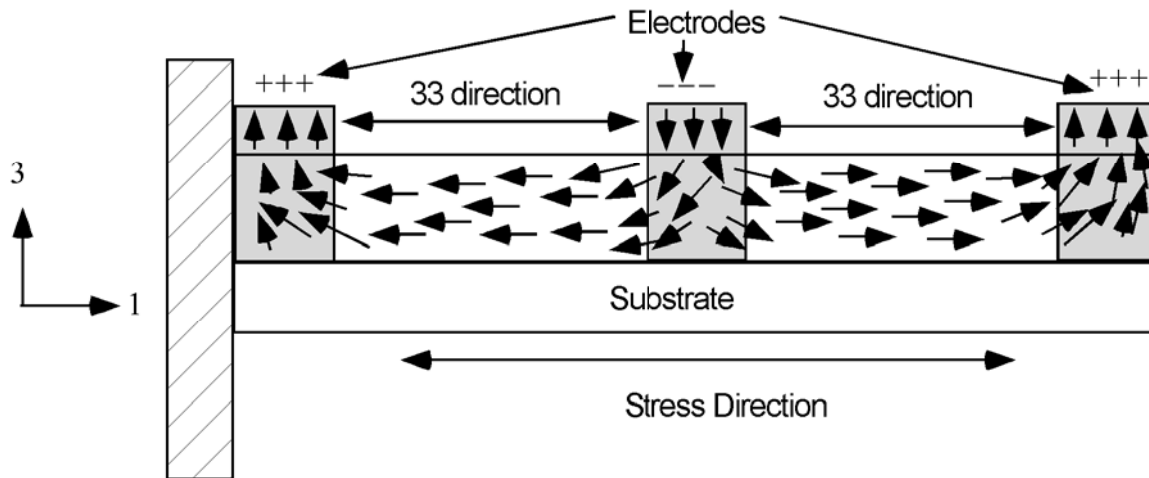
Figure 2.8. 33 Piezoelectric Cantilever Bender

It is difficult to realize the 15 mode in a standard cantilever bender. However, since the d_{15} constant is larger than the d_{33} and d_{31} constants, if the bender could experience shear in the 1-3 plane, mechanical to electrical conversion or electrical to mechanical conversion may be able to be increased as compared with operating in the d_{33} and d_{31} modes . Figure 2.9 depicts a cantilever beam manufactured to operate in the 15 mode. Since the electrodes are on the ends of the beam, when the beam bends, a shear stress would develop in the 1-3 plane and the d_{15} constant would be exhibited. In reality, this configuration would be very difficult to manufacture and would not be a likely candidate for an energy harvester.
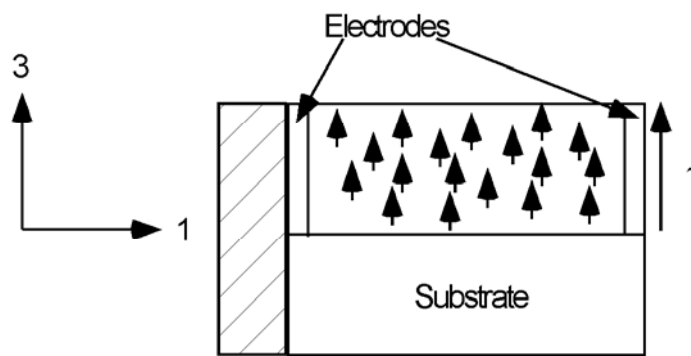
Figure 2.9. Cross section of cantilever beam employing 15 mode

12

3.0   LITERATURE REVIEW

In the last few years, there has been increasing research in the area of power or energy harvesting. This is defined as the process of acquiring the energy surrounding a system and converting it into usable electrical energy. This chapter will review some of the work that has been done previously in the energy harvesting area. It will begin with a look at piezoelectric based energy harvesting and possible applications for these devices. Reviewing research that investigates storing the energy harvested from the environment will follow this. The basis of the capacitive shunt method used for tuning purposes in this thesis is discussed and is followed by a section outlining frequency-tuning concepts used in previous work.

3.1   PIEZOELECTRIC BASED ENERGY HARVESTING AND APPLICATIONS

The concept of using piezoelectric material for energy generation has been the focus of much research over the past few decades. Numerous studies involving energy harvesting with piezoelectric material in various disciplines demonstrates the wide variety of applications that can be employed. Hausler and Stein (1984) studied the expansion and contraction of the rib cage during breathing as a means to generate energy. A polyvinylidene fluoride (PVDF) film was implemented *in vivo* on a dog. It was demonstrated to produce a peak voltage of 18V and power

of approximately 17μW. Starner (1996) explored the possibility of using a person's everyday actions to generate power to run a computer and thus reduce or eliminate the use of batteries. An analysis of the amount of energy generated from leg motion is presented along with a survey of other possible sources of energy such as blood pressure and body heat. Kymissis et al. (1998) studied the use of capturing energy parasitically while walking. Three different devices were built into the sole of a shoe and analyzed. The three devices were a piezoceramic Thunder sensor/actuator placed in the heel of the shoe, a PVDF foil laminate patch in the sole of the shoe, and an electromagnetic generator. Both the Thunder and PVDF devices translated each heel strike into electrical energy. As for the generator, each time the heel struck the ground, a flywheel was spun which could extract power from the walking motion. Ramsay and Clark (2001) investigated the capabilities of powering an *in vivo* MEMS system with a piezoelectric transducer. It was shown that by driving a thin square plate with blood pressure, there was enough energy to run the electronics if they were used intermittently. Priya (2005) demonstrated the possibility of using piezoelectric bimorphs to harvest energy from the wind using a piezoelectric windmill. 12 bimorphs were arranged along the circumference of the mill. As the wind caused the mill to rotate, a camshaft gear mechanism provided a torque that excited the harvesters. A rectified power of 10.2 mW was produced at an oscillating frequency of 6 Hz.

One of the most effective ways to implement a piezoelectric harvesting device is to use mechanical vibrations to induce strain energy into the piezoelectric ceramic. By using ambient vibrations as an energy source, otherwise wasted energy can be converted into useful electrical energy and used to power other devices. Umeda et al. (1996) investigated the characteristics of a piezoelectric generator. The authors quantified the amount of energy that could be produced from a steel ball impacting a piezoelectric plate. An equivalent circuit model was used to predict

the generated energy and several parameters were modified to find the optimum conditions. It was determined that a large amount of kinetic energy was returned to the steel ball causing it to leave the plate. If the ball instead vibrated with the plate, more energy could be produced. It was also determined that efficiency increases if the mechanical quality factor increases, the electromechanical coupling coefficient increases and the dielectric loss decreases.

Williams and Yates (1996) propose a device that when embedded in a vibrating environment, can convert the mechanical energy into electrical energy. The energy can be used to power other devices. In this case a harmonic analysis was performed on an electromagnetic transducer and not a piezoelectric one. However, the application is much the same. Theoretical values of generated power for a range of frequencies of excitation, amplitude, and seismic mass displacement were calculated. It was determined that the amount of power generated was proportional to the cube of the vibration frequency and in order to generate large amounts of power, large deflections of the mass must be incorporated into the design.

Goldfarb and Jones (1999) analyzed the efficiency of the piezoelectric material in an energy harvesting stack configuration via an analytical model. From the model it is suggested that a major problem in generating power from a piezoelectric material is that it stores a majority of the energy produced. The energy is then transferred back to the vibration source that initially caused the generated charge. The authors claim the maximum efficiency of power generation can be achieved by minimizing the amount of energy stored inside the piezoelectric material.

Roundy et al. (2002) surveyed the potential to use ambient energy as a power source when vibrations are present. In this work, possible energy sources for wireless sensor nodes were presented. Of particular interest for this work are vibration energy sources. The authors collected acceleration and frequency data from common sources that could be used to scavenge

energy from. Table 1 presents the acceleration magnitude and frequency of the fundamental vibration mode of several common sources.

Table 1. Acceleration (m/s^2) magnitude and frequency of fundamental vibration mode for various sources. (Roundy et al. (2002))

Vibration Source	A (m/s^2)	F$_{peak}$ (Hz)
Car engine compartment	12	200
Base of 3-axis machine tool	10	70
Blender casing	6.4	121
Clothes dryer	3.5	121
Person nervously tapping their heel	3	1
Car instrument panel	3	13
Door frame just after door closes	3	125
Small microwave oven	2.5	121
HVAC vents in office building	0.2-1.5	60
Windows next to a busy road	0.7	100
CD on notebook computer	0.6	75
Second story floor of busy office	0.2	100

Designs for both capacitive and piezoelectric converters are investigated and evaluated. The analysis indicates that piezoelectric converters are capable of producing more power per unit volume than capacitive converters. Piezoelectric materials also prove to have the capability of

16

producing a significant amount of energy at low frequencies that make them attractive for certain applications.

Sodano et al. (2002) investigated the amount of power that could be generated by vibrating a cantilever plate. An electromagnetic shaker was used to drive the plate at both resonant and random excitation signals. At resonance, the plate could generate 2 mW of power. It was also shown the piezoelectric plate could be used to charge a capacitor circuit and also to replenish a fully discharged battery.

Kim (2002) investigated the use of diaphragm elements for power harvesting. In this work, unimorph and bimorph diaphragm structures were studied. Several different poling configurations were investigated. The thickness ratios and poling directions at various locations were varied and the amount of energy generated was calculated. It was determined that a regrouped electrode pattern resulted in maximum electrical energy generation.

Sood et al. (2005) presents an energy-harvesting device utilizing the d_{33} mode that can produce as much as 20 times more voltage than the d_{31} mode. The manufacturing process is discussed. The device was mechanically excited via base excitation. It was shown that the device could deliver 1μW of power to a 5.2 MΩ resistive load at 2.4 V DC.

3.2   POWER ESTIMATION MODELS FOR PIEZOELECTRIC DEVICES

Along with experimental studies, many researchers have done analytical studies to predict the amount of energy that could be harvested from an energy harvester.

Smits et. al. (1991) discusses the electromechanical characteristics of a piezoelectric bender subjected to various boundary conditions, both electrical and mechanical. In this work a

beam containing two piezoelectric layers is studied. Using free bender analysis and assuming thermodynamic equilibrium, the constitutive equations of the bender are derived by calculating the internal energy of the system. Wang and Cross (1999) followed a similar process for a triple layer piezoelectric bender. The bender contained a substrate layer, sandwiched between two piezoelectric layers. The constitutive equations were again derived using energy methods. In another paper, Wang et. al. (1999) presents a discussion on electromechanical coupling mechanisms in piezoelectric unimorph and bimorph bending actuators. The electromechanical coupling coefficient, maximum energy transmission coefficient, and maximum mechanical output energy were characteristic parameters discussed in the paper. It was determined that in a unimorph actuator to obtain a higher coupling coefficient, a stiffer material is desired. Also bending mode actuators have lower electromechanical coupling coefficients compared to longitudinal, transverse, or shear mode actuators because internal stresses are built up when converting transverse motion into bending motion.

Eggborn (2003) investigated three different analytical models to predict the power output of a cantilever beam containing piezoelectric materials. A pin-force method, enhanced pin-force method, and Euler-Bernoulli method were studied. A parametric study was also conducted to determine optimum location and dimensions of a PZT patch and forcing function of the system. It was shown experimentally that the Euler-Bernoulli method produced the most accurate power predictions.

Richards et al. (2004) developed a formula to predict the power conversion efficiency for devices that contain a piezoelectric material. The formula reveals a trade-off on efficiency between the quality factor and electromechanical coupling factor. The largest efficiency increase

comes from decreasing structural stiffness. This is followed by decreasing the mechanical damping of the structure and next by increasing the effective mass.

Lu et al. (2004) presents a simple model for the analysis of piezoelectric power generator in MEMS. From the model, the output power and conversion efficiency are obtained and are used to evaluate the generator performance. It is found that there is an optimal load resistance that produces the maximum output power. Also, increasing frequency of vibration can increase generated power up to a certain point, where at the power ceases to improve.

Sodano et al (2004a) developed a model to predict the amount of power capable of being generated via the vibration of a cantilever beam containing PZT elements. The model was adaptable to account for various boundary conditions or layouts of PZT patches. Through experiment, the model proved to be very accurate.

Mo et al. (2005) examined a unimorph piezoelectric cantilever beam with interdigitated electrodes for use in power harvesting. A theoretical model to predict power output of the device is first presented and is followed by parametric simulations to determine optimal parameters to generate the greatest amount of energy. It was determined that keeping the piezoelectric and substrate layers the same thickness results in the best performance. Also, keeping the width of the interdigitated electrode narrow, results in larger energy generation.

3.3   ENERGY HARVESTING CIRCUITS AND STORAGE METHODS

Just as there has been much research done with energy harvesting devices, there also have been investigations involving ways to store the harvested energy. As well as looking at harvesting energy from human motion, Starner (1996) also discussed the advantages and disadvantages of

19

using either a rechargeable battery or capacitor and was one of the earliest researchers to investigate the concept.

Umeda et al. (1997) continued their previous work and studied the characteristics of energy storage. Using the steel ball and piezoelectric generator as before, a bridge rectifier and capacitor were connected to the setup. By changing parameters of the circuit, they were able to determine energy storage characteristics both theoretically and experimentally.

After evaluating the performance of their piezoelectric generators, Kymissis et al. (1998) developed a circuit used to take energy generated from walking and power a radio transmitter. The circuit utilized a capacitor as the storage device as well as other components used to control the charging cycle. The capacitor was first charged to a desired level and then allowed to discharge. Once the capacitor was discharged to a predetermined level, an electronic switch would be triggered and the capacitor would recharge. It was determined that it was possible to use the piezoelectric devices to power a transmitter to send data to a wireless receiver.

Much research has gone into optimizing harvesting devices and developing storage circuits. Some researchers have also looked at developing circuitry to extract more energy from the piezoelectric material. Kasyap et al. (2002) developed a lumped element model to predict the energy generated from a cantilever beam with a piezoelectric element undergoing forced vibration. Energy was harvested and stored using a flyback converter to increase efficiency. The flyback converter allows the circuit impedance to match that of the piezoelectric device and hence maximized the amount of energy stored.

In most applications, a capacitor is used as a storage device. However, since a capacitor is only good at delivering short bursts of energy, it is not well suited for long term storage. Sodano et al. (2004) showed that a rechargeable battery could be used with piezoelectric

materials as an alternative to the capacitor. In a paper that followed, Sodano et al. (2005) investigated the ability to use three piezoelectric devices to recharge various capacity nickel metal hydride batteries. The three materials were stock PZT used in a manufactured bender, a macro-fiber composite, and a bimorph Quick-Pack actuator. It was found that the PZT and Quick Pack were capable of recharging the batteries, with the PZT being more efficient in a random vibration environment. It was also shown that the macro-fiber composite was not suited for power harvesting.

Guan and Liao (2006) compared several energy storage devices for use in piezoelectric power harvesting. The storage devices included conventional capacitors, rechargeable batteries, and supercapacitors. Parameters studied were charge/discharge efficiency, adaptability, lifetime, and self-discharge. From experimental results, it was determined that supercapacitors are suitable for energy harvesting and are more attractive than rechargeable batteries as energy storage devices.

Ottman et al. (2002) studied the use of an adaptive step down DC-DC converter to maximize energy transfer between a vibrating piezoelectric transducer and a battery. It was experimentally shown that the use of the converter increases power transfer by as much as 400% as compared to a standard AC-DC rectifier circuit used alone. A drawback to this circuit is that additional power was required due to the dissipative effects of added components. It was also determined that there exists an optimal rectifier voltage to harvest the maximum amount of energy. In an AC-DC rectifier circuit, the optimal rectifier voltage should be one-half of the peak open circuit voltage from the piezoelectric element.

Shu (2006) investigates the optimal AC-DC power generation for a piezoelectric device. In this work an analytic expression for the AC-DC power generation is derived under steady

state operation. From the derivation, it was shown that the harvested power is dependent on the frequency and acceleration of the input vibration, the mass of the generator, the electrical load, the natural frequency, damping, and electromechanical coupling coefficient of the system. Several design guidelines are given for devices with large coupling coefficients and quality factors.

3.4   CAPACITIVE TUNING METHOD

The majority of research involving the use of piezoelectric harvesters requires the fundamental mode of the harvesters to match the frequency of the vibration source to obtain maximum power output. Manufacturing processes or changes in the vibration frequency can make frequency matching difficult. Using a piezoelectric element's capacitive nature as a means of changing structural properties and hence natural frequency would be beneficial in the energy harvesting field. Little has been done in using a passive tuning concept on a piezoelectric harvesting device. However, such a concept was investigated for use in structural damping and in tuning resonators used for frequency applications.

Hagood and von Flotow (1991) initially investigated using passive elements to provide damping in structures. By connecting piezoelectric materials with passive electrical networks (in this case using resistor-inductor networks), it was shown that damping could be developed in the system. Wang et al. (1994) adapted the initial circuit to improve dissipation.

Davis and Lesieutre (1998) investigated the use of a capacitive network to create a tunable vibration absorber. The effective stiffness of the device was adjusted electrically, utilizing piezoelectric ceramic elements. It was shown that by using a passive capacitive shunt

22

circuit, the absorber had a tuning range dependent on the short and open circuit conditions of the piezoelectric element.

Clark (2000) presented a piezoelectric actuator that was used for energy dissipation in a simple mechanical system. The system utilizes an electrical shunt circuit to switch the actuator from high to low stiffness. When the system is moving, the actuator is held in its high stiffness state such that energy can be stored in the actuator. The actuator is switched to a low stiffness when the system's motion would cause it to receive energy back from the actuator, and in turn dissipating the energy.

Muriuki (2004) utilized a shunt capacitive concept to tune self-oscillating piezoelectric resonators. In this work, a piezoelectric cantilever beam resonator was modeled as a single degree of freedom system. From this work the natural frequency of a single degree of freedom resonator is shown in equation 1. As can be seen, an equivalent stiffness of the cantilever beam can be equated to a mechanical stiffness combined with the product of the square of the electromechanical coupling and the inverse of the capacitance of the piezoelectric element. Hence, the natural frequency of the beam can be altered via the capacitance term.

$$\omega = \sqrt{\frac{K_{eff} + C^{-1}d^2}{m_{eff}}} \tag{1}$$

Frederick (2005) used a similar approach to achieve a wide range of tunability utilizing the d_{33} piezoelectric response of an interdigitated resonator. In a similar approach, this work investigates the tuning range of a piezoelectric bimorph that utilizes the d_{31} response and also incorporates effects on generated energy.

3.5   OTHER FREQUENCY TUNING CONCEPTS

Among the vast research being done in studying piezoelectric energy harvesters, the concept of tuning plays a major role in the amount of energy able to be recovered. Along with the piezoelectric shunt mechanism described in the previous section, there is other research aimed at eliminating or at least reducing the dependence on matching a harvesting devices natural frequency to a source.

Chandrashekhara and Bangera (1993) demonstrate the influence of beam geometry, tip mass and material properties on the frequencies of symmetric laminated composite beams. In this work, the natural frequencies of a symmetrically laminated composite beam with a tip mass are determined. The equations account for the Poisson effect, rotary inertia and transverse shear deformation.

Lesieutre and Davis (1997) preceded their previously mentioned work by investigating the dependence of electromechanical coupling in a piezoelectric device on mechanical axial pre-loads and hence show an alternative method of tuning piezoelectric devices. By applying a preload equal to half of the buckling load to a symmetric piezoelectric bimorph device, the coupling coefficient increased by more than 40%. Leland and Wright (2006) later used this method to adjust the natural frequency of an energy harvester. A simply supported piezoelectric bimorph was used to evaluate harvester performance. It was determined that an axial pre-load can reduce the resonance frequency of the harvester up to 24% and increase the coupling coefficient up to 25%. Using this method, a harvesting device can be tuned across a bandwidth of frequencies.

Shahruz (2005) presents a design for a mechanical band-pass filter for use in energy scavenging.   A systematic procedure for designing the filter is given. The filter contains and

ensemble of cantilever beams with proof masses at their ends. By appropriately choosing dimensions of the beams and the size of the mass, energy can be harvested from a range of frequencies and is not limited to just one.

Tieck et al. (2006) investigates a new approach using a frequency multiplication technique to harvest electrical energy from mechanical energy using cantilever piezoelectric bimorphs. The work involves using a linearly traveling beam exciter or rack to impart vibrational motion to a beam. If the rack is traveling at a lower frequency than the natural frequency of the energy harvester, it is possible to gather energy from a source using a harvester whose natural frequency is unrelated. The authors claim more energy can be generated than using a standard harvester driven at resonance.

4.0   CAPACITIVE TUNING METHOD

The tuning concept used in this work is based on utilizing the variable stiffness capabilities of piezoelectric material. In this case, the piezoelectric material is a layer of a cantilever beam or plate structure. By adjusting shunt circuit conditions applied across the piezoelectric layer, the effective elastic modulus of the layer changes and hence the overall stiffness of the structure changes. Since the natural frequency of the structure is dependent on its stiffness, by varying the shunt conditions, the natural frequency can be adjusted or tuned to a desired value. This chapter will begin by investigating shunt circuit effects on stiffness of a single degree of freedom beam model. It will be shown that a ratio of open circuit to short circuit stiffness (or frequency) can be used to determine a tuning range for the device. This model will then be used to determine parameters to gain the most tuning. A binary capacitor array concept for use in tuning a piezoelectric harvester will be explained next.

4.1   PIEZOLECTRIC SHUNT CONDITIONS

In a network of parallel capacitors, the equivalent capacitance of the system is the sum of the capacitances. If a piezoelectric element has a capacitance, C_p, and it's shunt has a capacitance, C_s, the total capacitance is equal to the sum $C_p + C_s$. Figure 4.1 presents the basic capacitive shunt method.

26
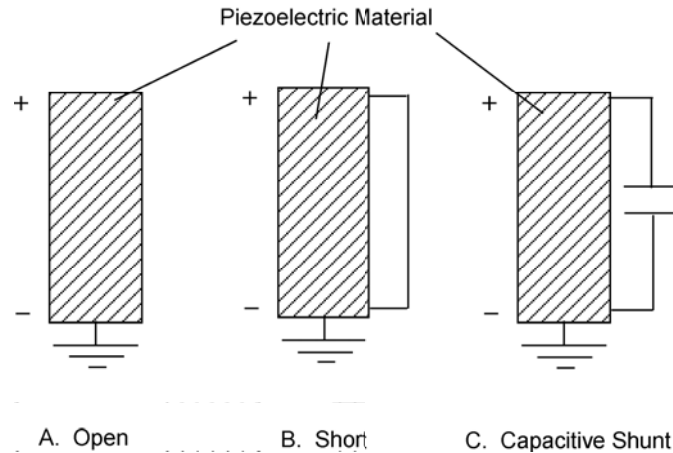
Figure 4.1. Shunt Capacitor Tuning Method

Case A of Figure 4.1 represents a piezoelectric element whose electrodes are left as an open circuit. Case B represents a short-circuited piezoelectric element and Case C depicts a piezoelectric element in parallel with a shunt capacitor. Since a piezoelectric element is a capacitive element, the total capacitance of the system is equal to the sum of the capacitance of the piezoelectric layer and its shunt. Combining this fact and Equation 1, the stiffness of the beam can be determined. Case A has a capacitance equal to the piezoelectric layer and defines the upper stiffness limit. For Case B, the electromechanical coupling term disappears because the equivalent capacitance is infinite and therefore the total structural stiffness only has a mechanical stiffness term, defining the lower stiffness limit. Since the reciprocal of the capacitance appears in the frequency equation, the effect of a shunt is to reduce the effect of the electromechanical coupling on the system. If shunt capacitors are added in parallel to the piezoelectric element, the stiffness and natural frequency of the beam can be adjusted between the two bounding conditions.

27

An example of this concept is demonstrated in the next section by changing the stiffness of a multi-layer cantilever beam containing piezoelectric layers. By adding capacitors in parallel with a piezoelectric layer, the stiffness of the layer changes and hence the overall structural stiffness changes.

4.2   SINGLE DEGREE OF FREEDOM BEAM MODEL

In this section, a model for a cantilever beam with a harvesting layer (piezoelectric), a substrate layer (non-piezoelectric), and tuning layer (piezoelectric) is developed. The harvesting and tuning layers are made of piezoelectric material and the substrate layer is constructed of metal. Two piezoelectric layers were chosen for this analysis so that the affect each layer had on tuning and harvesting could be isolated for each case. Since piezoelectric materials are brittle, a substrate was included to add stiffness and durability to the structure. By varying the position and thickness of each layer, effects on stiffness and hence tunability can be studied. Three cases are given in Figure 4.2
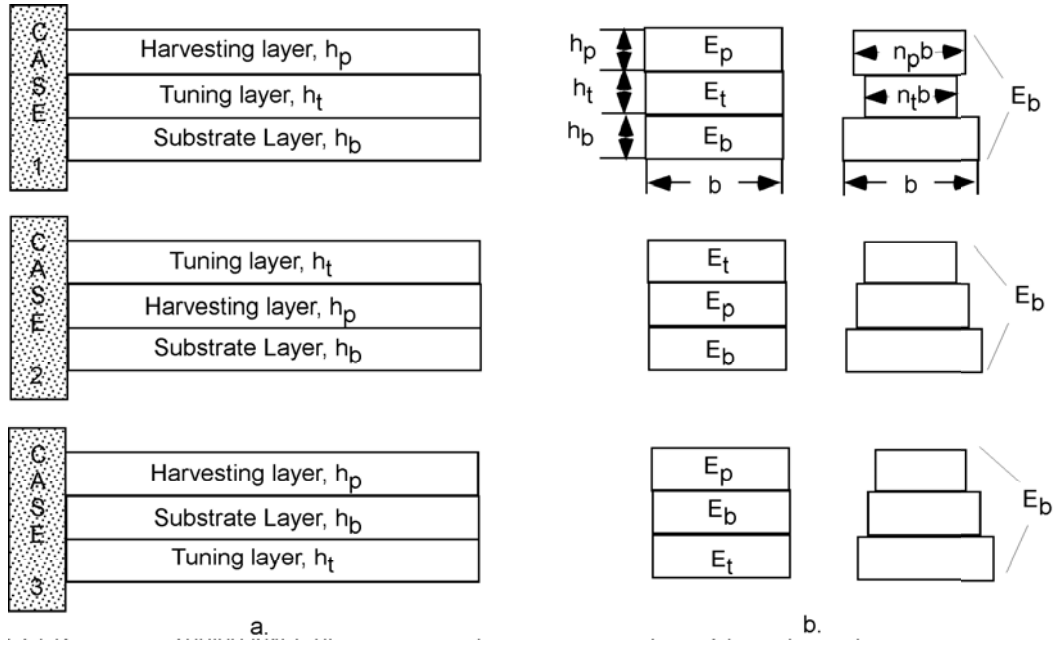
Figure 4.2. (a) Cantilever beam with piezoelectric harvesting and tuning layers and a metal substrate. (b) Conversion of beam cross-section dimensions from original beam to one made of entirely substrate material.

For easier reference later, Case 1 is the case with the order of layers (from the bottom of the beam) being substrate layer, tuning layer, and harvesting layer. Case 2 is the case with the order being substrate layer, harvesting layer, and tuning layer. Case 3 is the case with the order of layers being tuning layer, substrate layer, and harvesting layer.

Utilizing a simplified analysis of the fundamental mode of a beam with effective stiffness and mass, the effective stiffness of a flexible beam can be found by using the equation for spring stiffness:

$$F = K_{eff}\, y \tag{2}$$

where F is a load applied to the end of the beam and y is the resulting deflection. This deflection can be written as (Riley, 2002):

$$y = \frac{F}{6EI}(-x^3 + 3L^2 x - 2L^3) \tag{3}$$

29

The deflection at the end of the beam ($x=0$) is equal to:

$$y = \frac{PL^3}{6EI}$$ (4)

hence the effective stiffness is:

$$k_{eff} = \frac{3EI}{L^3}$$ (5)

Since the beam has three layers of different materials, the flexural rigidity, EI, is not constant through the depth of the beam. By converting the beam to an equivalent one made entirely of the substrate material, the effective stiffness can be determined. Figure 2b shows equivalent beams for each case where the heights of each layer have remained the same and the widths have been multiplied by a ratio of the layer's elastic modulus to that of the substrate. The ratios are:

$$n_p = \frac{E_p}{E_b} \qquad n_t = \frac{E_t}{E_b}$$ (6)

The subscript, p, is for the harvesting layer, b is for the substrate, and t is for the tuning layer. Letting all distances be measured from the interface of the upper two layers, an effective moment of inertia, I, can be calculated for each case. For case 1:

$$
\begin{aligned}
I_{eff} &= \frac{bh_b^3}{12} + (h_b b)\left[y_c - \left(-h_t - \frac{h_b}{2}\right)\right]^2 \\
&+ \frac{n_t bh_t^3}{12} + (n_t h_t b)\left[y_c - \left(-\frac{h_t}{2}\right)\right]^2 \\
&+ \frac{n_p bh_p^3}{12} + (n_p h_p b)\left[y_c - \left(\frac{h_p}{2}\right)\right]^2
\end{aligned}
$$ (7)

where h is the thickness of the specific layer, and y_c is the distance to the centroid of the beam and is also known as the position of the neutral axis. For this case, y_c is defined as:

$$y_c = \frac{\sum A_n y_n}{\sum A_n} = \frac{n_t bh_t(\frac{-h_t}{2}) + n_p bh_p(\frac{h_p}{2}) + bh_b(-h_t - \frac{h_b}{2})}{n_t bh_t + n_p bh_p + bh_b}$$ (8)

30

where A_n is the area of a layer, and y_n is the distance to the centroid of each layer.

For case 2:

$$I_{eff} = \frac{bh_b^3}{12} + (h_b b)\left[y_c - \left(-h_p - \frac{h_b}{2}\right)\right]^2$$
$$+ \frac{n_t bh_t^3}{12} + (n_t h_t b)\left[y_c - \left(\frac{h_t}{2}\right)\right]^2$$
$$+ \frac{n_p bh_p^3}{12} + (n_p h_p b)\left[y_c - \left(-\frac{h_p}{2}\right)\right]^2 \tag{9}$$

$$y_c = \frac{\sum A_n y_n}{\sum A_n} = \frac{n_t bh_t(\frac{h_t}{2}) + n_p bh_p(-\frac{h_p}{2}) + bh_b(-h_p - \frac{h_b}{2})}{n_t bh_t + n_p bh_p + bh_b} \tag{10}$$

For case 3:

$$I_{eff} = \frac{n_t bh_t^3}{12} + (n_t h_t b)\left[y_c - \left(-h_b - \frac{h_t}{2}\right)\right]^2$$
$$+ \frac{bh_b^3}{12} + (h_b b)\left[y_c - \left(-\frac{h_b}{2}\right)\right]^2$$
$$+ \frac{n_p bh_p^3}{12} + (n_p h_b b)\left[y_c - \left(\frac{h_p}{2}\right)\right]^2 \tag{11}$$

$$y_c = \frac{\sum A_n y_n}{\sum A_n} = \frac{n_t bh_t(-h_p - \frac{h_t}{2}) + n_p bh_p(\frac{h_p}{2}) + bh_b(-\frac{h_b}{2})}{n_t bh_t + n_p bh_p + bh_b} \tag{12}$$

In all three cases, the effective rigidity and hence the effective stiffness can be changed by short or open circuiting the tuning layer. For the harvesting layer (assuming a piezoelectric material), the elastic modulus is:

$$E_p = \left(s_{11}^E - \frac{d_{31}^2}{\varepsilon} \zeta Z_{sh} \right)^{-1} \tag{13}$$

where the permittivity $\varepsilon = \dfrac{tC}{A}$, with t being capacitor thickness, C is capacitance, and A is capacitor area, s_{11} is the mechanical compliance of the piezoelectric material, d_{31} is the electromechanical coupling coefficient, ζ is a Laplace variable and Z_{sh} is the impedance of the piezoelectric material and it's shunt, defined by

$$Z_{sh} = ((C_p + C_s)\zeta)^{-1} \tag{14}$$

where $C_p = \dfrac{\varepsilon A}{t}$.

If the tuning layer (a piezoelectric material) is short circuited, C_s approaches infinity and therefore Z_{sh} approaches 0. Hence the compliance is equal to the inverse of the Young's modulus:

$$E_{tsc} = (s_{11}^E)^{-1} \tag{15}$$

If the tuning layer is open circuited, C_s is equal to zero and the modulus becomes:

$$E_{toc} = \left(s_{11}^E - \frac{d_{31}^2}{\varepsilon} \right)^{-1} \tag{16}$$

When a capacitive shunt is applied, it can be seen from equation 13 that the modulus of the beam will fall between the short circuit and open circuit conditions. Equations 5 through 16 show that by changing the shunt condition on the tuning layer, the effective beam modulus, and hence stiffness of the beam can be changed (Equation 5). Since this stiffness term also appears in the frequency equation (1), it can be seen that the natural frequency of the beam can be adjusted using this capacitive shunt concept. A summary of each shunt condition is presented in Table 2.

Table 2. Summary of shunt conditions and effect on Stiffness

Shunt Condition	C_s	Z_{sh}	E	Stiffness State
Open Circuit	0	$(C_p \zeta)^{-1}$	$E_{toc} = \left(s_{11}^E - \dfrac{d_{31}^2}{\varepsilon} \right)^{-1}$	High Stiffness
Short Circuit	∞	0	$E_{tsc} = (s_{11}^E)^{-1}$	Low Stiffness
Capacitive Shunt	C_s	$((C_p+C_s)\,\zeta)^{-1}$	$E = (s_{11} - \dfrac{d_{31}^2 A}{t(C_p + C_s)})^{-1}$	Stiffness between High and Low

Assuming the natural frequency $\omega = \sqrt{\dfrac{k_{eff}}{m_{eff}}}$, and inserting the appropriate modulus into equation

5, the upper and lower frequency bounds are shown in equations 17 and 18.

$$\omega_{upper} = \sqrt{\frac{3(s_{11} - \frac{d_{31}^2}{\varepsilon})^{-1} I}{L^3 m_{eff}}} \tag{17}$$

$$\omega_{lower} = \sqrt{\frac{3I}{L^3 s_{11} m_{eff}}} \tag{18}$$

By varying the capacitance of the shunt, the frequency can be varied between these two bounds

and is shown in equation 19.

$$\omega_{upper} = \sqrt{\frac{3(s_{11} - \frac{d_{31}^2 A}{t(C_p + C_s)})^{-1} I}{L^3 m_{eff}}} \tag{19}$$

4.2.1 AVAILABLE STIFFNESS RESULTS

Table 3 gives the parameters used in modeling each beam configuration. Aluminum was chosen as the substrate material from previous experience and Lead Zirconate Titanate (PZT) was chosen as the material for both the substrate layer and the tuning layer.

Table 3. Parameters Used in Available Stiffness and Energy Analysis

Parameter	Variable	Value	Units
PZT strain constant	d_{31}	-320e-12	m/V
PZT relative permittivity	ε	3800	m/V
PZT elastic modulus	$E_{p \text{ or }} E_t$	6.2e10	Pa
Aluminum Elastic Modulus	E_b	7e10	Pa

Clark (2000) demonstrated that for a unimorph cantilever beam shunted between open circuit and short circuit states, by varying the ratio of the thickness of the substrate layer to the piezoelectric layer, the available change in stiffness of a beam could be determined. In this study, an additional layer is added to the beam. A ratio of the thickness of the substrate layer to the tuning layer and a ratio of the thickness of the harvesting layer to the tuning layer is used as a baseline parameter for quantifying the change in stiffness for different layer configurations. Figures 4.3 and 4.4 show the results for varying the ratios for Case 1. Figure 4.3 uses both tuning and harvesting layers for tuning and Figure 4.4 only uses the tuning layer. Note that the vertical axis in each case shows the open-circuit to short-circuit stiffness (koc/ksc), so higher values indicate greater change. Also, the tuning layer thickness in each case remains constant.

As the thickness ratios increase, the stiffness change and thus the amount of tunability in the

beam decreases since the frequency change is related to the square root of stiffness change. This

makes sense because the relative amount of tuning material decreases as the ratio increases. On

the following plots, the change in frequency can be found by taking the square root of the

stiffness change.
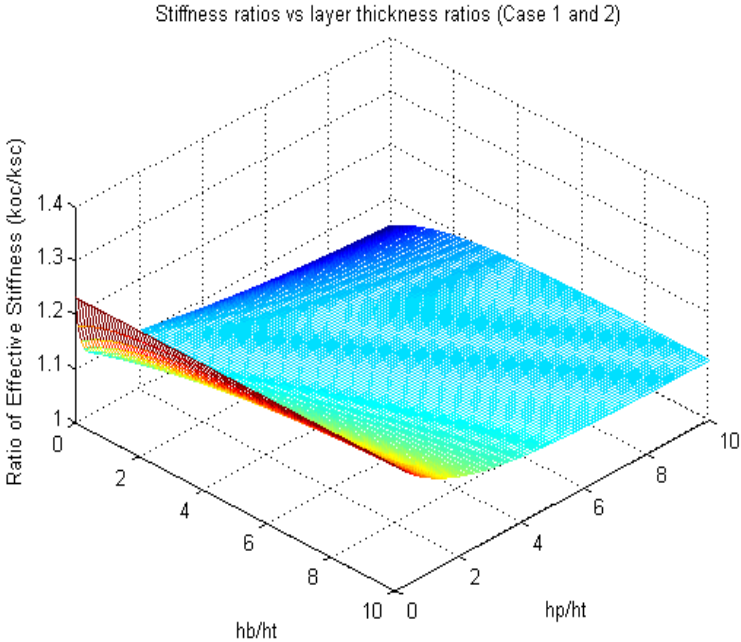
Figure 4.3. Beam Stiffness Ratio versus Layer Thickness Ratio for Case 1 and 2 (Tuning and harvesting
layers used for tuning)
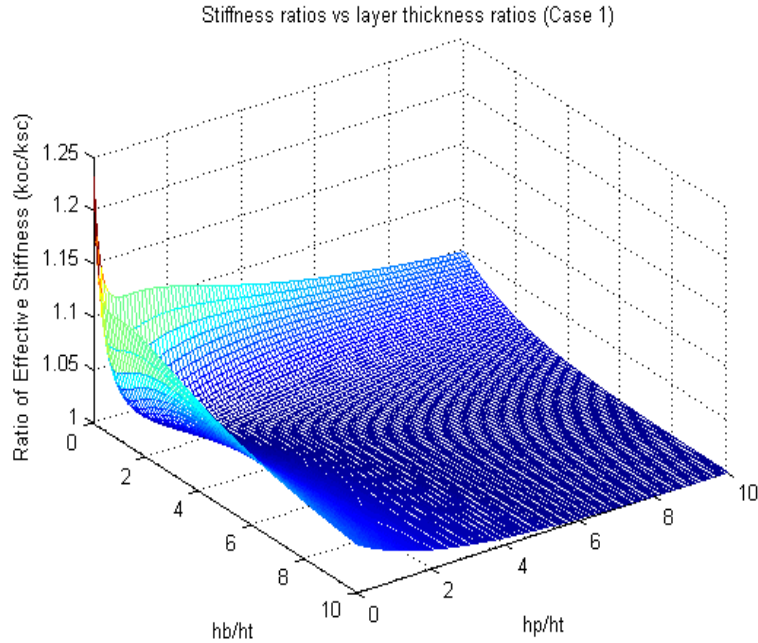
Figure 4.4. Beam Stiffness Ratio versus Layer Thickness Ratio for Case 1 (Tuning layer used for tuning)

Figure 4.3 shows the result of using both the harvesting and tuning layer for tuning for Case 1 and 2. The plots for each case look the same because the layers are in the same relative places on the beams and therefore their effect on stiffness is the same. From the plot, the maximum ratio of stiffness and hence maximum amount of tunability occurs when the thickness ratios are small (between 0 and 2). Figure 4.4 shows the results when only the tuning layer is used for tuning. This condition could be considered as a lower limit on the available tuning. For this case, the maximum amount of tunability again occurs when the thickness ratios are small. However, in this case, when the ratios are equal to each other the stiffness ratio drops dramatically. This is due to the neutral axis of the beam being inside of the tuning layer and hence causing a cancellation effect inside the piezoelectric material. It is important to note that there is more tuning available for a larger range of thickness ratios when both layers are used due

36

to a greater stiffness change. However, using both layers entirely would result in not being able to harvest any energy when approaching a short circuit condition.
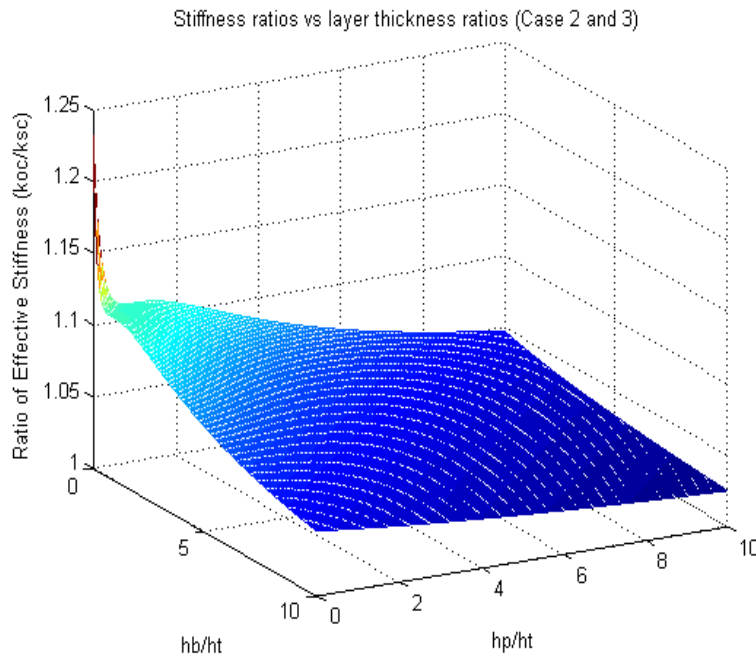
Figure 4.5. Beam Stiffness Ratio versus Layer Thickness Ratio for Case 2 and 3 (Tuning Layer used for tuning)

Figures 4.5 and 4.6 represent the resulting stiffness ratios from varying the thickness ratios for cases 2 and 3. Figure 4.6 uses both harvesting and tuning layers for tuning. Figures 4.5 uses only the tuning layer. In cases 2 and 3, the tuning layer is in the same relative position, therefore by changing the stiffness of the tuning layer both cases produce the result of Figure 4.5. Again as the thickness ratios increase, the amount of available change in stiffness decreases. The maximum amount of tunability occurs when the ratios are small. Again, when only the tuning layer is used for tuning as in cases 2 and 3, the plots are the same. This is because the layers are in the same relative places on the beams and therefore their effect on stiffness is the same.
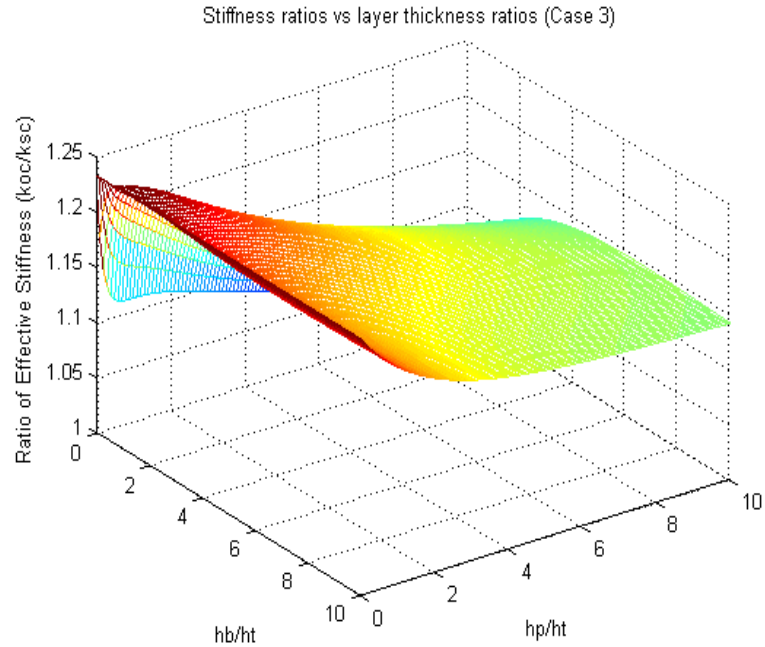
Figure 4.6. Beam Stiffness Ratio versus Layer Thickness Ratio for Case 3 (Tuning and harvesting layers used for tuning)

It can be seen from Figure 4.6 that the most tuning is provided from Case 3. For this case there is still a decrease in tuning for smaller substrate to tuning ratios. However, the amount of tuning is in general greater than for the other cases. For this reason, a bimorph is chosen as the structure to be used in all future analyses. Figures 4.5 and 4.6 show that keeping the ratio of the substrate layer thickness to the tuning layer thickness between .5 and 1 and the harvesting layer thickness to tuning layer thickness between 0 and 2 provides the largest available tuning. Also, there is up to 20 percent change in stiffness in this range that corresponds to approximately 10 percent change in frequency.

In order to ensure the neutral axis remains in the substrate material and hence charge cancellation is prevented, all layer thickness ratios were chosen to be unity. Also, unless otherwise mentioned, the harvesting layer will be used exclusively for harvesting and the tuning

layer exclusively for tuning. Since stiffness of the beam is dependent on the capacitance of the piezoelectric layer and its shunt, by plotting the ratio of the stiffness of the system to the short circuit stiffness vs. the ratio of the shunt capacitance to that of the piezoelectric layer, the effect of the shunt capacitance on the system can be observed.
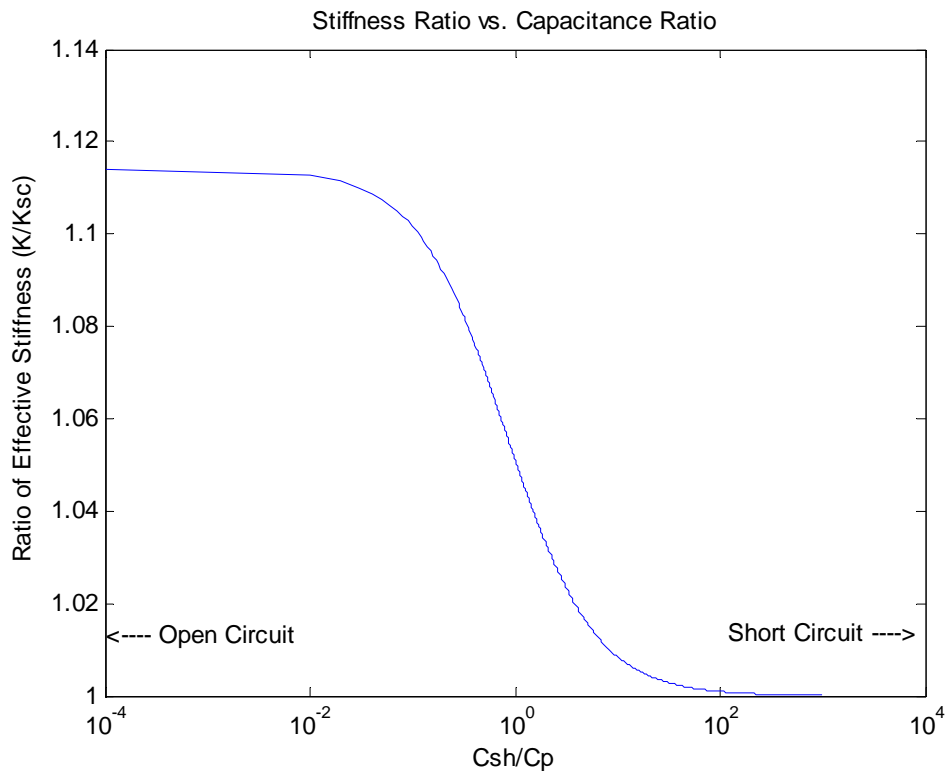
Figure 4.7. Ratio of effective stiffness versus ratio of shunt capacitance to piezoelectric capacitance

As can be seen in Figure 4.7, an effective stiffness of 1 represents a short circuit condition and anything above this represents stiffness between short and open circuit. As the capacitance of the shunt increases, the stiffness approaches short circuit conditions and as the capacitance of the shunt decreases, the stiffness approaches open circuit conditions. It is important to note it takes approximately a four-order magnitude change in shunt capacitance to

go from open to short circuit. Also, small capacitance ratios and large capacitance ratios affect the change in stiffness less than when the capacitance ratios are around one.

4.3   CAPACITOR BINARY ARRAY

The previous section showed that by adding capacitors in parallel with a piezoelectric layer in a piezoelectric bimorph, the stiffness of the layer changes and hence the overall stiffness of the device changes. To implement this concept on a real structure, a capacitor array similar to the one shown in Figure 4.8 could be used. By closing a certain combination of switches, the shunt capacitance can be adjusted from an open circuit condition to a short circuit condition.
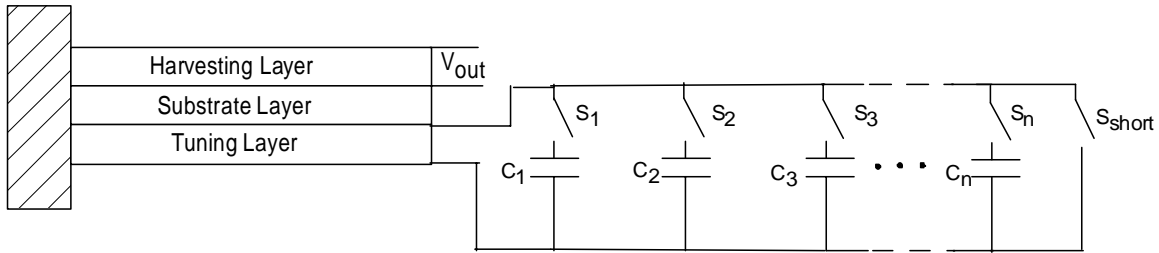
Figure 4.8. Capacitor array attached in parallel to tuning layer of a piezoelectric bimorph

If each capacitor in the array is chosen appropriately, the array will be able to count in a binary fashion with a resolution equal to the smallest capacitor (or bit) in the array. If the lowest bit in the array has a value equal to C pF, then each consecutive bit will have a value of

$$C_n = 2^n C \quad \text{pF} \tag{20}$$

where n ranges from 0 to m-1 and m is the number of bits in the array. Therefore the total capacitance that can be obtained from the array is

40

$$C_{total} = \sum_{n=0}^{m-1} 2^n C \qquad (21)$$

and the capacitance in parallel with the harvesting device at any given time is

$$C_s = \sum_{n=0}^{m-1} 2^n C\delta(S_n) \qquad (22)$$

where δ is the Kronecker delta function.

$$S_n = \begin{cases} 0 & S_n \text{ is closed} \\ 1 & S_n \text{ is open} \end{cases} \qquad (23)$$

For easier computation, the capacitance values in the array can be put into matrix form. Each bit of the array can either be on or off which is equivalent to a binary one or zero. By multiplying a vector with the binary equivalent of the array with the transpose of the vector containing the value of each bit, the value of the total capacitance of the array can be determined. For example, let the capacitance array be an 8 bit array with the lowest bit, C, being equal to 1 pF. Therefore, the capacitance vector is

$$C_{array} = \begin{bmatrix} 128 & 64 & 32 & 16 & 8 & 4 & 2 & 1 \end{bmatrix} \qquad (24)$$

If switches 1, 3, and 7 are on, a matrix, b, representing this (in binary form) is the vector

$$b = \begin{bmatrix} 0 & 1 & 0 & 0 & 0 & 1 & 0 & 1 \end{bmatrix} \qquad (25)$$

The capacitance of the array is now equal to

$$C_s = b * C_{array}^T \qquad (26)$$

41

5.0   ENERGY HARVESTING ANALYSIS

The purpose of tuning a piezoelectric energy harvester is to match its fundamental mode with that of its excitation frequency and hence maximize the amount of energy able to be generated. This chapter will present several models to predict the amount of energy that can be generated via an excited piezoelectric bimorph. This chapter will begin by presenting a model representing a beam bimorph excited by a static force. A continuous beam model will follow and mode shapes will be plotted for use in following energy calculations. Finally a plate model is developed for the purpose of comparing to experimental results. A dynamic beam bimorph energy model will follow this. Utilizing the fact that the first mode of a plate is pure bending, the last section of this chapter will analyze a dynamic plate bimorph model based on the dynamic beam model. It will be shown that each model is based on the modulus of each layer. Hence if each structure contains piezoelectric layers, by shunting the layers with capacitors, the stiffness and hence natural frequencies can be adjusted. The three models are presented to provide alternatives to calculating energy depending on the particular situation. Similar energy calculations have been performed by Smits et. al. (1991), Kim (2002), and Wang and Cross (1999) for unimorph and bimorph benders. In these works it was assumed that each piezoelectric layer had the same properties. To account for tuning and be able to change the stiffness of a particular layer, this work assumes each layer has different properties. By adding an extra layer, the resulting energy equations are rather large. Due to the length of the resulting equations, the

method will be discussed and the results presented in Appendices C and D. For convenience,

Table 4 lists the variables used in the calculations.

Table 4. Variables used in energy calculations

Young's Modulus	E_{letter}
Moment of Inertia	I
Length of Beam	L
Moment	M
Load	F
Width of Beam	b
Piezoelectric Coefficient	d
Thickness of Beam Layer	t
Position Along the Beam	x
Position Across Beam	z
Compliance	s
Deflection	y
Piezoelectric Permittivity	ϵ
Frequency	ω
Electric Displacement	D
Strain	ε
Stress	σ
Electric Field	E_{number}

Table 4. (continued)

Charge	Q
Voltage	V
Modulus Ratio	n
Energy	U
Curvature	ρ
Neutral Axis	y_c
SUBSCRIPTS	
1 direction	1
2 direction	2
3 direction	3
Piezoelectric 31 mode	31
Piezoelectric 33 mode	33
Substrate	b
Harvesting layer	p
Tuning layer	t
SUPERSCRIPTS	
Constant Electric Field	E
Constant Stress	T

5.1   STATIC BEAM ENERGY HARVESTING MODEL

By assuming a static load, the equations used to describe the system are reduced dramatically and therefore is easier to model. Multiplying the resulting energy by a driving frequency can approximate the amount of energy generated from a dynamic situation. When a point force, F, is applied to the end of a cantilever beam, as shown in Figure 5.1, strain is developed in the beam. If the beam is made of a piezoelectric material, this strain causes a charge to develop that can be harvested.
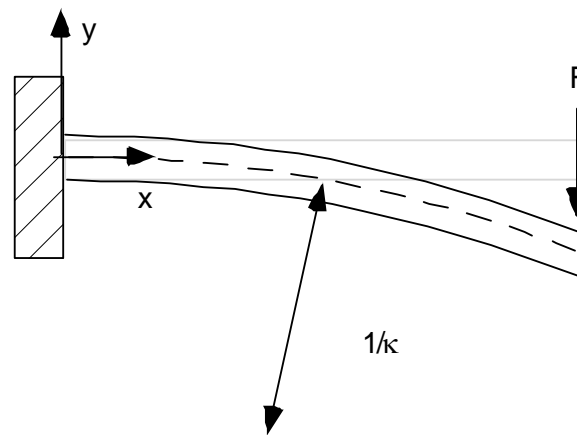
Figure 5.1. Cantilever beam with applied load, F, at the tip

Figure 5.2 represents the bimorph to be analyzed. It is assumed that each layer is completely isolated from each other. Since the electrodes of the piezoelectric material are on the 3 surface and the stress will develop in the 1 direction when the force is applied, the bimorph will operate in the 31 mode.
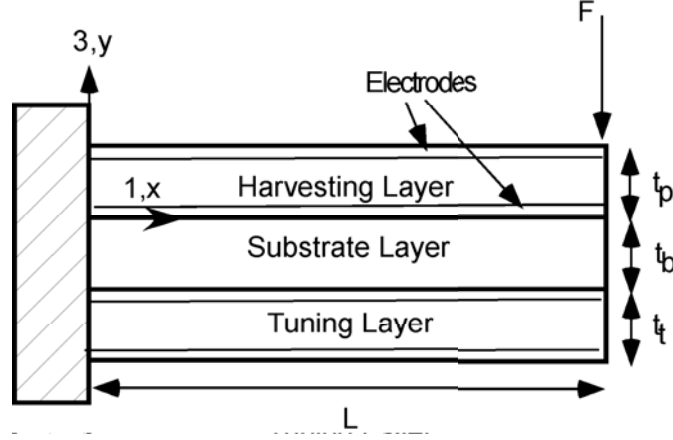
Figure 5.2. Piezoelectric bimorph with static excitation

The strain can be described in terms of curvature of the beam.

$$\varepsilon_1 = \kappa(y - y_c) \tag{27}$$

where y_c is the position of the neutral axis. From mechanics, the moment at any point along the

beam can be calculated as

$$M = F(L - x) \tag{28}$$

The moment can also be calculated from stresses on a cross section.

$$M = \int_t \sigma_{1t}(y - y_c)bdy + \int_b \sigma_{1b}(y - y_c)bdy + \int_p \sigma_{1p}(y - y_c)bdy \tag{29}$$

From the IEEE standard 176, the constitutive equations for a piezoelectric material in the 31

mode are

$$\left\{ \begin{array}{l} \varepsilon_1 = \dfrac{1}{Ep}\sigma_1 + d_{31}E_3 \\ D_3 = d_{31}\sigma_1 + \in_{33}^T E_3 \end{array} \right\} \tag{30}$$

The stresses in each layer can now be written for a piezoelectric layer and a non-piezoelectric

layer and are given in equations 31 and 32, respectively.

$$\sigma_1 = E_p(\varepsilon_1 + d_{31}E_3) \tag{31}$$

$$\sigma_1 = E_b\varepsilon_1 \tag{32}$$

Substituting equation 27 into 31 and 32 and inserting the result into equation 29 results in

$$M = \int_0^{t_p} E_p(\kappa(y-y_c) + d_{31}E_3)(y-y_c)bdy + \int_{-t_b}^0 E_b\kappa(y-y_c)^2 bdy + \int_{-t_b-t_t}^{t_b} E_p(\kappa(y-y_c) + d_{31}E_3)(y-y_c)bdy \tag{33}$$

Setting equation 33 equal to equation 28, the curvature, κ can be solved for.

$$\kappa = G_1 F + G_2 E_{3p} + G_3 E_{3t} \tag{34}$$

where G_1, G_2, and G_3 are constants. The curvature can then be substituted into the stress equations for each layer and used in the following procedure.

In thermodynamic equilibrium, an infinitesimally small volume element in the piezoelectric material has an internal energy density of:

$$dU = \frac{1}{2}\varepsilon_1\sigma_1 + \frac{1}{2}D_3E_3 \tag{35}$$

Therefore the energy in a piezoelectric layer can be described as

$$dU_p = dU_t = \frac{1}{2}(\frac{1}{E_p}\sigma_1 + d_{31}E_3)\sigma_1 + \frac{1}{2}(d_{31}\sigma_1 + \in_{33}E_3)E_3$$
$$= \frac{1}{2E_p}\sigma_1^2 + d_{31}\sigma_1 E_3 + \frac{1}{2}\in_{33}E_3^2 \tag{36}$$

and for the non-piezoelectric layer

$$dU_b = \frac{1}{2E_b}\sigma_1^2 \tag{37}$$

The total energy is found by integrating the energy equations for each layer over the volume of the beam.

$$U_{total} = \int_0^L\int_0^b(\int_0^{t_p} dU_p dy + \int_{-t_b}^0 dU_b dy + \int_{-t_b-t_t}^{-t_b} dU_t dy)dzdx \tag{38}$$

47

Electric field in a piezoelectric layer can be defined as the voltage across the layer divided by the thickness of the layer. Using this relation, the electric field terms in the result of equation 38 can be replaced according to equations 39 and 40. For the harvesting layer,

$$E_{3p} = \frac{V_p}{t_p} \tag{39}$$

and for the tuning layer,

$$E_{3t} = \frac{V_t}{t_t} \tag{40}$$

Making the appropriate substitution into equation 38 and differentiating with respect to the voltage across the layer being harvested from, the general charge output equation can be found.

$$Q = \frac{\partial U}{\partial V} = G_4 F + G_5 V_p + G_6 V_t \tag{41}$$

where G_4, G_5, and G_6 are constants. The charge generation from only the mechanical force input is

$$Q_{gen} = G_4 F \tag{42}$$

The second and third terms are the charge generation due to electrical excitation. Since the relationship of voltage to charge is capacitance, the terms in front of the voltages are the capacitance of the system. Therefore the open circuit capacitance is

$$C_{free} = \frac{\partial^2 U}{\partial U^2} \tag{43}$$

Using the capacitance and the generated charge, the voltage that appears on the electrodes of the harvesting layer can be calculated.

$$V_{gen} = \frac{Q_{gen}}{C_{free}} \tag{44}$$

The generated energy from the applied load is

$$Ugen = \frac{1}{2}C_{free}V_{gen}^2 = \frac{1}{2}Q_{gen}V_{gen} \tag{45}$$

In order to maximize the amount of energy generated from the harvester, the impedance of the harvester must match that of the load. The power across the load can be determined using basic circuit equations. Figure 5.3 shows a simple resistive circuit with a rectified voltage, V_p, from the piezoelectric harvester, internal harvester resistance, R_p, and load resistance R_l.
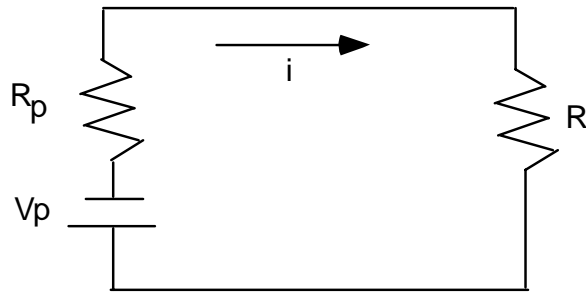
Figure 5.3. Resistive Circuit

The equivalent resistance of the circuit is

$$R_{eq} = R_p + R_l \tag{46}$$

The current, i, is

$$i = \frac{V_p}{R_{eq}} = \frac{V_p}{R_p + R_l} \tag{47}$$

Therefore the power generated across the load resistor can be found.

$$P = i^2 R_l = \frac{V_p^2 R_l}{(R_p + R_l)^2} \tag{48}$$

5.2   MODE SHAPES OF BEAMS AND PLATES

In the section 4.2, a single degree of freedom model was developed to classify the effect of changing capacitance on tuning. In this section, mode shapes of beams and plates will be derived as well as equations for natural frequencies. The natural frequency equation can be used in a similar manner to the single degree of system model and show it's dependence on shunt circuit conditions. The mode shapes will be used in sections 5.3 and 5.4 in a vibrational energy analysis of the system.

5.2.1   Continuous Beam Model

Equation 49 is the Euler-Bernoulli equation representing the dynamics of a beam.

$$\rho A \frac{\partial^2 w(x,t)}{\partial t^2} + EI \frac{\partial^4 w(x,t)}{\partial x^4} = F(x,t) \tag{49}$$

where, w is the displacement of the beam, ρ is the density of the beam, and F is the external force applied to the beam. If no external force is applied, then F(x,t) is equal to 0 and the equation can be rewritten as:

$$\frac{\partial^2 w(x,t)}{\partial t^2} + c^2 \frac{\partial^4 w(x,t)}{\partial x^4} = 0 \quad c = \sqrt{\frac{EI}{\rho A}} \tag{50}$$

A separation of variables solution is assumed to be $w(x,t) = X(x)T(t)$. This is substituted into equation 50 which becomes:

$$c^2 \frac{X'''(x)}{X(x)} = -\frac{\ddot{T}(t)}{T(t)} = \omega^2 \tag{51}$$

By rearranging equation 51, the spatial equation of the system can be found:

$$X'''(x) - \left(\frac{\omega}{c}\right)^2 X(x) = 0 \tag{52}$$

Defining,

$$\beta^4 = \frac{\omega^2}{c^2} = \frac{\rho A \omega^2}{EI} \tag{53}$$

And assuming a solution of the form

$$X(x) = Ae^{\alpha x} \tag{54}$$

The general solution of equation 52 can be calculated as

$$X(x) = a_1 \sin(\beta x) + a_2 \cos(\beta x) + a_3 \sinh(\beta x) + a_4 \cosh(\beta x) \tag{55}$$

The value of β and constants of integration can be determined using boundary conditions. If a

beam in transverse vibration is free at one end, the bending moment and shear force at that end

must vanish:

$$EI \frac{\partial^2 w}{\partial x^2} = 0 \quad EI \frac{\partial^3 w}{\partial x^3} = 0 \tag{56}$$

If the end of the beam is clamped, the deflection and slope must vanish at that end:

$$w = 0 \quad \frac{\partial w}{\partial x} = 0 \tag{57}$$

Using these boundary conditions and substituting into equation 55, the mode shape of a

cantilever beam becomes

$$X_n(x) = \cosh \frac{\beta_n x}{L} - \cos \frac{\beta_n x}{L} - \alpha(\sinh \frac{\beta_n x}{L} - \sin \frac{\beta_n x}{L}) \tag{58}$$

$$\alpha = \left(\frac{\sinh(\beta_n L) - \sin(\beta_n L)}{\cosh(\beta_n L) + \cos(\beta_n L)}\right) \tag{59}$$

where L is the length of the beam. The characteristic equation which is used to calculate β and

hence the natural frequency of the beam is:

$$\cos(\beta L) \cosh(\beta L) = -1 \tag{60}$$

Inman (2001) presents weighted frequencies and values for α for the first five modes of several

different boundary conditions. Values for a clamped-free beam are shown in Table 5. A plot of

the first 5 normalized modes is shown in Figure 5.4.

Table 5. Weighted natural frequencies and clamped free mode shape coefficient α_n

Weighted frequencies $\beta_n a$	α_n
1.875	.734
4.694	1.018
7.854	.999
10.995	1.000
14.137	1.000
$\dfrac{(2n-1)\pi}{2}$ for $n > 5$	1 for $n > 5$
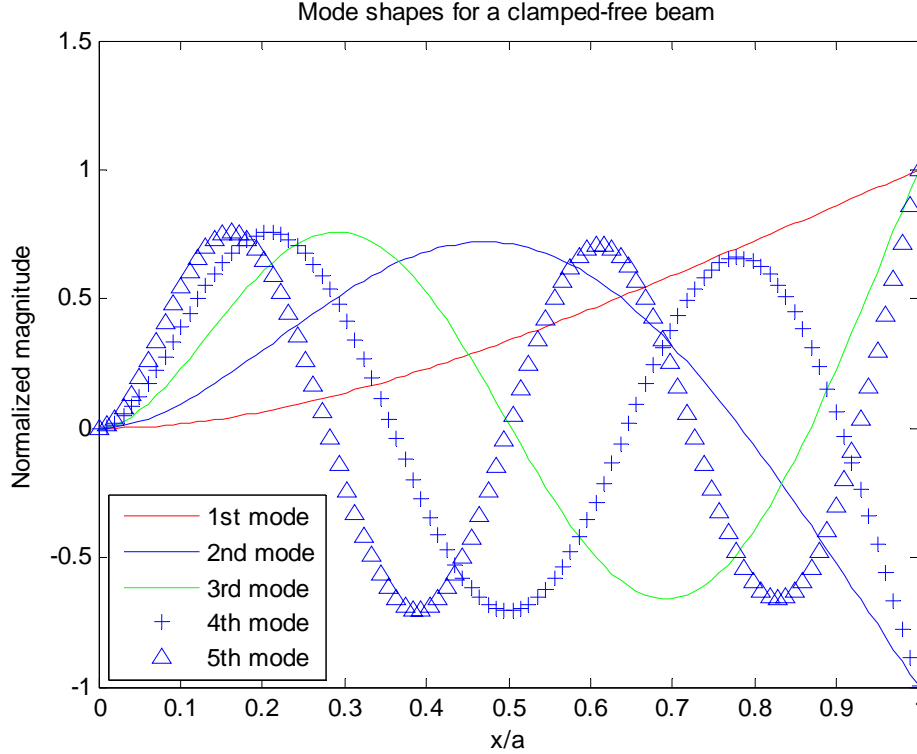
Figure 5.4. Normalized mode shapes of a clamped-free beam

5.2.2 Plate Mode Shapes

In an Euler-Bernoulli beam, the length is assumed to be 10 times the width. When this does not hold true, the structure can be considered a plate. The equation representing a plate's vibration is

$$D\nabla^4 w(x, y, t) + \rho A \frac{\partial^2 w(x, y, t)}{\partial t^2} = F(x, y, t)$$

$$\nabla^4 = \frac{\partial^4}{\partial x^4} + 2\frac{\partial^4}{\partial x^2 \partial y^2} + \frac{\partial^4}{\partial y^4}$$

(61)

where F is an applied load and D is the modulus of rigidity, which is similar to the stiffness term, EI in a beam. The equation is similar to the Euler-Bernoulli equation for a beam however it is now dependent on two directions x and y. For a plate constructed of a single material, the modulus of rigidity is defined as

53

$$D = \frac{Et^3}{12(1-v^2)} \tag{62}$$

where E is the modulus of the material, t is the thickness and υ is Poisson's ratio. For a laminated plate with 2n+1 symmetrical isotropic layers as shown in Figure 5.5, Ugural (1999) defines a transformed flexural rigidity as

$$D_t = \frac{2}{3}\left[\sum_{k=1}^{n} \frac{E_k}{1-\upsilon_k^2}(t_k^3 - t_{k+1}^3) + \frac{E_{n+1}t_{n+1}^3}{1-\upsilon_{n+1}^2} \right] \tag{63}$$

This can be substituted into equation 61 in place of D.
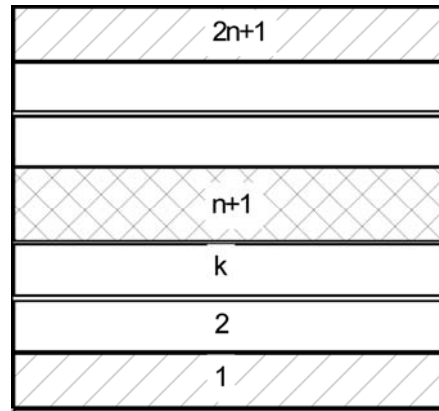
Figure 5.5. Cross section of a symmetrically constructed layered plate

The mode shape of a plate can be defined as

$$\Phi = X_m(x)Y_n(y) \tag{64}$$

The mode shapes of the plate can be thought of as combinations of two beam mode shapes: a clamped-free beam mode shape, X(x), running along the length of the beam and a free-free mode shape Y(y), running along the width of the beam. This is shown in Figure 5.6.

54
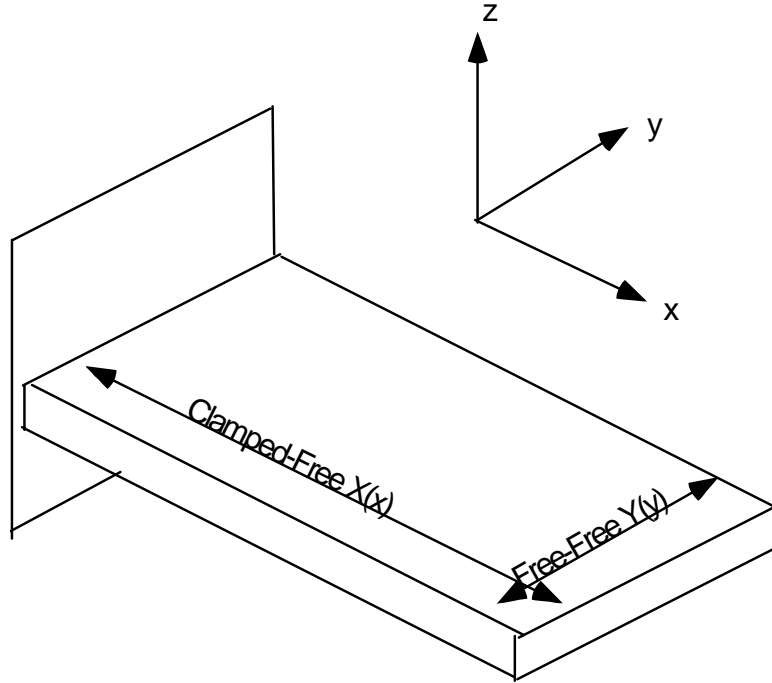
Figure 5.6. Representation of plate mode shapes: Clamped-free beam mode in x-direction, Free-free beam mode in y-direction

Following a similar procedure for the clamped-free beam, the equations for the mode shapes of a free-free beam are given in equations 65, 66, and 67.

$$Y_1(y) = 1 \tag{65}$$

$$Y_2(y) = \sqrt{3}\left(1 - \frac{2y}{b}\right) \tag{66}$$

$$Y_j(y) = \cosh\frac{\mu_j y}{b} + \cos\frac{\mu_j y}{b} - \eta_j\left(\sinh\frac{\mu_j y}{b} + \sin\frac{\mu_j y}{b}\right) \tag{67}$$

$$\eta_j = \frac{\cosh\mu_j b - \cos\mu_j b}{\sinh\mu_j b - \sin\mu_j b} \qquad j=3,4,5\ldots \tag{68}$$

The characteristic equation for a free-free beam is:

$$\cos\mu b \cosh\mu b = 1 \tag{69}$$

55

Equations 65 and 66 represent the rigid body and twisting 1st mode, respectively. Equation 67

satisfies the free-free boundary conditions. Values for a clamped-free beam are shown in Table

6 (Inman (2001)). A plot of the first 5 normalized modes is shown in Figure 5.7.

Table 6. Weighted natural frequencies and free free mode shape coefficient η_j (j=3,4,5...)

Weighted frequencies $\mu_j b$	η_j
4.730	.982
7.853	1.000
10.995	.999
14.137	1.000
17.278	.999
$\dfrac{(2n+1)\pi}{2}$ for $n > 5$	1 for n > 5
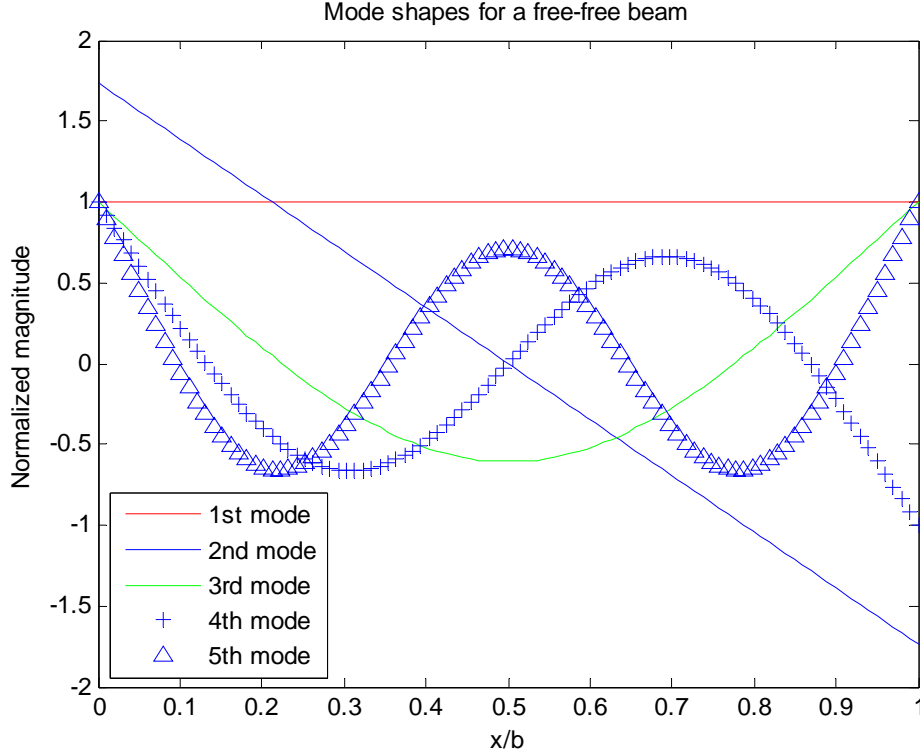
Figure 5.7. Normalized mode shapes of a free-free beam

In order to find the correct mode shape combinations and natural frequencies of a thin elastic plate, the Ritz method is employed. A comprehensive analysis using this method for several plates with various boundary conditions was performed by Young (1950) and therefore a brief overview will be given instead of an in depth analysis.

The maximum potential energy for a uniform plate vibrating harmonically with amplitude w(x,y) and frequency ω is given by

$$V = \frac{D}{2} \iint \left[\left(\frac{\partial^2 w}{\partial x^2} \right)^2 + \left(\frac{\partial^2 w}{\partial y^2} \right)^2 + 2\upsilon \frac{\partial^2 w}{\partial x^2} \frac{\partial^2 w}{\partial y^2} + 2(1-\upsilon) \left(\frac{\partial^2 w}{\partial x \partial y} \right)^2 \right] dxdy \qquad (70)$$

and the maximum kinetic energy is

$$T = \frac{1}{2} \rho h \omega^2 \iint w^2 dxdy \qquad (71)$$

57

Equating equations 70 and 71 leads to

$$\omega^2 = \frac{2}{\rho h} \frac{V}{\iint w^2 \, dxdy} \tag{72}$$

The natural frequencies are determined by finding expressions for w that satisfy the boundary conditions and minimize equation 72. The deflection is assumed to be in the form of a series approximation as shown in equation 73 with A_{mn} being a coefficient of each term in the series and X and Y are beam mode shapes along the length and width of the plate, respectively.

$$w(x, y) = \sum_{m=1}^{p} \sum_{n=1}^{q} A_{mn} X_m(x) Y_n(y) \tag{73}$$

Equation 73 is then substituted into equation 72. The right hand side of the equation becomes a function of the coefficients A_{mn}. Taking partial derivatives with respect to each coefficient and setting equal to zero minimizes this result. Each equation is of the form

$$\frac{\partial V}{\partial A_{ik}} - \frac{\omega^2 \rho h}{2} \frac{\partial}{\partial A_{ik}} \iint w^2 \, dxdy = 0 \tag{74}$$

where A_{ik} is one of the coefficients A_{mn}. Equation 74 represents a system of linear homogeneous equations with unknowns A_{mn}. The natural frequencies of the system are determined from finding the coefficients that make the determinant of the system vanish. The natural frequencies of the plate can be obtained using the equation

$$\omega_n = \lambda_n \sqrt{\frac{D}{\rho h a^3 b}} \tag{75}$$

where λ_n is dependent on the A_{mn} coefficients. Young (1950) provides values for A_{mn} and λ_n for plates with various boundary conditions. Table 7 contains values for λ for the first five modes of a square cantilever plate (a=b). Leissa (1969) provides a compilation of papers on the vibration of plates. Such papers provide tables containing values for λ for non-symmetrical plates.

Table 7. Values of characteristic value for 1st five modes of a square cantilever plate.

Mode	1	2	3	4	5
λ	3.494	8.54	21.44	27.46	31.17

It is also important to note that for each mode there is one value of A_{mn} that dictates the shape of the modes. Hence, the values of m and n determine the correct beam mode shape combinations. Table 8 lists the X and Y combinations for each mode and can be found in Equation 58 for the X modes, and 65, 66 and 67 for the Ymodes.

Table 8. Beam mode shape combinations for plate mode shapes

Mode	Mode Shape
1	$\Phi_1 = X_1(x)Y_1(y)$
2	$\Phi_2 = X_1(x)Y_2(y)$
3	$\Phi_3 = X_2(x)Y_1(y)$
4	$\Phi_4 = X_1(x)Y_3(y)$
5	$\Phi_5 = X_2(x)Y_2(y)$

Figures 5.8 to 5.12 show plots of the first five normalized mode shapes of a square cantilever plate. As can be seen from the plots, the first mode is a pure bending mode. The

second mode is a 2-d bending mode. The third mode is again a bending mode and the fourth and

fifth modes are combinations of bending in two directions.
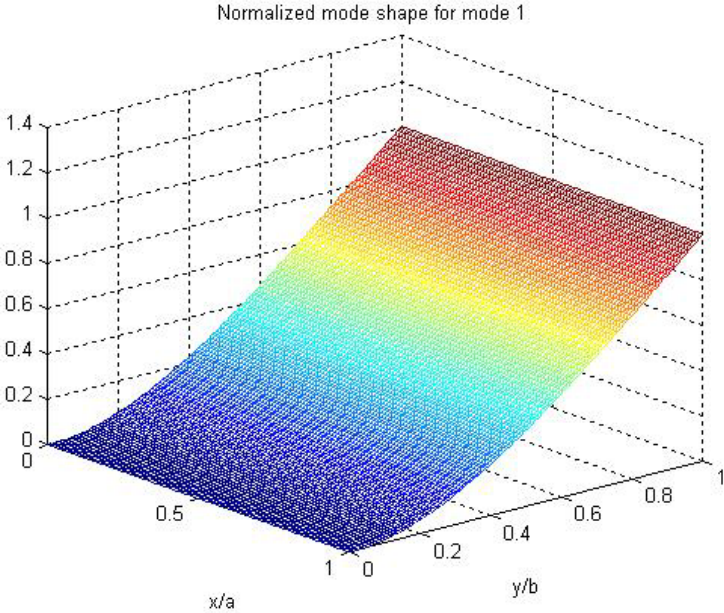
Figure 5.8. Normalized 1st mode shape of a cantilever plate
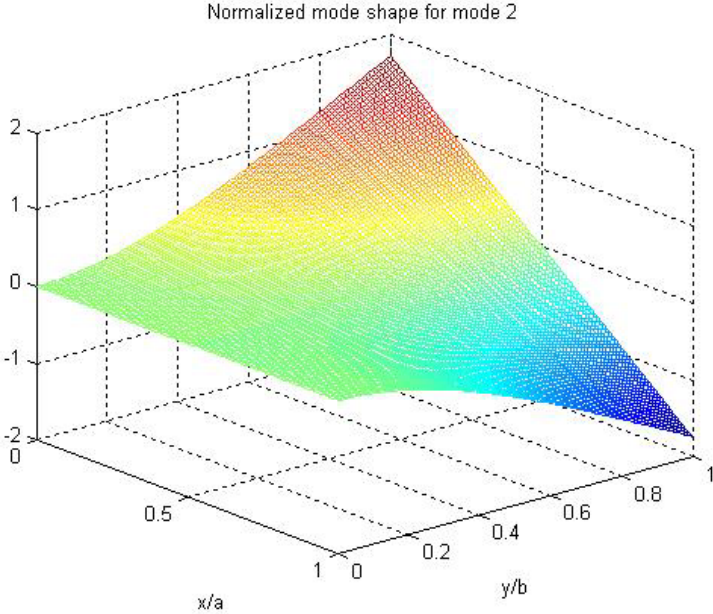
Figure 5.9. Normalized 2nd mode shape of a cantilever plate

60
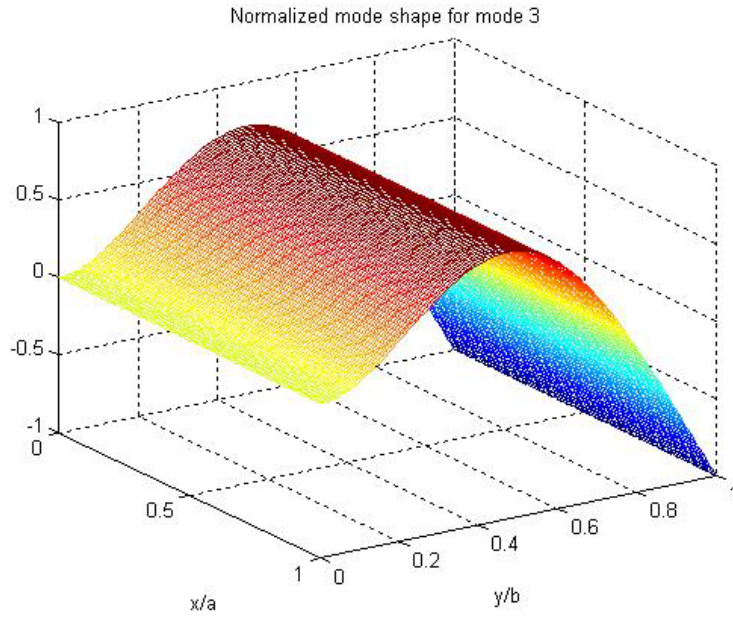
Figure 5.10. Normalized 3rd mode shape of a cantilever plate
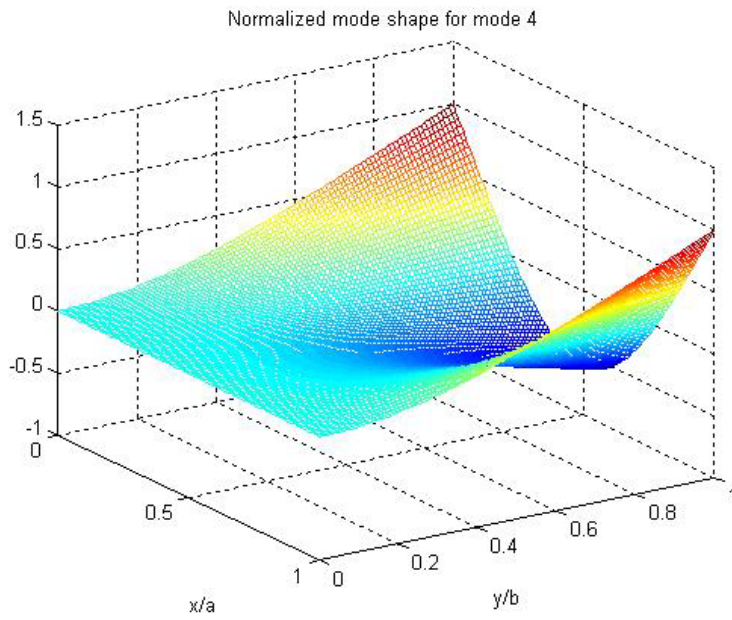
Figure 5.11. Normalized 4th mode shape of a cantilever plate

Normalized mode shape for mode 5
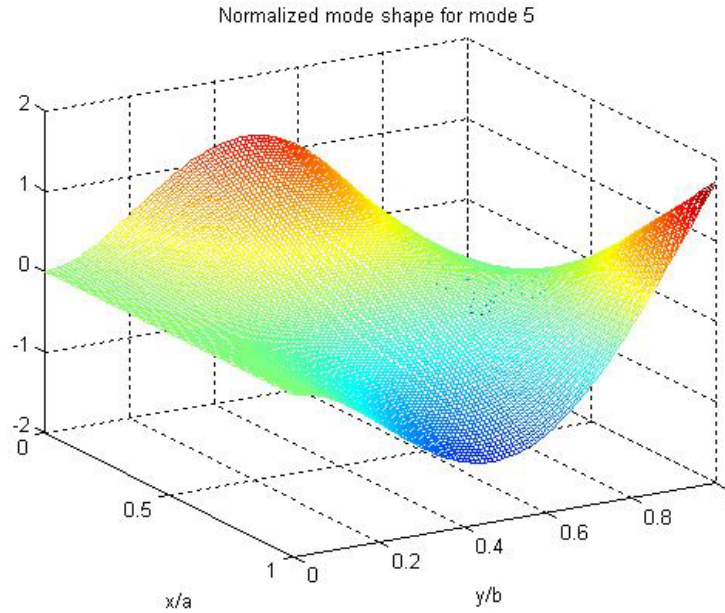
Figure 5.12. Normalized 5th mode shape of a cantilever plate

The next chapter will use the previously derived mode shapes to develop a model that will be used to calculate the amount of power that can be generated from a piezoelectric bimorph energy harvester.

5.3   DYNAMIC BEAM ENERGY HARVESTING MODEL

The Euler-Bernoulli method is used to model a bimorph energy harvester being excited by a harmonic vibration source. This is shown in Figure 5.13.
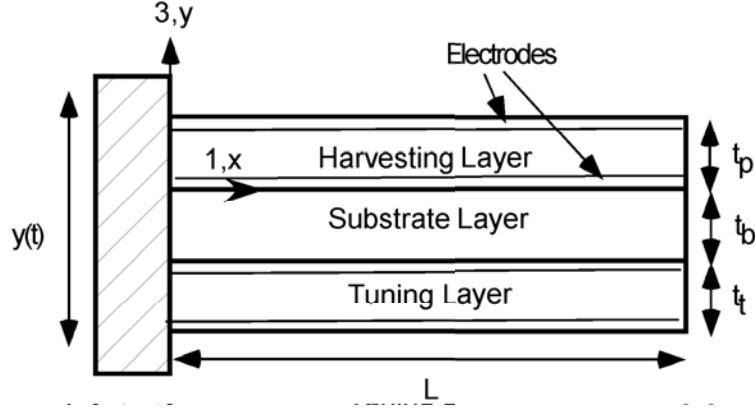
Figure 5.13. Base excited piezoelectric bimorph

The Euler-Bernoulli equation from the previous chapter now becomes

$$\rho A \frac{\partial^2 w(x,t)}{\partial t^2} + EI \frac{\partial^4 w(x,t)}{\partial x^4} = -\rho A \frac{\partial^2 y(t)}{\partial t^2} \qquad (76)$$

where ρ is the density, A is the cross-sectional area and y(t) is the excitation of the beam. The term on the right hand side of the equation is representative of base excitation. The solution to equation 76 is assumed to take the form of equation 77 that is a series solution containing the multiplication of a spatial solution and a temporal solution.

$$w(x,t) = \sum_{i=1}^{\infty} X_i(x) q_i(t) \qquad (77)$$

X_i is the *i*-th mode shape of the beam and $q_i(t)$ are generalized coordinates. The convolution integral is used to evaluate $q_i(t)$ and takes the form

$$q_i(t) = \frac{1}{\omega_d} e^{-\zeta \omega_{ni} t} \int_0^t F_i(\tau) e^{\zeta \omega_{ni} t} \sin(\omega_{di}(t-\tau)) d\tau \qquad (78)$$

where ω_d is the damped natural frequency, ω_n is the natural frequency, ς is the damping ratio and F is a generalized force. The generalized force from the distributed inertia is

$$F_i(t) = \int_0^L -\rho A \frac{\partial^2 y(t)}{\partial t^2} X_i(x) dx = \int_0^L -X_i(x) dx \rho A \frac{\partial^2 y(t)}{\partial t^2} \tag{79}$$

Inserting equations 58 and 78 into equation 77 the deflection w(x,t) can be found as

$$w(x,t) = \sum_{i=1}^{\infty} q_i(t)[\cosh(\beta_i x) - \cos(\beta_i x) - \alpha_i(\sinh(\beta_i x) - \sin(\beta_i x))] \tag{80}$$

The moment caused by the base excitation is

$$M(x,t) = EI \frac{\partial^2 w(x,t)}{\partial x^2} = \sum_i EI \beta_i^2 (q_i(t)[\cosh(\beta_i x) + \cos(\beta_i x) - \alpha_i(\sinh(\beta_i x) + \sin(\beta_i x))] \tag{81}$$

The procedure for calculating the generated energy from the harvester is now similar to section 5.1. Since the beam structure remains the same, the constitutive equations for stress and strain are the same. However the equation for curvature is slightly different due to a different forcing function.

$$\kappa = G_7 EI \frac{\partial^2 w(x,t)}{\partial x^2} + G_8 E_{3p} + G_9 E_{3t} \tag{82}$$

where G_7, G_8, and G_9 are constants. Hence, the equation for total energy, generated charge, generated voltage, capacitance, and generated energy are slightly different as well.

$$U_{total} = \int_0^L \int_0^b (\int_0^{t_p} dU_p dy + \int_{-t_b}^0 dU_b dy + \int_{-t_b-t_t}^{-t_b} dU_t dy) dz dx \tag{83}$$

$$Q = \frac{\partial U}{\partial V} = G_{10} H_i + G_{11} V_p + G_{12} V_t \tag{84}$$

where G_{10}, G_{11}, and G_{12} are constants, and

$$H_i = EI \beta_i q_i(t)(\alpha_i[\cosh(\beta_i L) - \cos(\beta_i L)] - (\sinh(\beta_i L) + \sin(\beta_i L)) \tag{85}$$

Therefore,

$$Q_{gen} = G_{10} H_i \tag{86}$$

64

$$C_{free} = \frac{\partial^2 U}{\partial U^2} \qquad (87)$$

$$V_{gen} = \frac{Q_{gen}}{C_{free}} \qquad (88)$$

$$Ugen = \frac{1}{2} C_{free} V_{gen}^2 = \frac{1}{2} Q_{gen} V_{gen} \qquad (89)$$

5.4   DYNAMIC PLATE ENERGY HARVESTING MODEL

The generated energy from a plate from a base excitation can be calculated in much the same way as the previous two sections. However, since a plate is wider than a beam, an addition width direction must be accounted for in the derivation of stress, strain, and curvature. Thus there will be two curvatures and each curvature equation will depend on two moment terms, one in each direction. It will be assumed that the plate will contain one neutral surface since the surface is dependent only on the cross section of the harvester and that each layer of the harvester is isotropic.
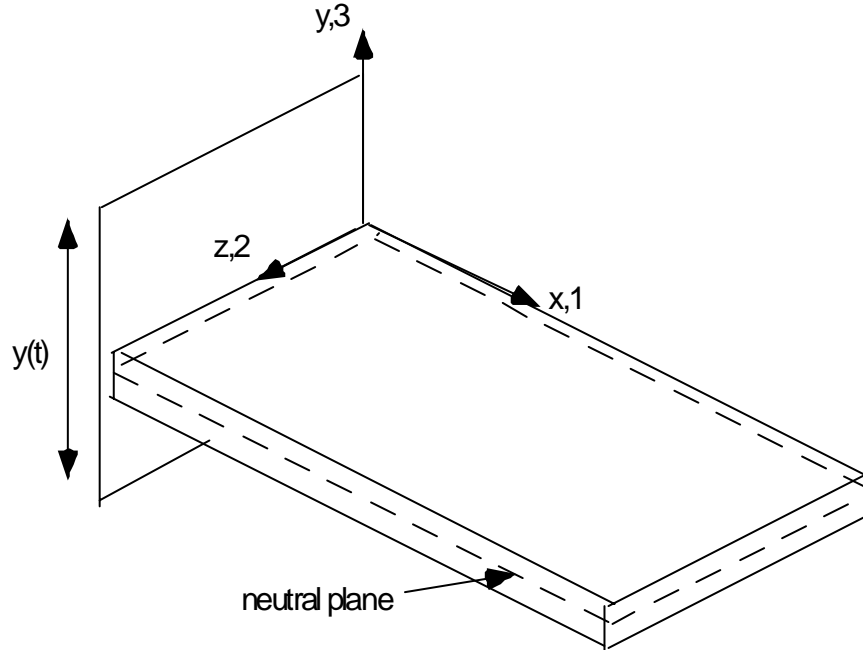
Figure 5.14. Plate used in energy calculations

The plate equation describing the vibration of a plate from the previous chapter becomes

$$DV^4 w(x,z,t) + \rho A \frac{\partial^2 w(x,z,t)}{\partial t^2} = -\rho A \frac{\partial^2 y(t)}{\partial t^2}$$

$$\nabla^4 = \frac{\partial^4}{\partial x^4} + 2\frac{\partial^4}{\partial x^2 \partial z^2} + \frac{\partial^4}{\partial z^4}$$

$$(90)$$

As with the dynamic beam model, the term on the right hand side is representative of base excitation. The solution to equation 87 is assumed to take the form of equation 88 that is a series solution containing the multiplication of a spatial solution and a temporal solution.

$$w(x,z,t) = \sum_{i=1}^{\infty} X_i(x) Z_i(z) q_i(t) \qquad (91)$$

$X_i Z_i$ is the i-th mode shape of the plate and $q_i(t)$ are generalized coordinates. The convolution integral is used to evaluate $q_i(t)$ remains the same as equation 78. However the generalized force F_i used to evaluate $q_i(t)$ becomes

66

$$F_i(t) = \int_0^b \int_0^L -\rho A \frac{\partial^2 y(t)}{\partial t^2} X_i(x) Z_i(z) dx dz = \int_0^b \int_0^L - X_i(x) Z_i(z) dx dz \rho z \frac{\partial^2 y(t)}{\partial t^2} \tag{92}$$

The moments in each direction of the plate can be described as

$$\left. \begin{aligned} M_1 &= -D\left(\frac{\partial^2 w}{dx^2} + v\frac{\partial^2 w}{dy^2}\right) \\ M_2 &= -D\left(\frac{\partial^2 w}{dy^2} + v\frac{d^2 w}{dx^2}\right) \end{aligned} \right\} \tag{93}$$

The strain in the x and z (1 and 2) directions are

$$\varepsilon_1 = \kappa_1(y - y_c), \qquad \varepsilon_2 = \kappa_2(y - y_c) \tag{94}$$

The constitutive equations can be rewritten to account for the extra direction.

$$\left. \begin{aligned} \varepsilon_1 &= \frac{1}{E}(\sigma_1 - v\sigma_2) + d_{31}E_3 \\ \varepsilon_2 &= \frac{1}{E}(\sigma_2 - v\sigma_1) + d_{31}E_3 \\ D_3 &= d_{31}(\sigma_1 + \sigma_2) + \in_{33} E_3 \end{aligned} \right\} \tag{95}$$

Hence, the stresses for the substrate layer and the piezoelectric layers can be written as

$$\left. \begin{aligned} \sigma_{1p} &= \frac{E_p}{1-v^2}(\varepsilon_1 + v\varepsilon_2 - (1+v)d_{31}E_3) \\ \sigma_{2p} &= \frac{E_p}{1-v^2}(\varepsilon_2 + v\varepsilon_1 - (1+v)d_{31}E_3) \end{aligned} \right\} \tag{96}$$

and for the substrate layer

$$\left. \begin{aligned} \sigma_{1p} &= \frac{E_b}{1-v^2}(\varepsilon_1 + v\varepsilon_2) \\ \sigma_{2p} &= \frac{E_b}{1-v^2}(\varepsilon_2 + v\varepsilon_1) \end{aligned} \right\} \tag{97}$$

The moments of the plate can be calculated using equation 98.

$$\begin{aligned} M_1 &= \int_t \sigma_{1t}(y - y_c)bdy + \int_b \sigma_{1b}(y - y_c)bdy + \int_p \sigma_{1p}(y - y_c)bdy \\ M_2 &= \int_t \sigma_{2t}(y - y_c)Ldy + \int_b \sigma_{2b}(y - y_c)Ldy + \int_p \sigma_{2p}(y - y_c)Ldy \end{aligned} \tag{98}$$

Inserting appropriate terms for strain into equations 96 and 97 and then inserting the result into 98 produces alternative equations for the moments in the plate. Setting equation 98 equal to 93, the curvatures in each direction can be found by solving the set of simultaneous equations. The curvatures are functions of the moments caused by the excitation force. Energies of each layer now include the stresses and strains in both 1 and 2 directions.

$$dU_p = \frac{1}{2}\varepsilon_1\sigma_1 + \frac{1}{2}\varepsilon_2\sigma_2 + \frac{1}{2}d_{31}(\sigma_1 + \sigma_2)E_3 + \frac{1}{2}\epsilon_{33}E_3^2$$
$$dU_b = \frac{1}{2}\varepsilon_1\sigma_1 + \frac{1}{2}\varepsilon_2\sigma_2$$

(99)

$$U_{total} = \int_0^L\int_0^b\int_0^{t_p}(\int dU_p dy + \int_{-t_b}^0 dU_b dy + \int_{-t_b-t_t}^{-t_b} dU_t dy)dzdx$$

(100)

The generated energy can now be calculated in the exact same manner as the previous two sections. In energy harvesting, the first mode of a harvester is designed to match that of the vibration source due to the first mode having the greatest energy. Since the first vibration mode of a cantilever plate is a pure bending mode, the stress in the 2 direction is assumed to be minimal. Hence, the method presented in this section reduces to that of section 5.3. If the energy from higher modes of the plate is desired the method from section 5.4 should be used.

6.0   EXPERIMENTAL TEST SETUP AND RESULTS

This chapter presents the test setup used to quantify the effects of using a capacitive shunt tuning method to tune a piezoelectric harvesting device. The bimorph construction process is first presented. This is followed by a description of the test rig used to measure the natural frequency of the harvesters and power output. It is followed by a presentation of experimental results.

6.1   BIMORPH CONSTRUCTION PROCESS

Five piezoelectric bimorphs were constructed using the following procedure. PZT (Lead Zirconate Titanate) type PSI-5H4E was chosen as the piezoelectric material and aluminum (Alloy 1100) was chosen as the substrate material. The dimensions of the materials are shown in Table 9. Note that the lengths of the PZT and Aluminum were made longer so that there was material available to clamp for testing. The actual clamped length and width dimensions are 30 mm by 30 mm.

Table 9. Dimensions of materials in bimorph

PZT thickness (mm)	.2667
PZT width (mm)	30

Table 9. (continued).

PZT length (mm)	36
Aluminum thickness (mm)	.254
Aluminum width (mm)	30
Aluminum length (mm)	76.2

The aluminum was cut to the proper dimensions. Next, using a straight edge and utility knife, the PZT was scored repeatedly until the proper size plate was obtained. This is shown in Figure 6.1.

Figure 6.1. Scoring a sheet of PZT

The substrate was next prepared for gluing by cleaning both sides with denatured alcohol. M-Bond 610 adhesive (Vishay) was then applied to the substrate in a thin layer as shown in Figure 6.2.
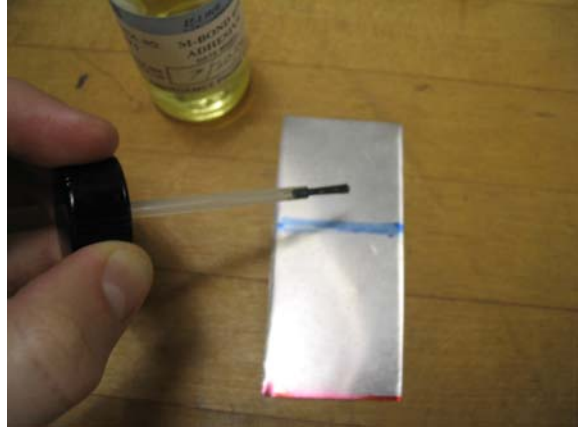
Figure 6.2. Adhesive is applied to the substrate

The previously cut PZT was then carefully placed onto the adhesive and substrate. The structure was turned over and the gluing process was repeated on the other side. In order to use the substrate as a common ground, the poling direction of each piezoelectric layer was kept pointing outward. If both layers are used to harvest energy, this also ensures positive voltage output from each layer. When the top layer is in tension, the bottom layer is in compression and therefore if the poling direction of each layer is opposite, the voltages will be of the same sign.
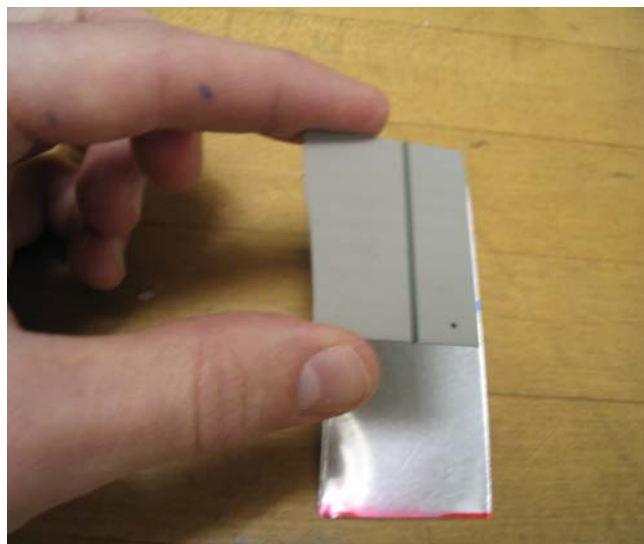
Figure 6.3. A piece of PZT being adhered to the substrate

71

Once both layers of PZT were adhered to the substrate, the structure was placed between two polycarbonate plates wrapped in Teflon tape (to prevent being glued to the plates) and a mass was placed on top to provide sufficient clamping. To cure the adhesive, the bimorph was placed in an environmental chamber (Model EC1X). The temperature was set to 110 °C and the glue was allowed to cure for 2 hours and 30 minutes.
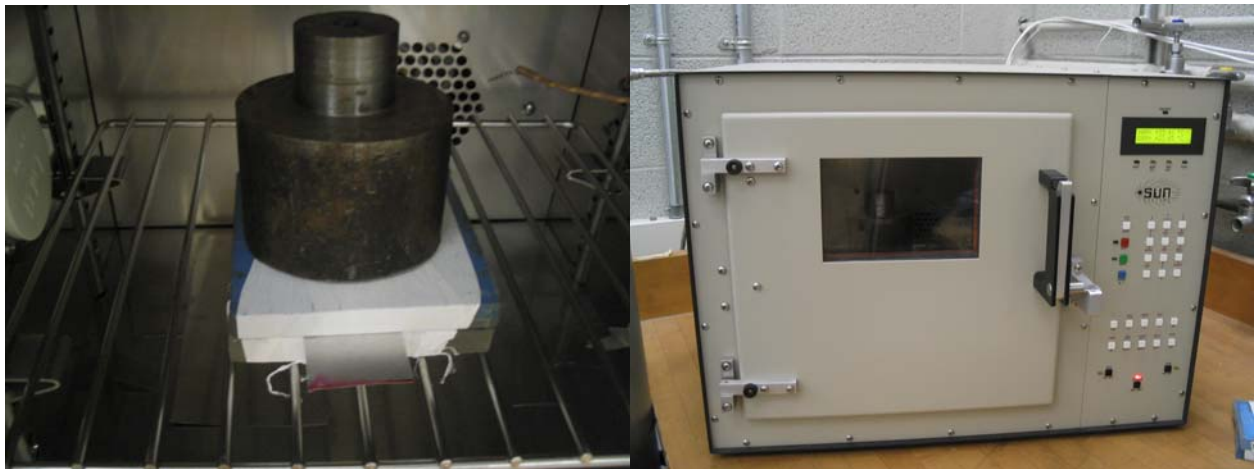
Figure 6.4. Left: Bimorph being clamped after gluing. Right: Environmental Chamber, Model EC1X

The bimorph was slowly allowed to cool in the environmental chamber to prevent cracking. Thermocouple wires (40 gage) were then attached to the upper and lower PZT layer via CircuitWorks two part conductive epoxy. Thermocouple wires were chosen because they had low resistance and mass. The epoxy was allowed to dry for four hours. The final product is shown in Figure 6.6.
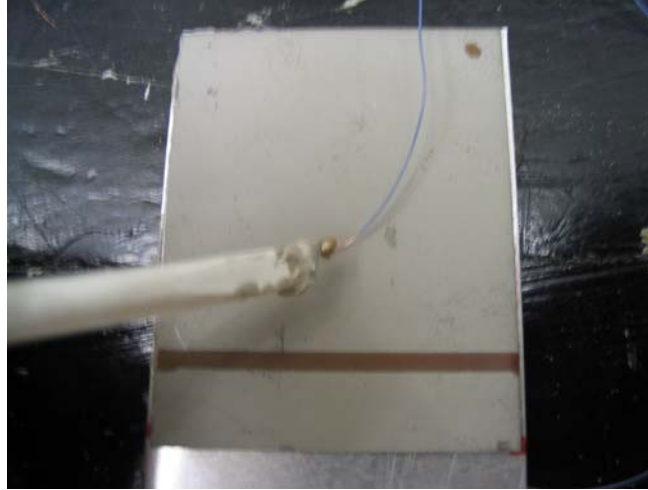
Figure 6.5. Attaching a lead to the surface of a piezoelectric bimorph
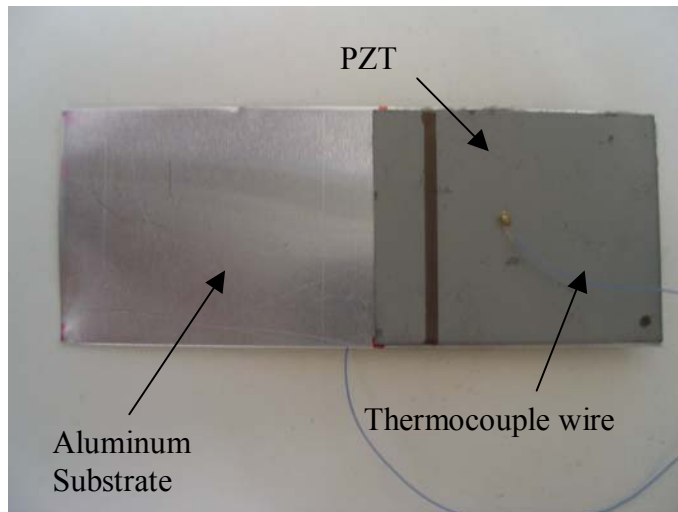
Figure 6.6. Finished piezoelectric bimorph

6.2   EXPERIMENTAL TEST SETUP AND PROCEDURE

The test rig used to perform tests on the previously constructed harvesters is shown in Figure 6.7.
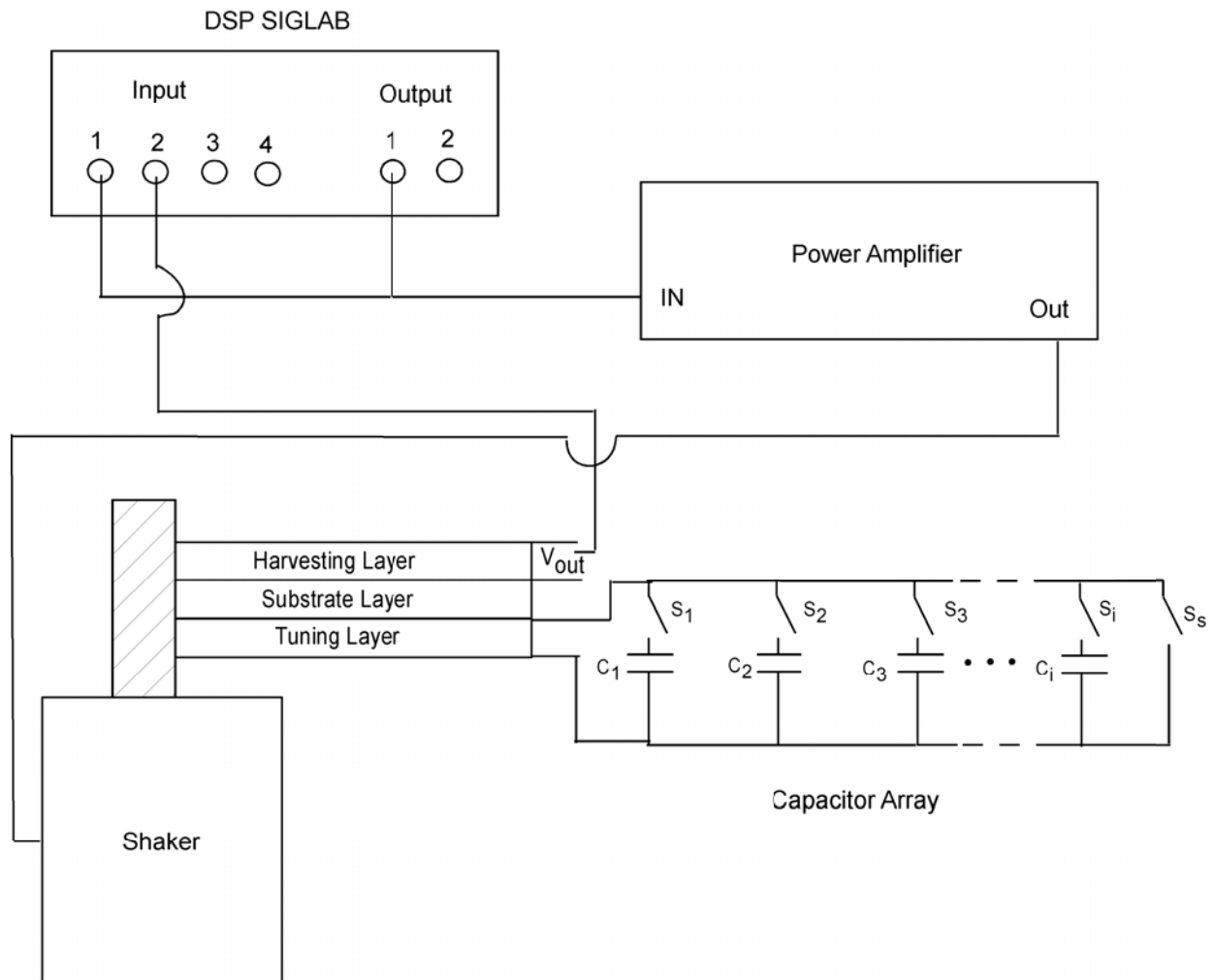
Figure 6.7. Test Setup

DSP Technologies SIGLAB (box model number 20-42, software V 3.26) is used to produce an excitation signal and also record data for frequency analysis. A signal is sent from Channel 1 of

the SIGLAB box, through a power amplifier that drives a shaker. The shaker is attached to a clamp that holds the harvester. One piezoelectric layer of the harvester is used to produce energy and sends a signal back to Channel 2 of the SIGLAB box. The other piezoelectric layer is attached to a capacitor array that is used to tune the bimorph. The actual SIGLAB box and harvester on the shaker is shown in Figures 6.8, and 6.9, respectively.

Figure 6.8. DSP SIGLAB box

Figure 6.9. Bimorph clamped on top of shaker.

The values of the capacitors in the capacitor array had to be chosen such that a full range of tuning (open to short circuit) could be observed with relative accuracy. After measuring the

capacitance of the tuning layer of the bimorphs, it was determined that each layer had a capacitance of approximately 100 nF. Analyzing Figure 4.7, the lowest capacitor value in the array was chosen to be 150 pF. A 14-bit array was used to cover the capacitance required for tuning. All other capacitance values are based off of the lowest bit. Since capacitors only come in select sizes, values were chosen so that each bit was approximately equal to that given by equation 20. The values used for each bit (nominal values) along with the calculated values are shown in Table 10. The actual array is shown in Figure 6.10.

Table 10. Calculated and commercial capacitance values for 14-bit capacitor array

Bit Number	Calculated Capacitance (pF)	Nominal Capacitance (pF)
1	150	100
2	300	300
3	600	630
4	1200	1200
5	2400	2530
6	4800	5030
7	9600	10000
8	19200	20000
9	38400	40000
10	76800	80000
11	153600	166000

Table 10. (continued).

12	307200	330000
13	614400	640000
14	1228800	1320000
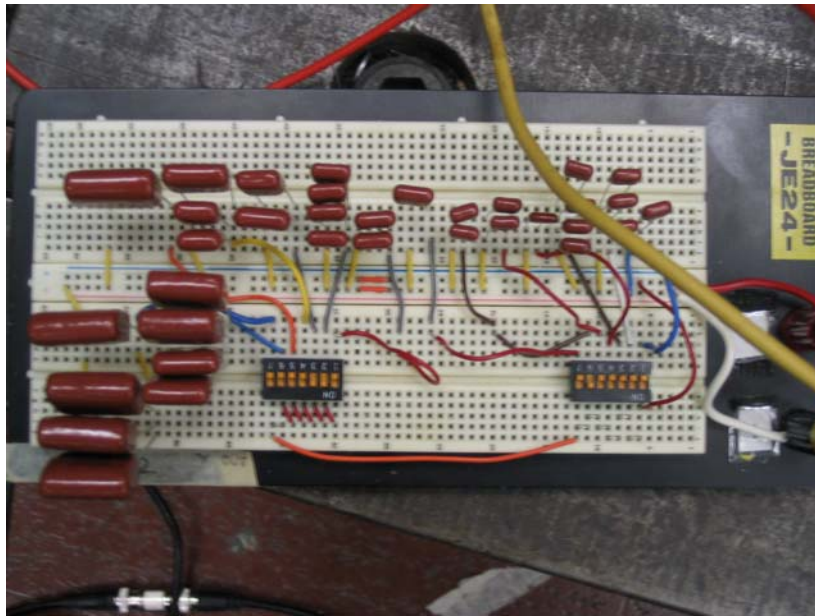
Figure 6.10. 14-bit capacitor array

6.2.1   Capacitive Tuning Procedure

To quantify the effects of the capacitive shunt on tuning, frequency responses were found for
each harvester at various shunt capacitances. First, a random signal of bandwidth 5kHz was
generated to characterize the modes of the device, particularly the first mode.   This was
performed using open circuit shunt conditions. By comparing the output of the harvester to the

input signal, the transfer function could be plotted and the natural frequencies of each mode determined. A random .707 Volt RMS random signal was used as the excitation signal. This correlated to a 1 g excitation that was verified using an accelerometer. Table 11 presents the characteristics of the signal.

Table 11. Characteristics of random signal with 5 kHz bandwidth

Averages	Samples	Frequency Resolution	Sampling Frequency	Window	Overlap
20	8192	1.563 Hz	12.8 kHz	Hanning	50 %

To obtain better frequency resolution for the first mode, the signal was then changed to a signal with 1 kHz bandwidth. The shunt capacitance was varied throughout its range and a response was found at 100 capacitance points. Each response was imported into MATLAB and the natural frequency of the bimorph at each capacitance was extracted. The characteristics of the 1kHz bandwidth signal are shown in Table 12.

Table 12. Characteristics of random signal with 1 kHz bandwidth

Averages	Samples	Frequency Resolution	Sampling Frequency	Window	Overlap
20	8192	.313 Hz	2.6 kHz	Hanning	50 %

6.2.2 Power Harvesting Procedure

Once the natural frequency-capacitance relationship was determined, the next objective was to determine effects the tuning concept had on power. Each harvester was excited by a .707 V RMS sine wave at its fundamental frequency (determined from the previous section) depending on the shunt capacitance. As the capacitance was changed, the input frequency was adjusted appropriately. The output of the harvesting layer was connected in parallel with a DC rectifying bridge circuit, shown in Figure 6.11. Power was dissipated through a resistive load. For several shunt capacitances ranging from open to short circuit, the load was varied so that the power output characteristics could be determined. The process was repeated for the tuning layer by putting the rectifying bridge circuit in parallel with the capacitor array.
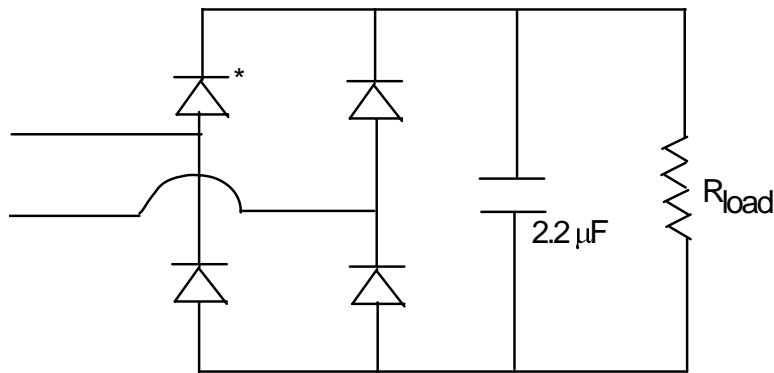
Figure 6.11. Schematic of DC rectifying circuit. (*Ultrafast diodes, p/n 1N414 from Digikey)

6.2.3 Frequency Tuning Results

By using equation 13, appropriate parameter values from Tables 5, and inserting into equation 53 the natural frequencies of the first five modes can be calculated. Table 13 shows these frequencies.

Table 13. Frequencies of the first five modes of a cantilever beam (open circuit)

Mode Number	Frequency (Hz)
1	351.151
2	2200.627
3	6161.819
4	12074.705
5	19960.353

Figures 6.12 to 6.16 show the frequency response of each beam being excited by a random signal. Due to the fact that each harvester was manufactured by hand the mode frequencies vary slightly from the predicted frequencies. However, the frequencies fall in the range where they are expected to be.
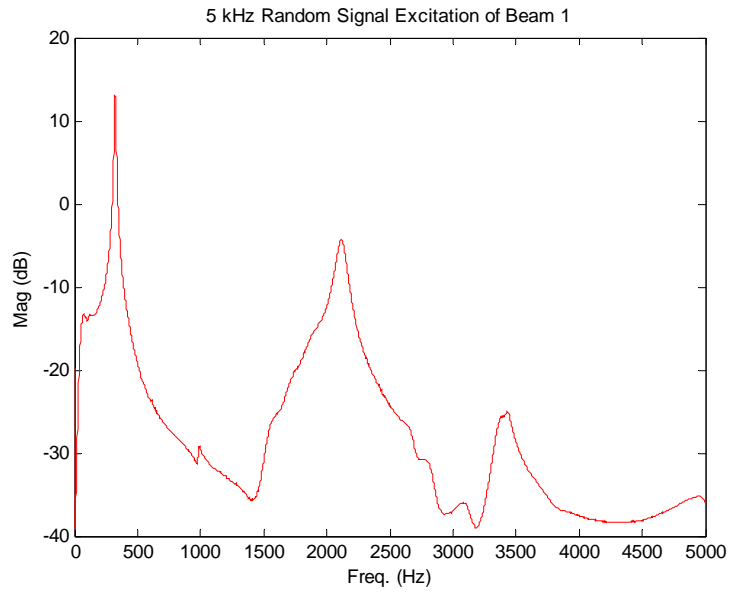
Figure 6.12. Response of a random signal excitation of beam 1
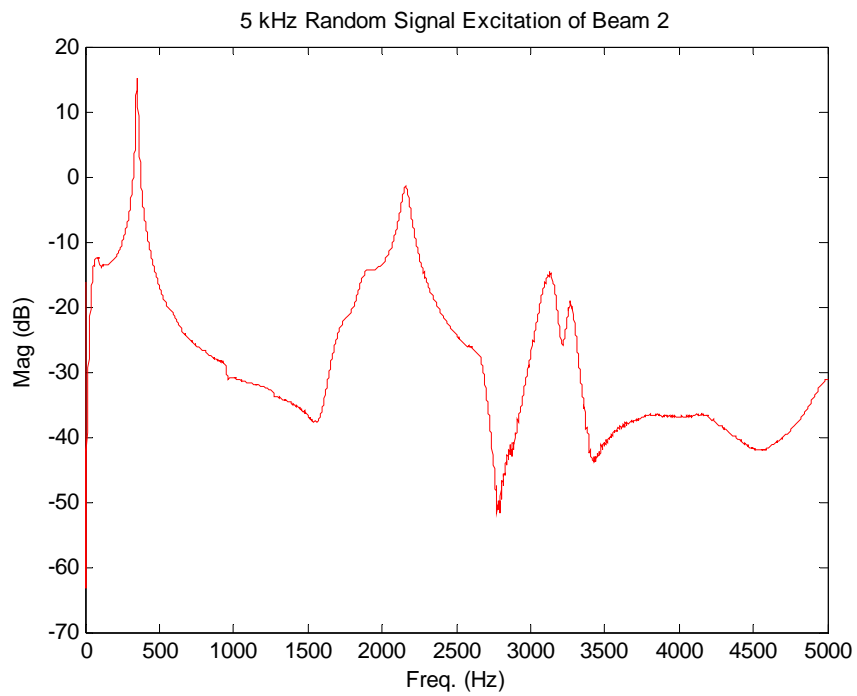
Figure 6.13. Response of a random signal excitation of beam 2

81
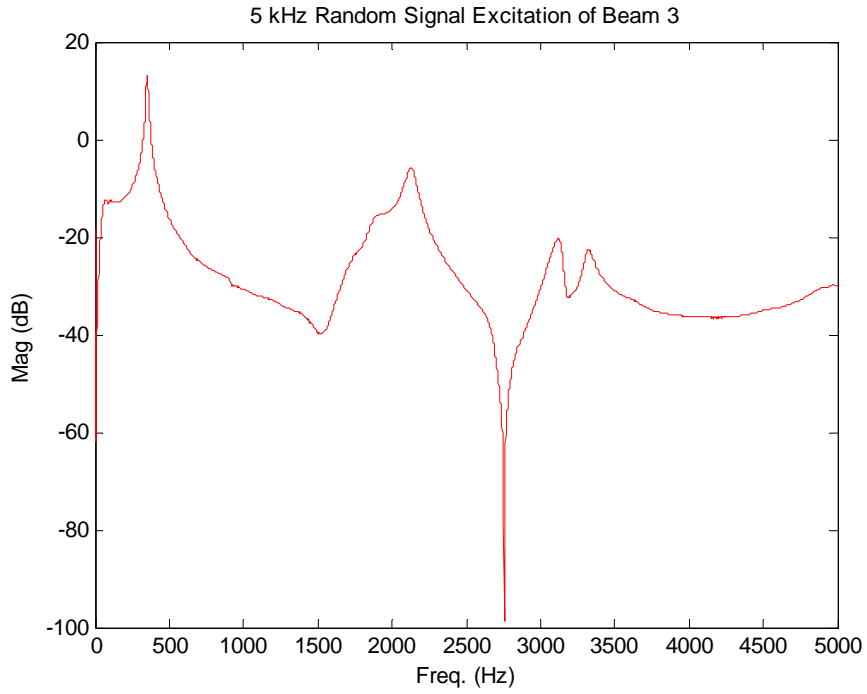
Figure 6.14. Response of a random signal excitation of beam 3
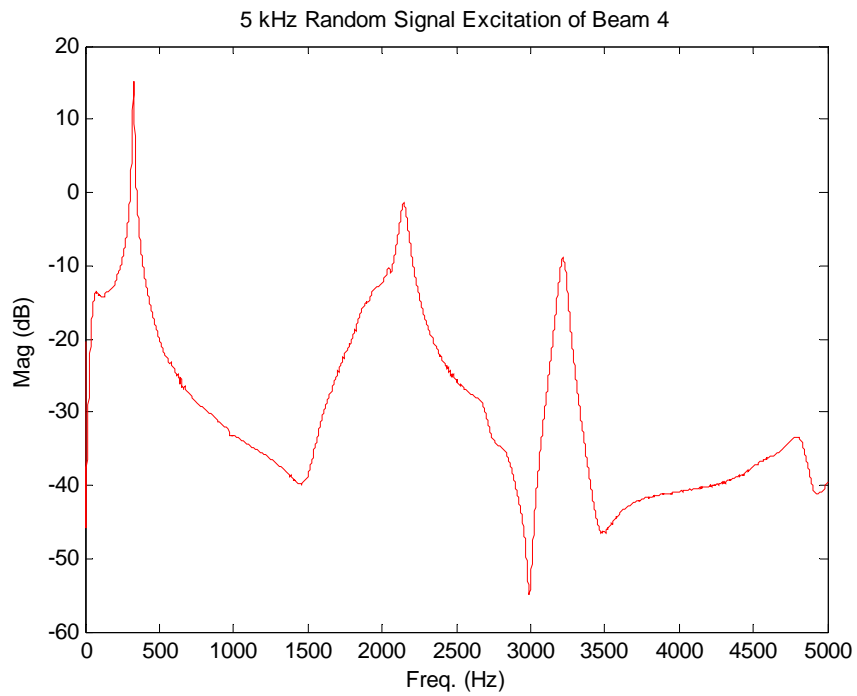
Figure 6.15. Response of a random signal excitation of beam 4
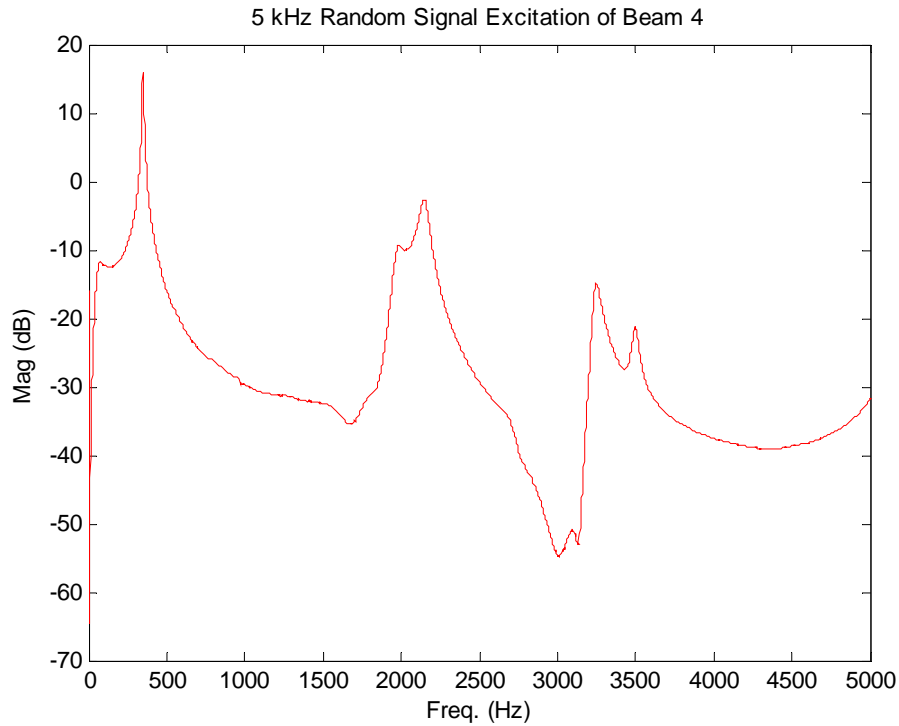
Figure 6.16. Response of a random signal excitation of beam 5

The same procedure was performed with one layer of the beams short-circuited. Table 14 and 15 present a comparison between the open and short circuit frequencies of each beam and compare them to theoretical values. The frequencies above the second mode are not reliable because the natural frequency of the shaker falls shortly above this range (> 3 kHz). Therefore only the first two modes are presented.

Table 14. Experimental and Theoretical open circuit frequencies for each beam

Mode	Beam 1	Beam 2	Beam 3	Beam 4	Beam 5	Theoretical
1	321.4	335.9	348.6	329.7	348.1	351.151
2	2103	2103	2125	2147	2159	2200.627

83

Table 15. Experimental and Theoretical short circuit (one layer used for tuning) frequencies for each beam

Mode	Beam 1	Beam 2	Beam 3	Beam 4	Beam 5	Theoretical
1	316.6	332.5	342.9	326.6	343.5	345.151
2	2064	2139	2108	2131	2147	2163.022

Once the open and short circuit frequencies of the beams were determined, the first mode was chosen to characterize the shunt capacitance effect on frequency. Using equation 13 and 53, the analytical frequency versus ratio of shunt capacitance to piezoelectric capacitance can be plotted for the piezoelectric bimorph and is shown in Figure 6.17.
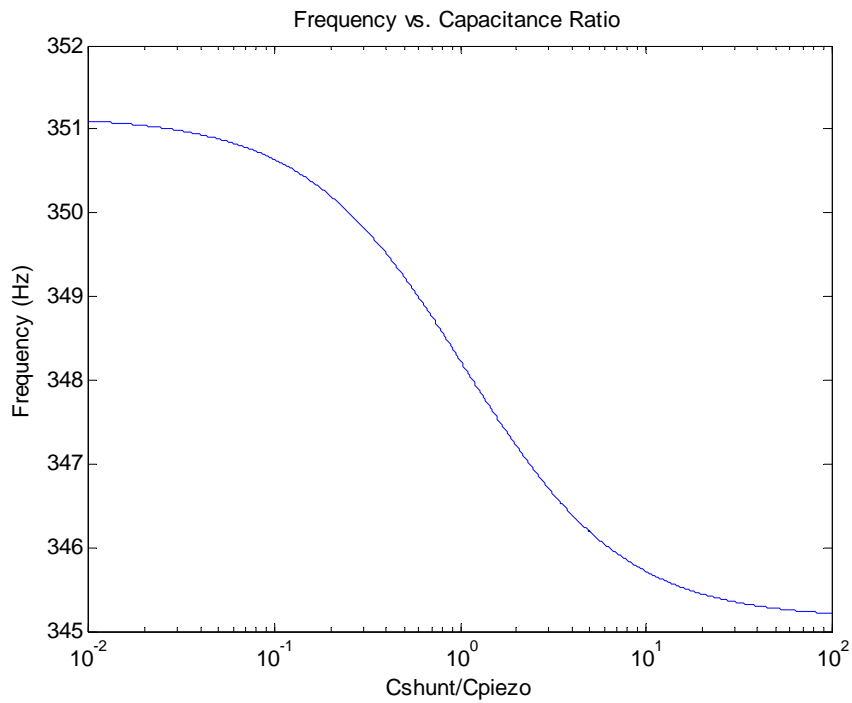
Figure 6.17. Frequency versus capacitance ratio for a bimorph harvester (one layer is used for tuning)

As can be seen in the plot, this case results in a tuning range of approximately 6 Hz, or 1.74 percent. If both layers are used for tuning, the tuning range can be increased. Figure 6.18 shows the analytical frequency versus ratio of shunt capacitance to piezoelectric capacitance if both layers are used for tuning.
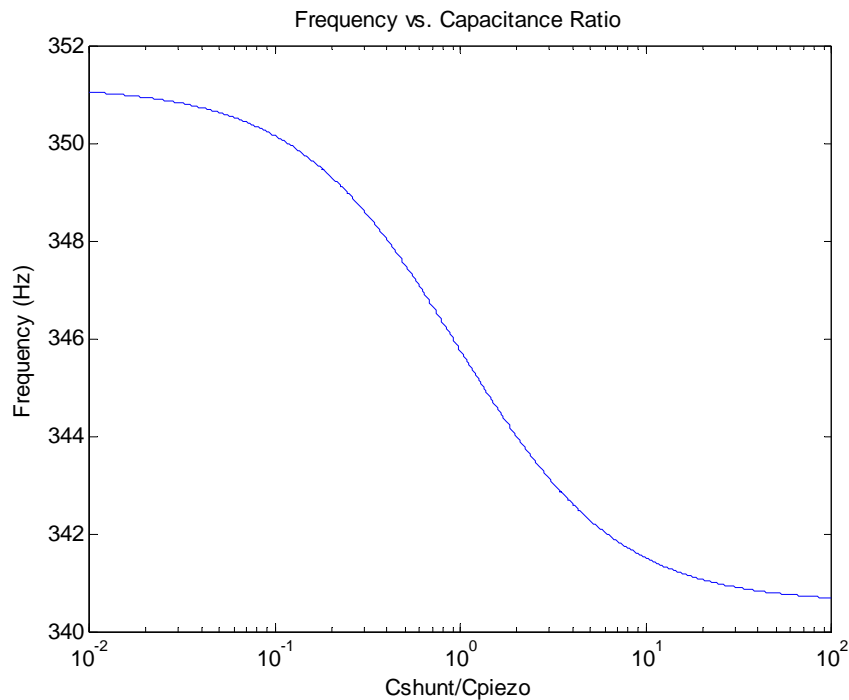
Figure 6.18. Frequency versus capacitance ratio for a bimorph harvester (both layers are used for tuning)

As can be seen in the plot, this case results in a tuning range of approximately 10 Hz, or 2.94 percent. Figures 6.19 to 6.23 show experimental plots of the natural frequency of each beam versus a ratio of the shunt capacitance to that of the piezoelectric material for the case when only one layer is used for tuning.
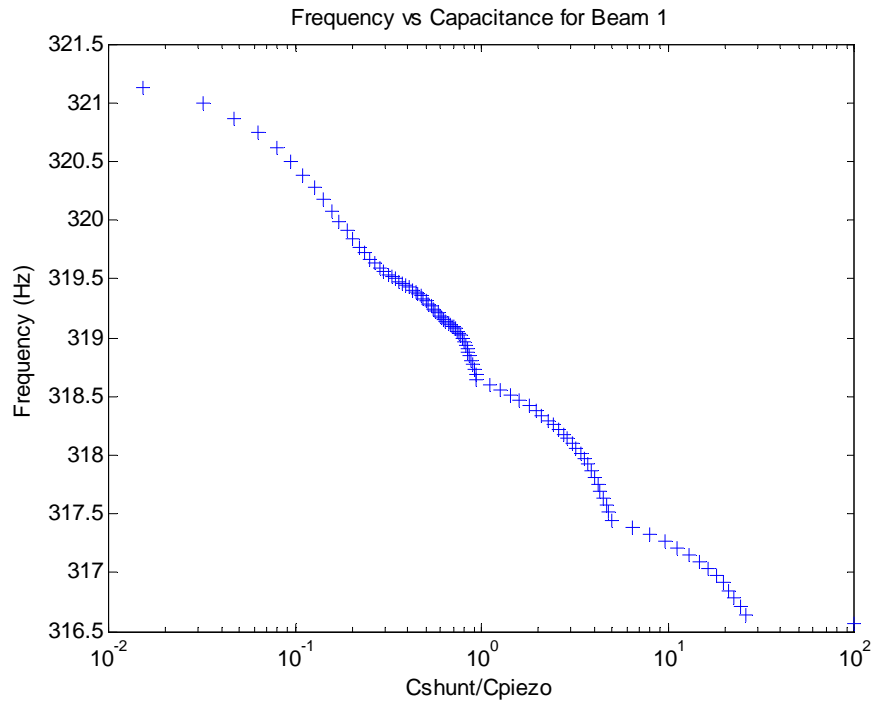
Figure 6.19. Frequency vs Capacitance Ratio for Beam 1 (one layer used for tuning)
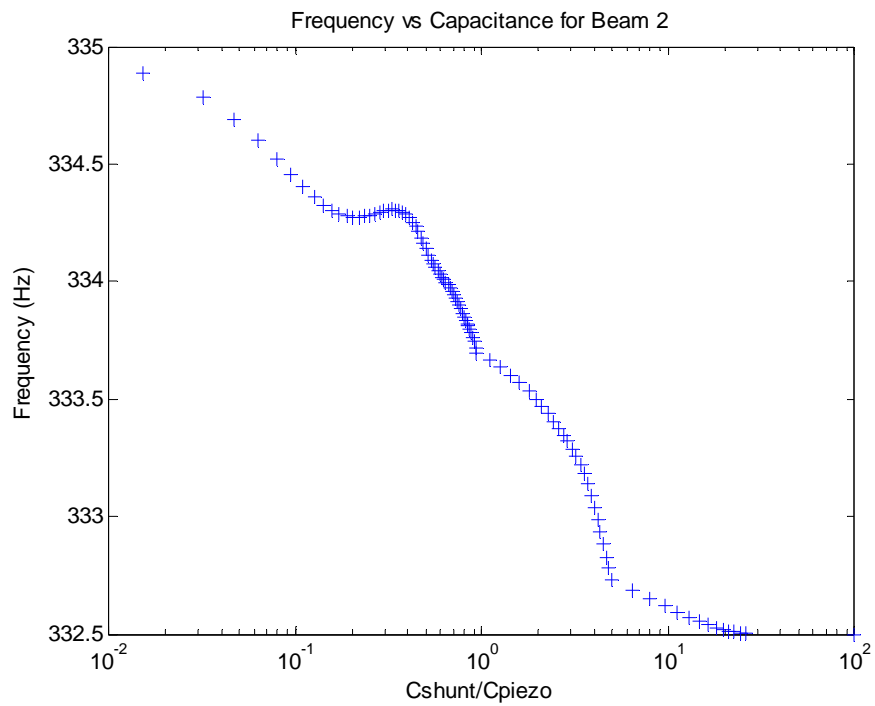
Figure 6.20. Frequency vs Capacitance Ratio for Beam 2 (one layer used for tuning)
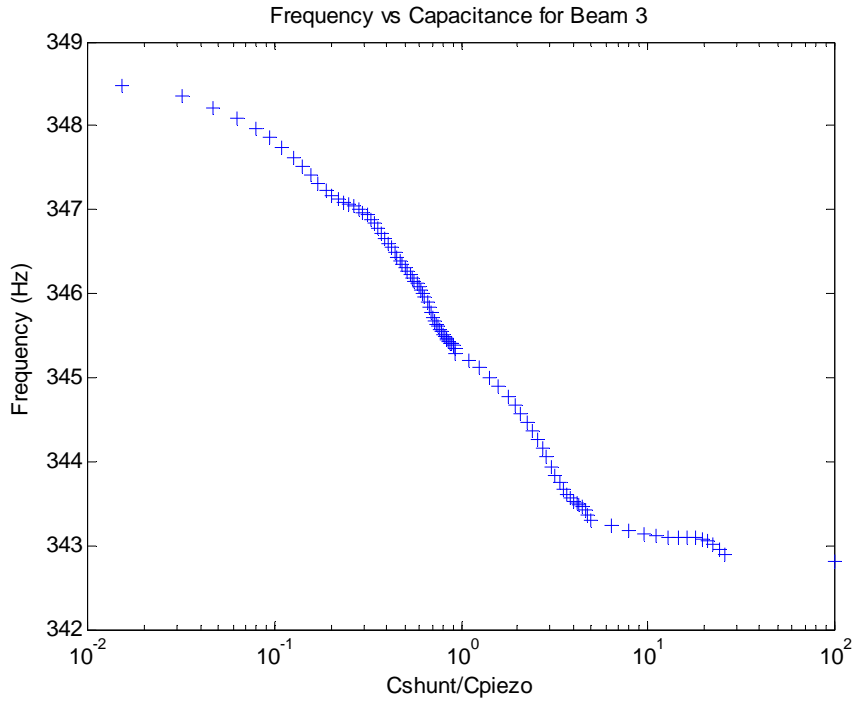
Figure 6.21. Frequency vs Capacitance Ratio for Beam 3 (one layer used for tuning)
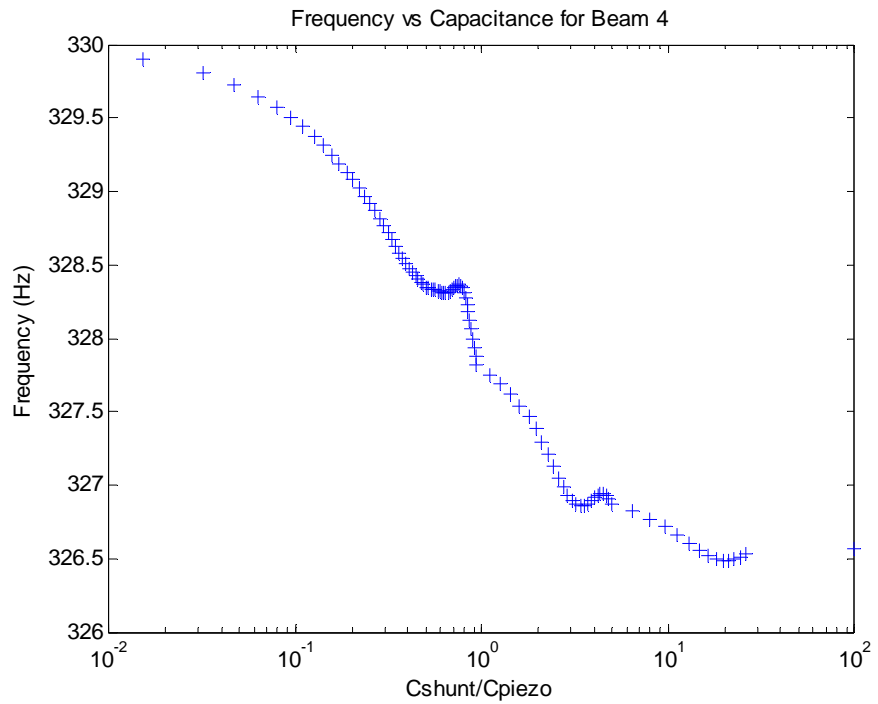
Figure 6.22. Frequency vs Capacitance Ratio for Beam 4 (one layer used for tuning)
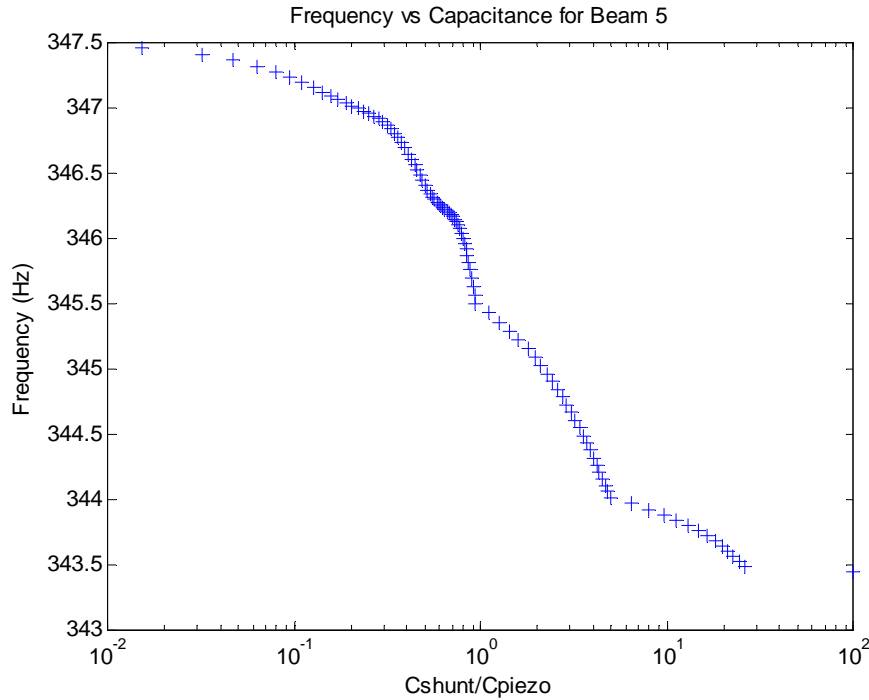
Figure 6.23. Frequency vs Capacitance Ratio for Beam 5 (one layer used for tuning)

From the plots, the amount of frequency change and percent of tuning can be determined and represent the amount of tuning using one of the piezoelectric layers for tuning. Table 16 summarizes the frequency tuning results. For the five beams tested, between 2.4 and 5.9 Hz frequency change was obtained. This corresponds to a range of 0.72 percent to 1.48 percent of tuning.

Table 16. Frequency change and percent of tuning results for each beam using one layer for tuning

Beam Number	Δf	% Tuning
1	4.7	1.48
2	2.4	0.72
3	5.9	1.71

Table 16. (continued).

| 4 | 3.3 | 1.01 |
| 5 | 4.1 | 1.19 |

Figures 6.24 to 6.27 show experimental plots of the natural frequency of each beam versus a ratio of the shunt capacitance to that of the piezoelectric material for the case when both layers are used for tuning. These tests were performed by adding an additional capacitor array to the second layer. By simultaneously changing the capacitance of each layer by the same amount, the stiffness of each layer could be adjusted and therefore at any given time, each layer would have approximately the same stiffness. Note that Beam 3 was damaged before this test was performed, and therefore was not used to gather data.
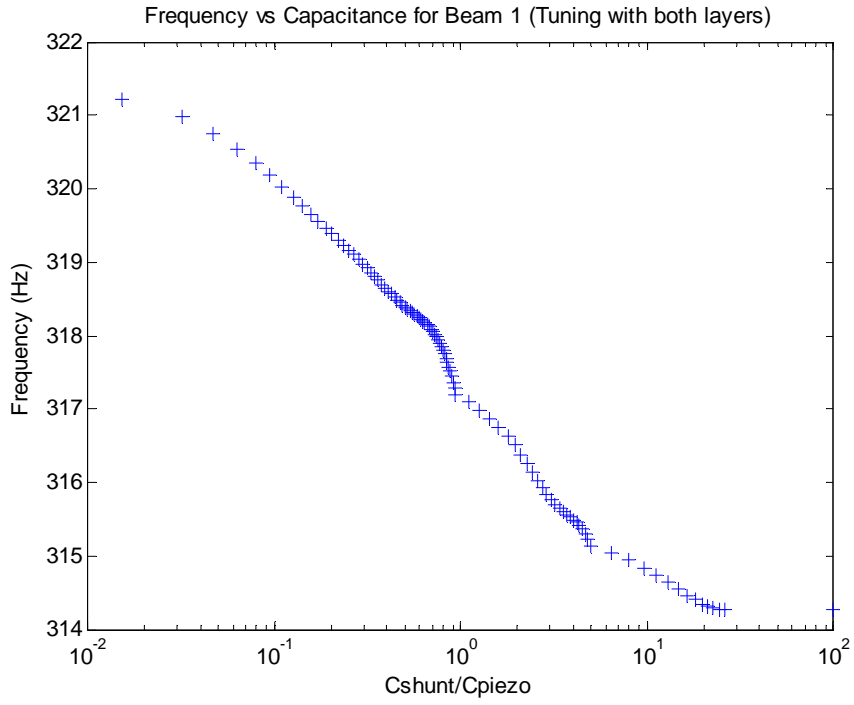
Figure 6.24. Frequency vs Capacitance Ratio for Beam 1 (both layers used for tuning)
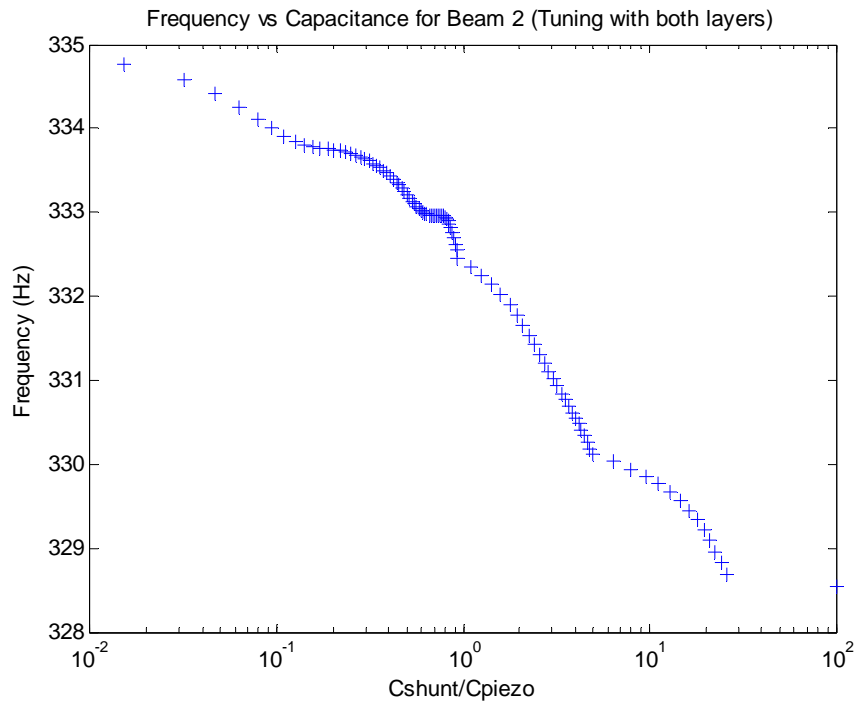
Figure 6.25. Frequency vs Capacitance Ratio for Beam 2 (both layers used for tuning)

90
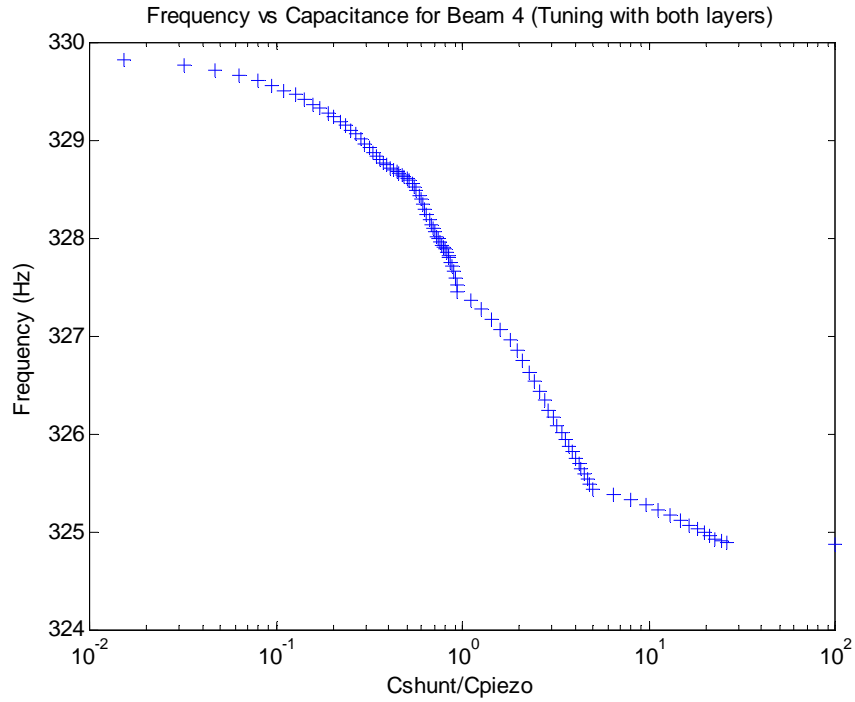
Figure 6.26. Frequency vs Capacitance Ratio for Beam 4 (both layers used for tuning)
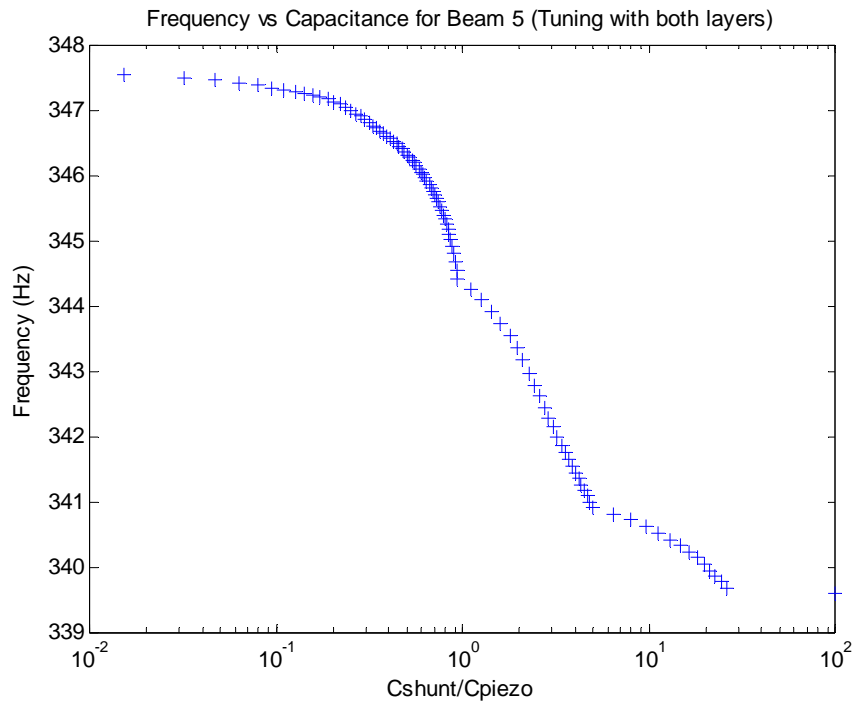
Figure 6.27. Frequency vs Capacitance Ratio for Beam 5 (both layers used for tuning)

Table 17 summarizes the tuning results using both layers for tuning. For the four beams tested, between 4.9 and 7.9 Hz frequency change was obtained. This corresponds to a range of 1.89 percent to 2.32 percent of tuning. Note that the frequencies were found by using the output of the beams and therefore the extreme case where both layers are shorted could not be found using this method. Therefore the measured tuning ranges are assumed to be close to the full tuning range (open circuit to short circuit) but may be slightly larger.

Table 17. Frequency change and percent of tuning results for each beam using both layers for tuning

Beam Number	Δf	% Tuning
1	6.9	2.19
2	6.2	1.89
4	4.9	1.51
5	7.9	2.32

From the results it can be seen that using a capacitive shunt method to adjust the natural frequency of a piezoelectric bimorph is a viable one. As long as the device is designed close to the desired frequency the harvester can be adjusted to the correct value. In this analysis, there was variability in the natural frequencies of the beams. To improve this, future studies should improve on the manufacturing process. It has been shown that if more layers are used for tuning, an increase in tunability occurs. It will be shown in the next section that it is possible to harvest energy and tune with the same layer (to a certain extent) and therefore for certain applications it may be possible to use more than one layer for both tuning and harvesting.

6.2.4　Energy Harvesting Results

By measuring across the load resistor in the energy harvesting circuit of Figure 6.11, the power output versus load resistance can be obtained. The first test involved using the bottom layer of the bimorph to tune the harvester and measure power from the top layer.

6.2.4.1 Harvesting from top layer (and tuning with bottom layer)

By varying the load the source resistance was determined to be approximately 10 kΩ and was approximately the same for all of the harvesters and remained constant even when the shunt capacitance and input frequencies were changed to match fundamental frequencies. Since the harvester only operated in the first bending mode, it was assumed it behaved like a beam and therefore the dynamic energy model was used for the theoretical power calculation due to it being much easier to calculate than the dynamic plate model. For the calculation, approximately 1% damping was assumed. Also, by varying the capacitance, the output voltage (and hence power) remained relatively constant and therefore only one theoretical power curve is plotted on each graph. Figures 6.28 to 6.32 present plots of power versus load resistance for the five beams.
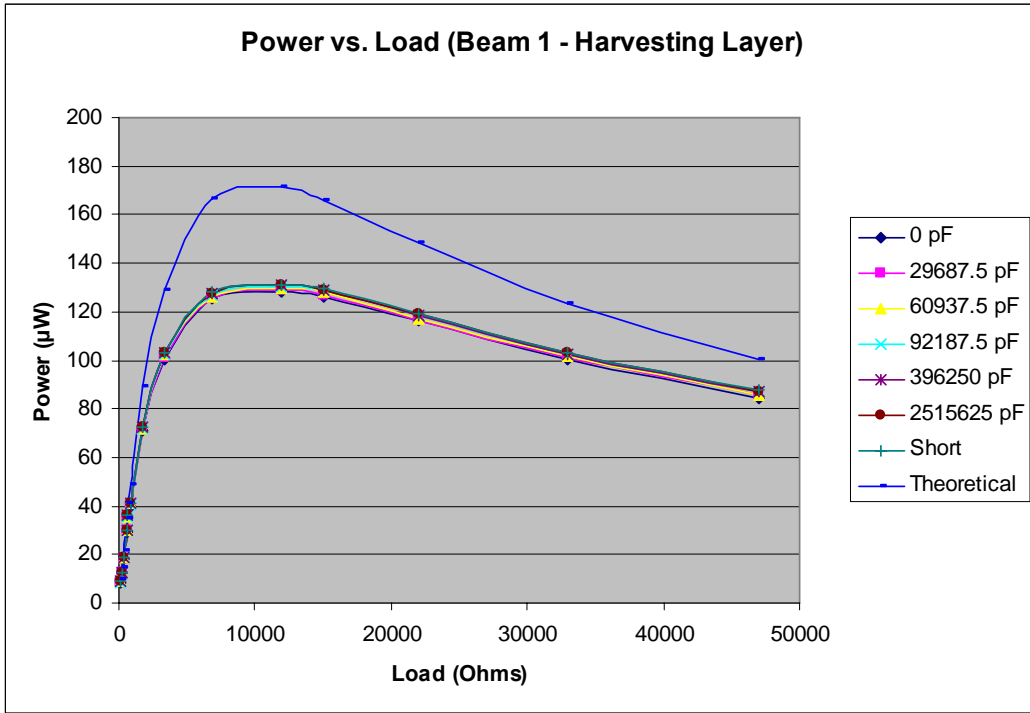
Figure 6.28. Power versus load resistance for Beam 1 (Harvesting from top layer, tuning with bottom layer)
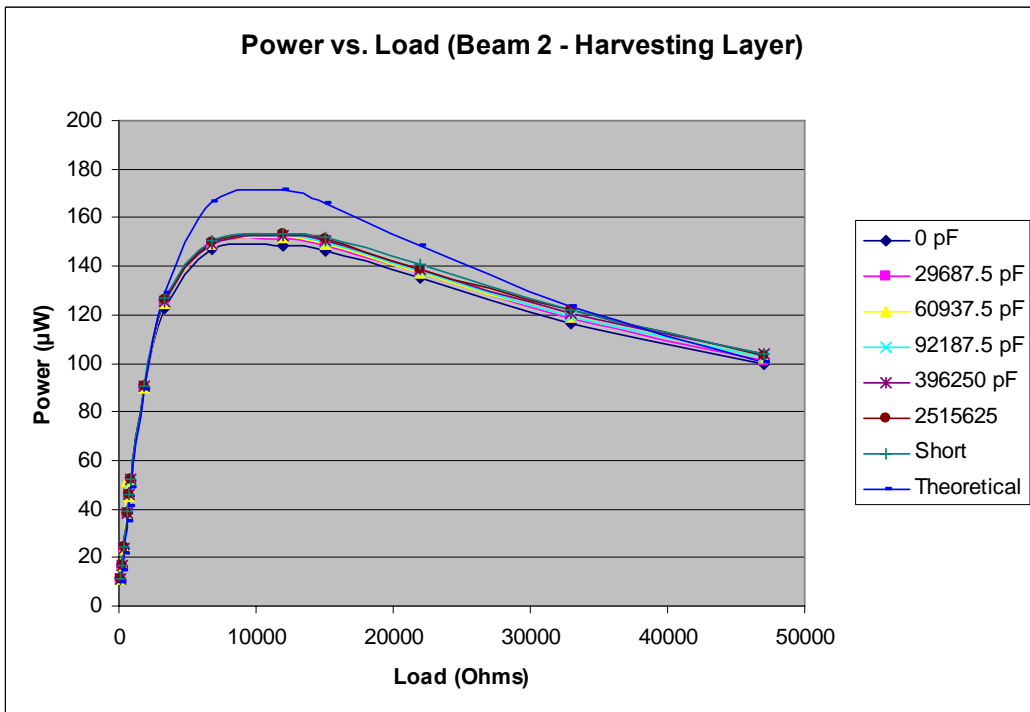
Figure 6.29. Power versus load resistance for Beam 2 (Harvesting from top layer, tuning with bottom layer)

94
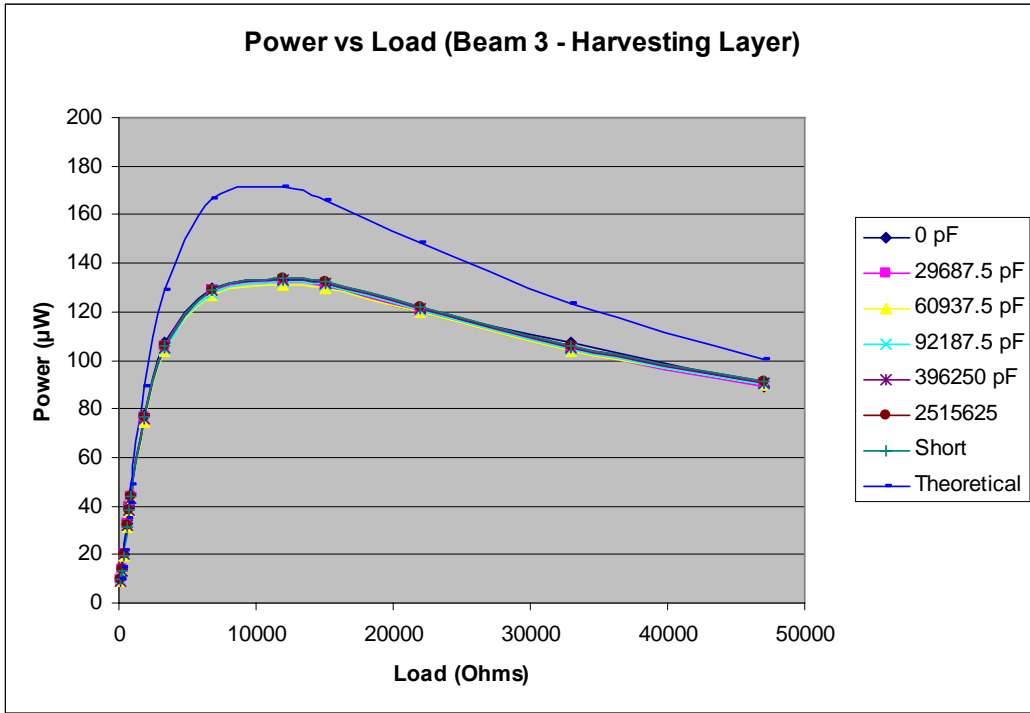
Figure 6.30. Power versus load resistance for Beam 3 (Harvesting from top layer, tuning with bottom layer)
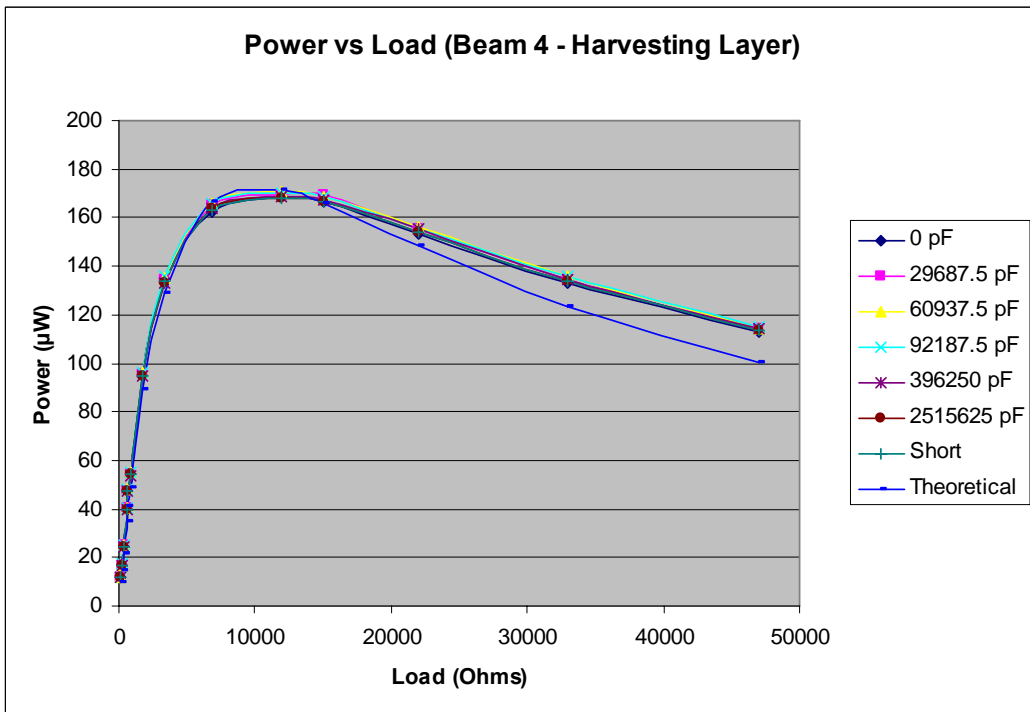
Figure 6.31. Power versus load resistance for Beam 4 (Harvesting from top layer, tuning with bottom layer)

Power vs Load (Beam 5 - Harvesting Layer)
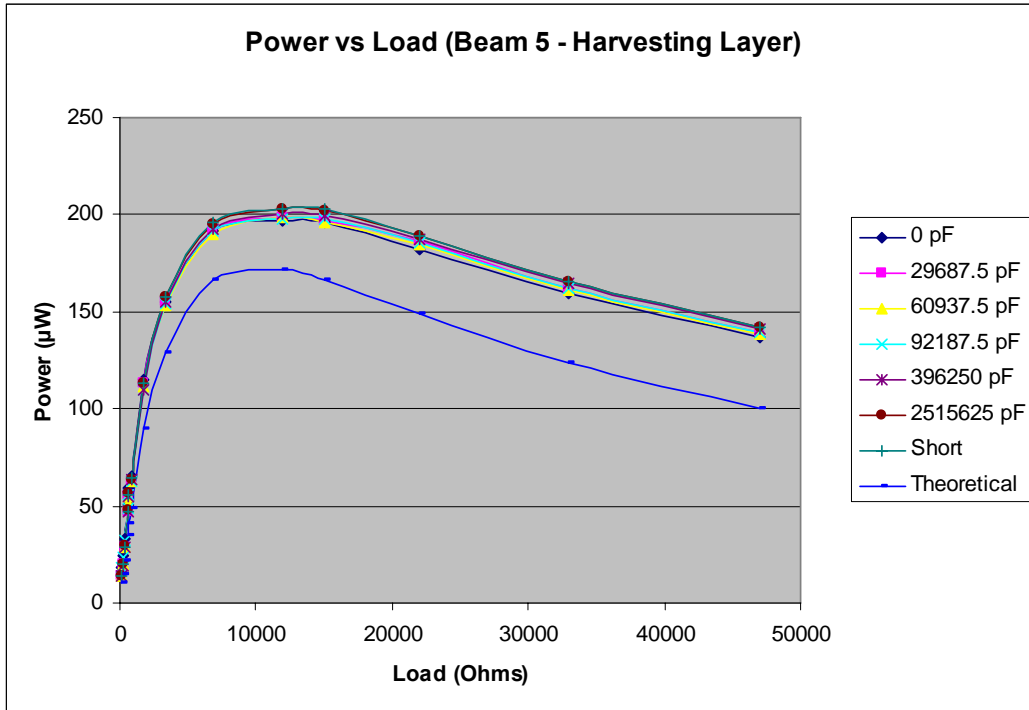
Figure 6.32. Power versus load resistance for Beam 5 (Harvesting from top layer, tuning with bottom layer)

From the plots it can be seen that the power ranges from 130 to 170 μW when the load is matched to that of the source. By adjusting the capacitance attached to the tuning layer, the plots show the power output and impedance of the harvesting layer is not affected, which provides evidence that the capacitive shunt method is a feasible means of tuning the natural frequency of a piezoelectric bimorph energy harvester.

The theoretical power over-predicts the power for beams 1, 2, and 3, and under predicts the power for beams 4 and 5. Several factors could attribute for this. The actual damping ratio for each beam is unknown and would need to be determined experimentally. The assumed damping could attribute to some discrepancies. Power is also dependent on material properties, dimensions of the structures, etc. Since each harvester was manufactured by hand, each is not an ideal replica of each other. As could be seen in the previous section, each device had slightly

different natural frequencies. Since the power calculation is based off calculated frequencies, there may be slight differences between calculated and actual values.

By selecting an excitation frequency in the middle of the range of tuning and varying the capacitance attached to the tuning layer (and holding the frequency constant), the effect on power can be determined as well as demonstrate the practical use of the capacitive shunt tuning method. Beam 1 was chosen to be used as an example. The results of this test are shown in Figure 6.33.
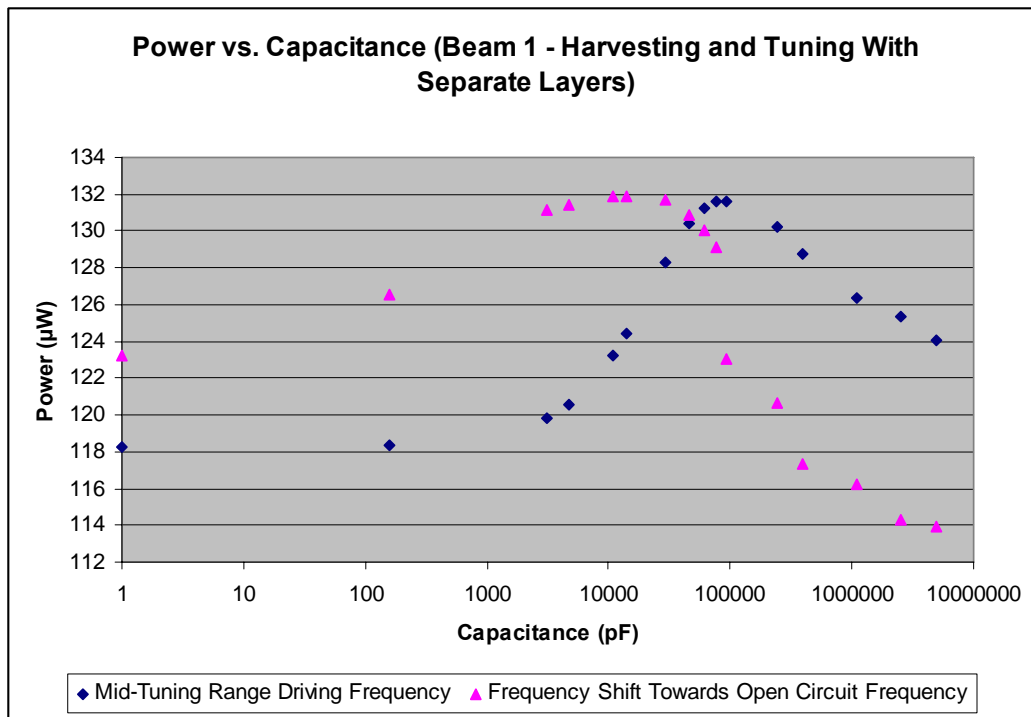
Figure 6.33. Plot of Power vs. Capacitance for Beam 1 holding frequency constant (mid-tuning range and shifted towards open circuit) and adjusting capacitance (Using separate layers for tuning and harvesting).

As can be seen from the plot, when the driving frequency is in the center of the tuning range, the power is significantly decreased at low capacitances (off resonance condition), and rises to a maximum when the natural frequency of the beam matches that of the shaker and then decreases as the capacitance continues to increase (off resonance once again). If the driving frequency is

shifted towards the open circuit natural frequency of the beam (increase in frequency), the resonant power peak occurs at a lower capacitance which makes sense since the open circuit shunt condition approaches zero. Therefore, it can be concluded that as long as the harvester is designed to resonate near the frequency of a vibration source, the shunt capacitance can be adjusted to move the harvester's natural frequency to that which produces maximum power.

An important characteristic for evaluating the performance of an energy harvester is to calculate the efficiency of energy conversion. For the test setup previously described, this can be defined as

$$\% \, efficiency = \frac{Electrical \, Output \, Power \, from \, Harvester}{Mechanical \, Input \, Power \, of \, Sha \, ker} * 100 \tag{101}$$

The power output from each harvester can be found using the maximum power values from Figures 6.28 to 6.32. The input power of the shaker can be found by measuring the mass of the beam-clamp structure and the force that is driving the structure. The power from the input can be written as

$$P_{input} = Fv \tag{102}$$

where F is the driving force and v is velocity of the structure. By attaching a force transducer between the shaker and harvester, the force can be found. Since force is equal to mass times acceleration, the acceleration of the system can be found. Acceleration can also be written as

$$a = A \, sin(\omega t) \tag{103}$$

where A is amplitude, and ω is the frequency of the source. Integrating, the magnitude of the velocity is

$$v = \frac{A}{\omega} \tag{104}$$

Substituting into equation 102, the mechanical input power is

98

$$P_{input} = \frac{FA}{\omega} \qquad (105)$$

With both the input and output power able to be calculated, the efficiency of each harvester can be determined. Table 18 presents the percent efficiency of each beam using the previous method. Note that the driving frequency will change slightly as the capacitance attached to the tuning layer is changed. Therefore, a frequency value in the center of each harvester's tuning range was chosen as the driving frequency for each efficiency calculation. Since the tuning ranges were not very large, the change in frequency does not have a large effect on the input power.

Table 18. Percent efficiency of each energy harvester (one layer used for tuning, one for harvesting)

Beam Number	% Efficiency
1	0.443
2	0.541
3	0.488
4	0.591
5	0.741

6.2.4.2 Harvesting (and tuning) with bottom layer

As in the previous test, the power versus resistive load was determined for the tuning layer. If the tuning layer could be used for both tuning and harvesting energy, the amount of energy generated by the beam could be increased while at the same time having tuning capabilities. For this test, the harvesting circuit was connected in parallel with the capacitor array. The results are shown in Figures 6.34 to 6.38.
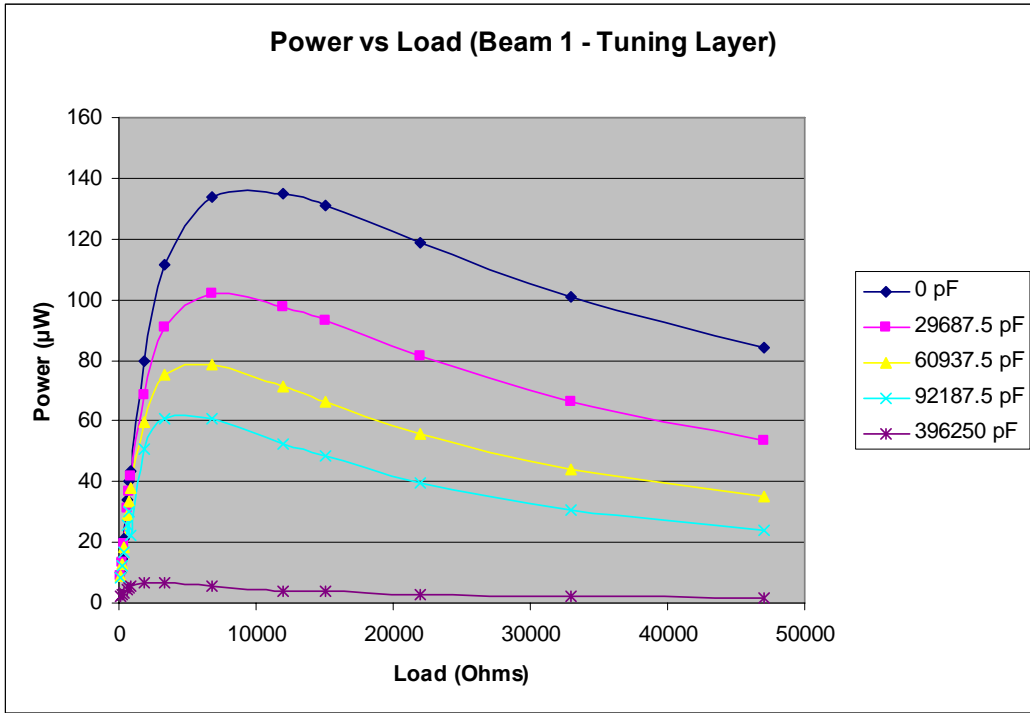
Figure 6.34. Power versus load resistance for Beam 1 (Harvesting and tuning with bottom layer)
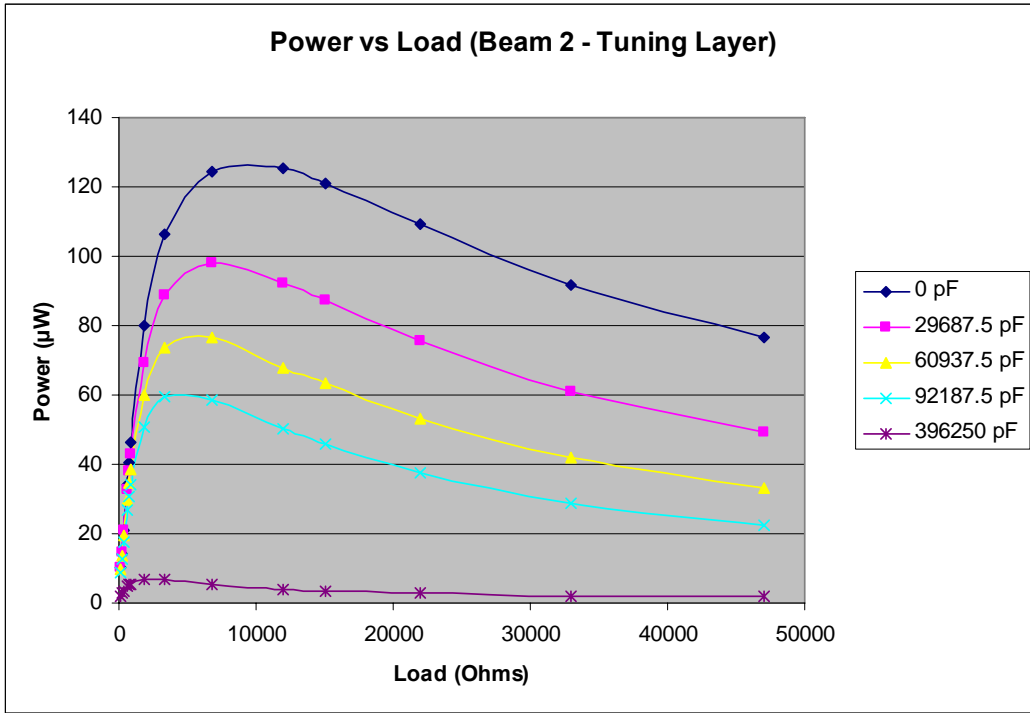
Figure 6.35. Power versus load resistance for Beam 2 (Harvesting and tuning with bottom layer)
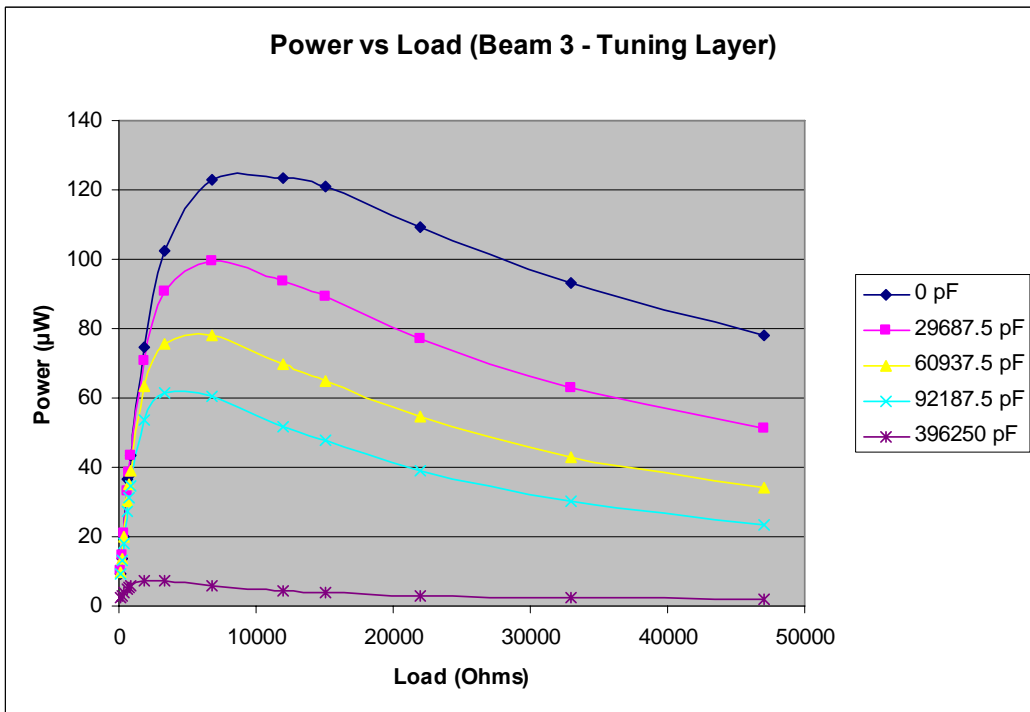
Figure 6.36. Power versus load resistance for Beam 3 (Harvesting and tuning with bottom layer)

101
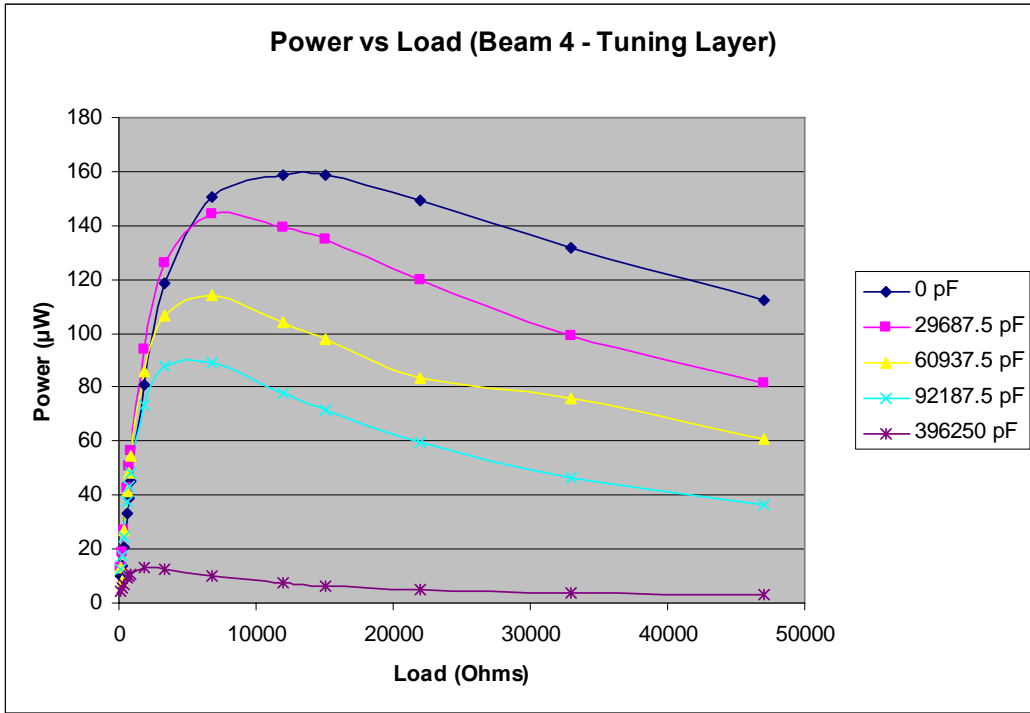
Figure 6.37. Power versus load resistance for Beam 4 (Harvesting and tuning with bottom layer)
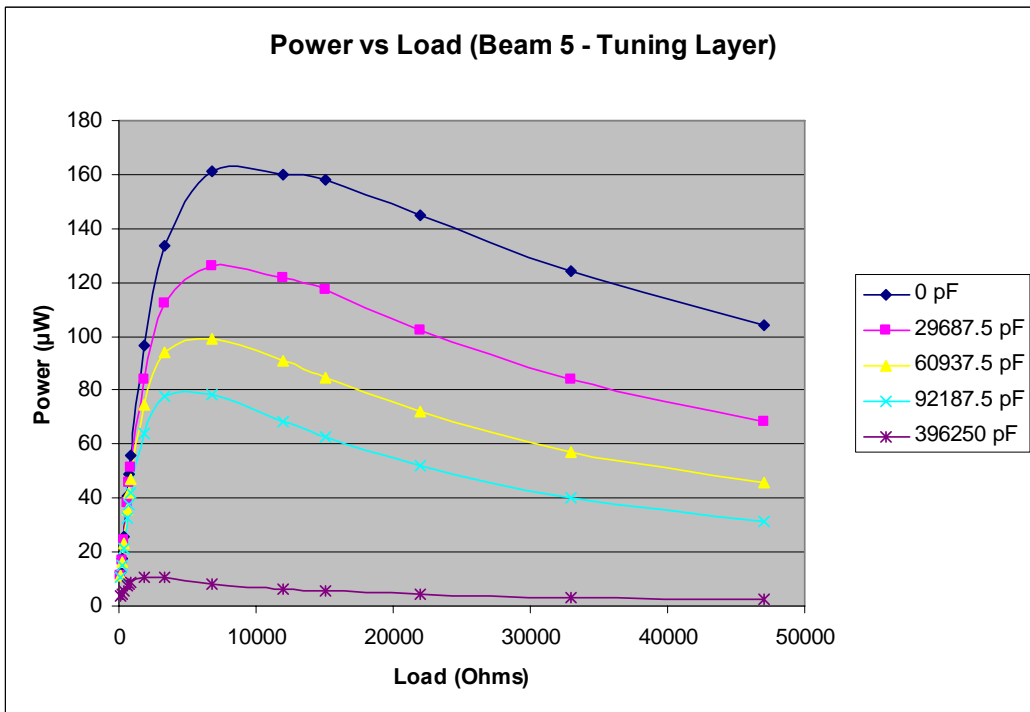
Figure 6.38. Power versus load resistance for Beam 5 (Harvesting and tuning with bottom layer)

From the plots, the open circuit power when the load matches the source impedance ranges from approximately 130 to 160 µW, similar to the previous results, as expected. As the capacitance of the array increases the amount of power generated decreases. This makes sense since as the capacitance of the shunt increases the shunt impedance approaches a short circuit condition. Obviously when the shunt is shorted, no power can be generated. Another observation is that as the capacitance of the array increases, the source impedance shifts slightly to the left (decreases). The impedance of a capacitive element is defined by

$$Z_c = \frac{1}{j\omega C} \tag{106}$$

where ω is frequency and C is capacitance. As capacitance increases, the impedance approaches zero. It is well known that maximum power transfer occurs when the impedance of the source matches that of the load. Treating the piezoelectric harvester and its shunt as a capacitive element and setting it equal to the impedance of the load, as the capacitance increases, the source and load impedance decrease.

Since both layers can possibly have different impedances, it is possible to harvest energy off of both layers at the same time by using a rectifying circuit like that of Figure 6.11 on each layer. However, if both voltages are different, the outputs of each circuit will not simply add together. It will be left to a future study to work this issue out.

As was done previously with the harvester with separate tuning and harvesting layers, if a driving frequency is held constant and capacitance is varied, the effect on power can be determined. Figure 6.39 shows the effects of power output of beam 1 by choosing a mid-tuning range frequency and varying the capacitance, along with shifting the frequency towards the open circuit frequency and varying the capacitance.
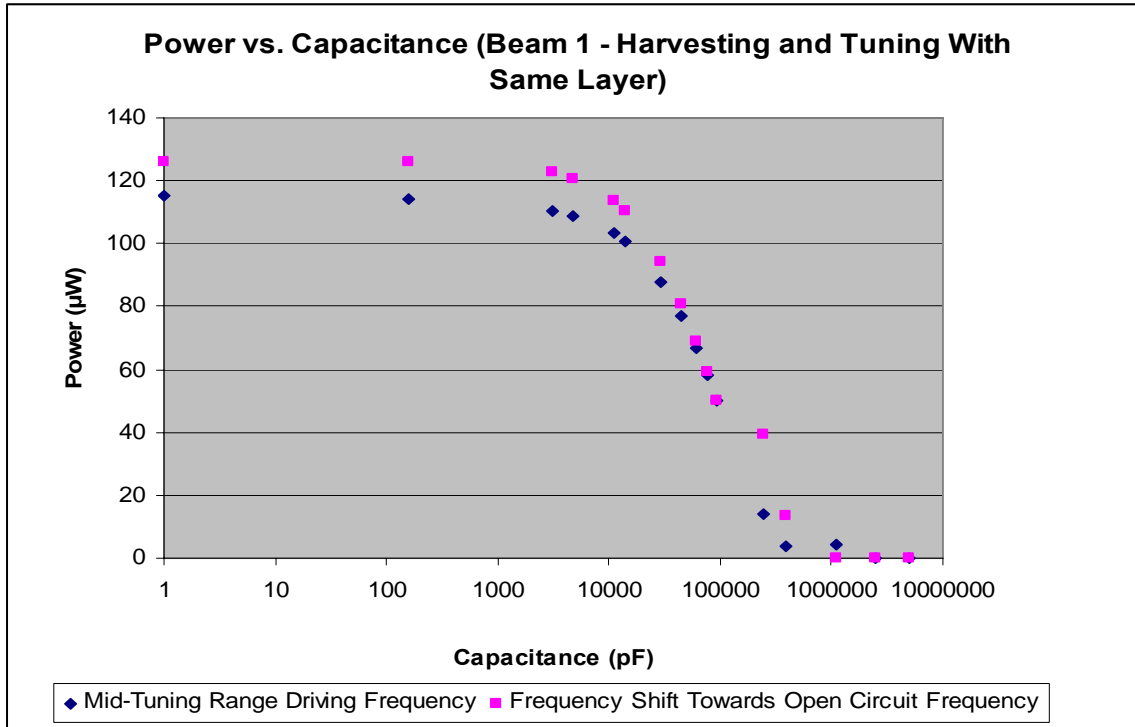
Figure 6.39. Plot of Power vs. Capacitance for Beam 1 holding frequency constant (mid-tuning range and shifted towards open circuit) and adjusting capacitance (Using same layer for tuning and harvesting).

As can be seen from the plot, the power output when the driving frequency is in the middle of the tuning range remains relatively constant and eventually falls off, similar to decrease of power observed in Figures 6.34 to 6.38. When the driving frequency is shifted towards open circuit, the initial power is larger but follows a similar trend as the mid range power plot. This makes sense because as the resonant frequency of the harvester approaches open circuit, the resonant power peak will occur at lower capacitance and hence will increase the power occurring at points close to the peak. The resonant power peaks should occur at similar locations as in Figure 6.33. However, the increase in capacitance of the capacitor array prevents these peaks from occurring and therefore the capacitive shunt concept is not as useful for maximizing power as when the harvesting and tuning layers are separate.

104

6.2.5 Summary

It has been shown that a capacitive shunt method can be used to tune a piezoelectric bimorph energy harvester. For a bimorph (with all layers approximately the same thickness) if both layers are used for tuning, theoretically it is possible to achieve up to 2.94 percent tuning. If only one layer is used for tuning the range is 1.74 percent. Experimentally up to 2.32 percent tuning was obtained using both layers for tuning and up to 1.7 percent tuning was obtained using only one layer.

Effects on power harvesting were also studied. When using the capacitive array on only one layer, effects on the other layer are minimal. It has been shown that the magnitude of the power versus impedance remains relatively constant as the value of the capacitive shunt is increased. Tuning and harvesting from the same layer is also possible. However, as capacitance increases, the amount of power able to be generated decreases. The source impedance also decreases.

7.0   CONCEPTS FOR REDUCING FREQUENCY DEPENDENCE OF PIEZOELECTRIC ENERGY HARVESTERS

The previous chapters have presented a method to passively tune a piezoelectric energy harvester. This chapter will provide a brief overview of several other methods that could be used to tune, or at least reduce the need to design a harvester to an exact frequency. To begin, a piezoelectric electro-mechanical filter concept to harvest from multiple frequencies will be presented. This will lead to another mechanical band pass filter using multiple beams. A frequency multiplier technique will follow. The chapter will conclude with a morphing beam concept.

7.1.1   Piezoelectric Electro-mechanical Filter

Dmuchoski (2000) provides an extensive investigation into using piezoelectric transducers as electromechanical filters. By coupling two beams together with a coupling spring, a band pass filter can be created which is dependant on the fundamental frequency of the two beams and the spring. Figure 7.1 shows an example of this type of filter.
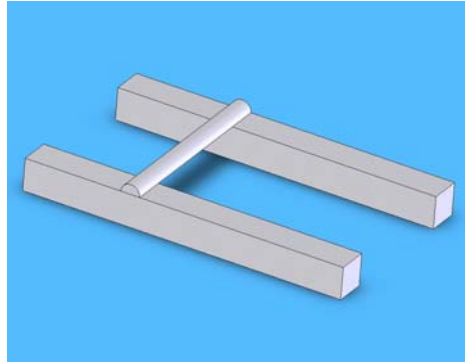
Figure 7.1. Mechanical filter

Figure 7.2 shows a free body diagram of the system for when one of the beams is excited by a signal or force.
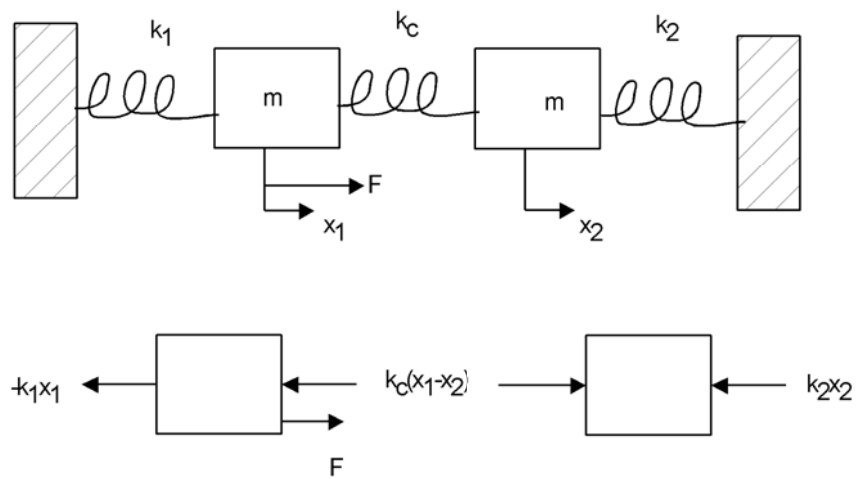
Figure 7.2. Free Body diagram of mechanical filter

Assuming both beams have the same stiffness, k, the equations of motion of the system are

$$F = m\ddot{x}_1 + (k + k_c)x_1 - k_c x_2$$
$$0 = m\ddot{x}_2 + (k + k_c)x_2 - k_c x_1$$

(107)

Taking the Laplace transform of the equations and writing in matrix form results in

107

$$\begin{vmatrix} \dfrac{F}{m} \\ 0 \end{vmatrix} = \begin{vmatrix} s^2 + \dfrac{k_1 + k_c}{m} & -\dfrac{k_c}{m} \\ -\dfrac{k_c}{m} & s^2 + \dfrac{k_2 + k_c}{m} \end{vmatrix} \begin{vmatrix} x_1 \\ x_2 \end{vmatrix} \tag{108}$$

Since the device is used as a resonator, the output of x_2 is of interest. Using Cramer's rule, the transfer function of the system can be found.

$$\frac{x_2}{F} = \frac{\dfrac{k_c}{m}}{(s^2 + \dfrac{k_1 + k_c}{m})(s^2 + \dfrac{k_2 + k_c}{m}) - (\dfrac{k_c}{m})^2} \tag{109}$$

The frequency response of the system (with $k_1=k_2=k$) can be seen in Figure 7.3. If both beams have the same stiffness then the peaks of the plot correspond to k and k+k_c.
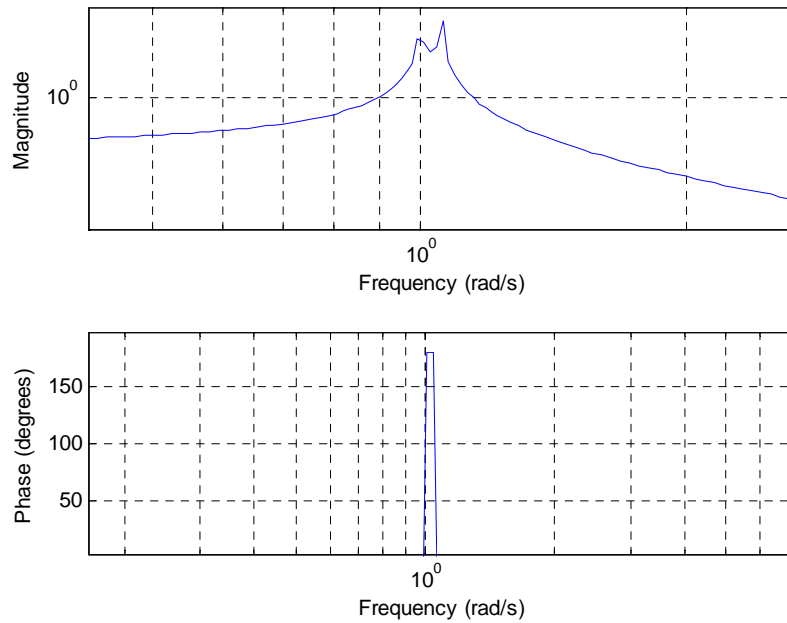
Figure 7.3. Frequency response of mechanical band pass filter

If this idea could be applied to two base excited energy harvesters, the point of maximum energy could be changed from just a single frequency (i.e. first mode of Figure 6.12) to a range of

frequencies. Changing the previous model so that both masses are excited by a base excitation, an energy harvesting analysis can be performed. The new model is shown in Figure 7.4.
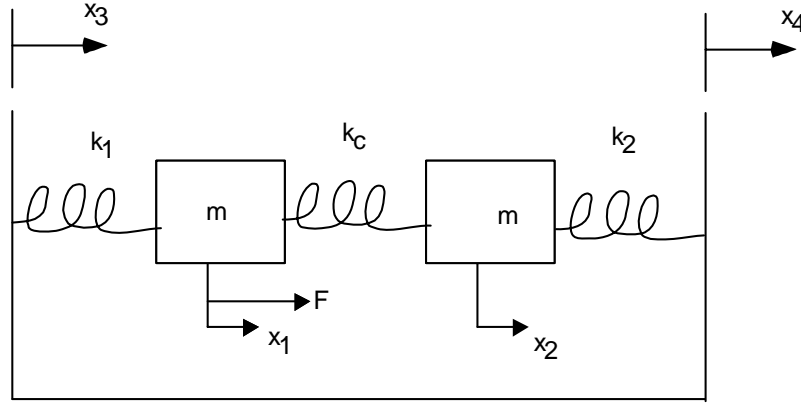
Figure 7.4. Base excited coupled energy harvesting model

Since the device is base excited, x_3 can be assumed to be equal to x_4. Following a similar procedure as before, the system can be described by equation 110.

$$\begin{vmatrix} \ddot{x}_3 \\ \ddot{x}_4 \end{vmatrix} = \begin{vmatrix} s^2 + \dfrac{k_1 + k_c}{m} & -\dfrac{k_c}{m} \\ -\dfrac{k_c}{m} & s^2 + \dfrac{k_2 + k_c}{m} \end{vmatrix} \begin{vmatrix} z_1 \\ z_2 \end{vmatrix} \tag{110}$$

Where $z_1 = x_1 - x_3$ and $z_2 = x_2 - x_4$ Using Cramer's rule, the transfer functions of the system can be found.

$$\begin{vmatrix} z_1 \\ \ddot{x}_3 \end{vmatrix} = \dfrac{s^2 + \dfrac{k_2 + 2k_c}{m}}{s^4 + \dfrac{(k_1 + k_2 + 2k_c)}{m}s^2 + \dfrac{k_1 k_2 + k_1 k_c + k_c k_2}{m^2}} \tag{111}$$

$$\begin{vmatrix} z_2 \\ \ddot{x}_3 \end{vmatrix} = \dfrac{s^2 + \dfrac{k_1 + 2k_c}{m}}{s^4 + \dfrac{(k_1 + k_2 + 2k_c)}{m}s^2 + \dfrac{k_1 k_2 + k_1 k_c + k_c k_2}{m^2}} \tag{112}$$

Since the same force is exciting both beams, by adding equations 111 and 112 together the total system response can be found.

$$\left| \frac{z_1 + z_2}{\ddot{x}_3} \right| = \frac{2s^2 + \dfrac{k_1 + k_2 + 4k_c}{m}}{s^4 + \dfrac{(k_1 + k_2 + 2k_c)}{m}s^2 + \dfrac{k_1 k_2 + k_1 k_c + k_c k_2}{m^2}} \tag{113}$$

Plotting the system response and varying the stiffness parameters, the effects on the system can be analyzed. Also, by integrating over each plot the available energy in each system can be determined. In Figures 7.5 to 7.8 this energy is found in between the magnitude and phase diagrams. As the number increases, the energy in the system does as well. Figure 7.5 shows the system response for $k_1=k_2=k_c$. Figure 7.6 shows the system response for $k_1=k_2$ and $k_c=0$. As can be seen in the plots, there is only one peak. This is due to there always being a pole-zero cancellation in the transfer function. The amount of energy in the system is also slightly more when the coupling spring is not present.
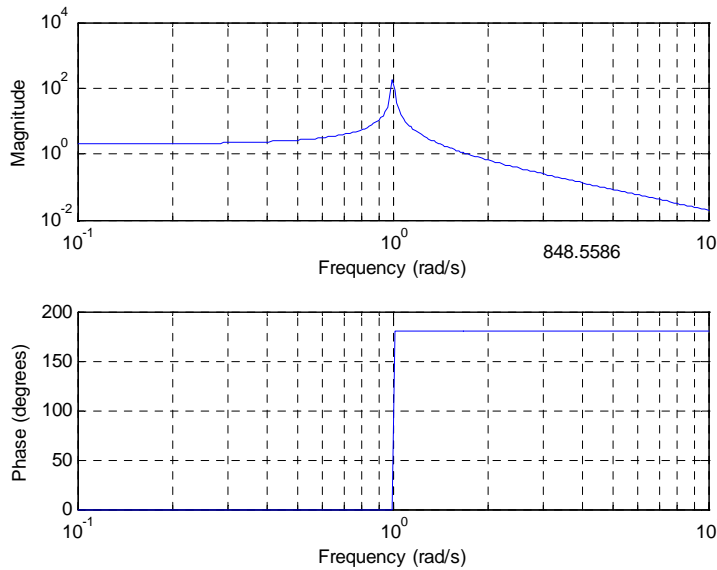
Figure 7.5. System response for $k_1=k_2=k_c$

110
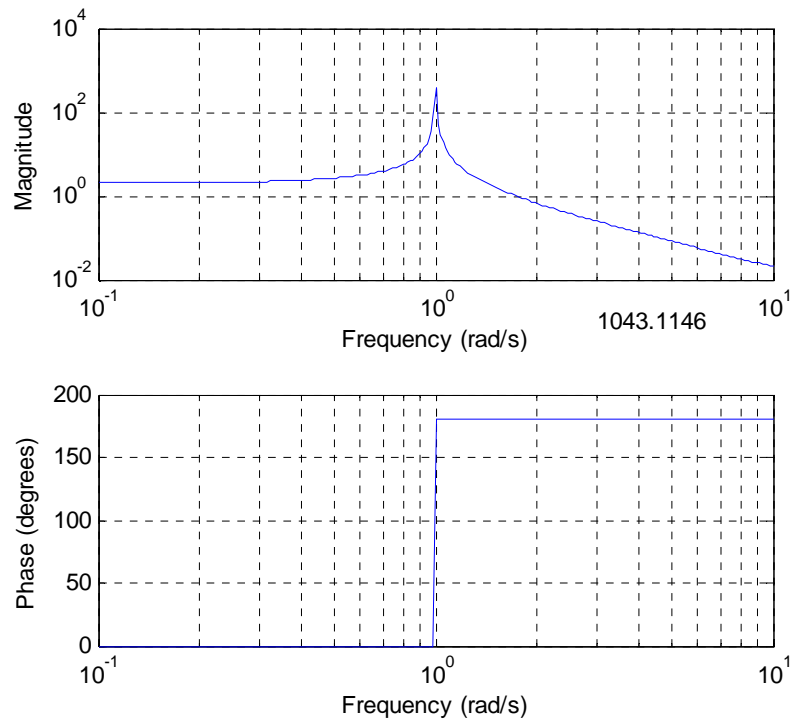
Figure 7.6. System response for $k_1=k_2$, $k_c=0$

Figures 7.7 and 7.8 show the system responses when the beam stiffness is not the same. Figure 7.7 is when $k_1=k_c$ and $k_2=3k_1$. Figure 7.8 is when $k_2=3k_1$ and $k_c=0$.
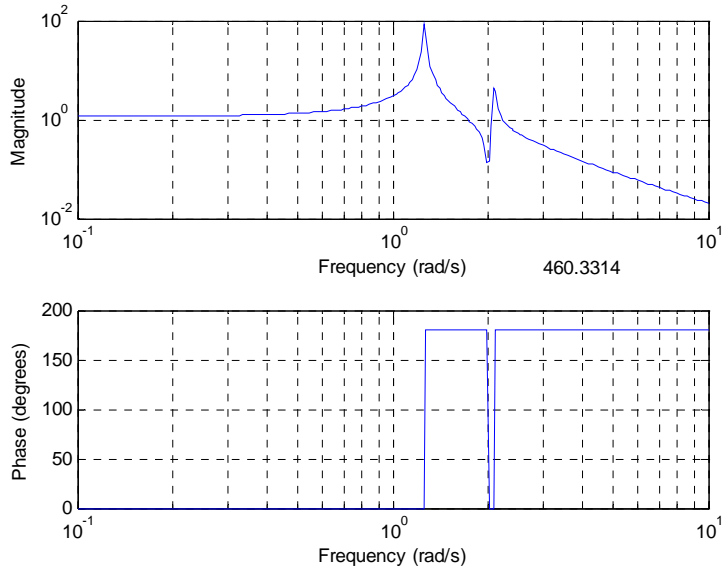
Figure 7.7. System response for $k_1=k_c$, $k_2=3k_1$
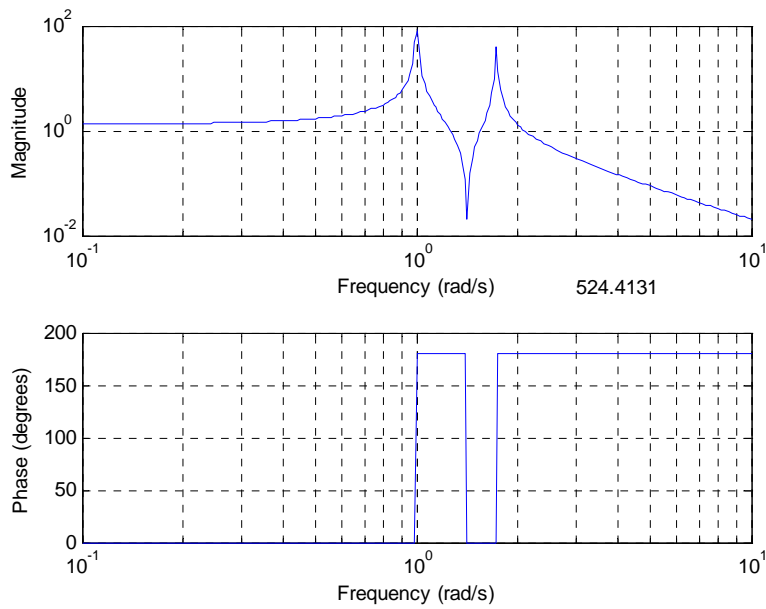
Figure 7.8. System response for $k_c=0$, $k_2=3k_1$

As can be seen from the plots, when the beam stiffness of each beam is different, two peaks occur due to poles in the system transfer function. When the coupling spring is in the system, the magnitude of the second peak decreases and therefore more energy is present in the system

without the coupling spring. From these results it is favorable to use a system lacking a coupling spring when the goal is to harvest energy from multiple frequencies. A better method would be to design a harvesting device containing an array of beams, each with different natural frequencies. If the frequencies are close enough together a response similar to a band-pass filter could be obtained. An example of such a device is shown in Figure 7.9. As can be seen in the figure, each beam is of different dimensions and also has proof masses on the ends. Both are also methods of tuning a harvester to a certain frequency.
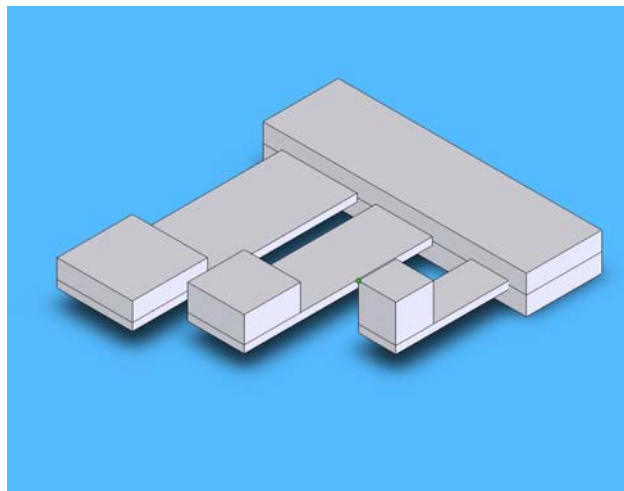
Figure 7.9. Energy harvesting beam array

In summary, in the case of a resonator, adding a coupling spring increases the bandwidth of the device and has a filtering effect. When using a coupling spring for the purpose of energy harvesting, there is always a pole-zero cancellation in the transfer function and the coupling spring has little effect. The coupling spring actually decreases the amount of energy in the system because of an added zero in the system. Multiple frequencies can be harvested by creating a multi-beam system in which each beam has a different stiffness.

7.1.2 Frequency multiplier

An idea from Tieck et al. (2006) provides a possible way to eliminate the need to manufacture a piezoelectric bimorph harvester to an exact natural frequency. The idea involves using a linear traveling rack that imparts vibrational motion to a beam (via impulses). As long as the natural frequency of the bimorph is larger than the source, each period of the rack will excite the beam, which will vibrate at its natural frequency. In a base excited beam, the beam would vibrate at the frequency of the source. In this case, the frequency is multiplied from the source frequency to that of beam. The two frequencies are unrelated. Figure 7.10 shows the motion of both the harvester and the source.
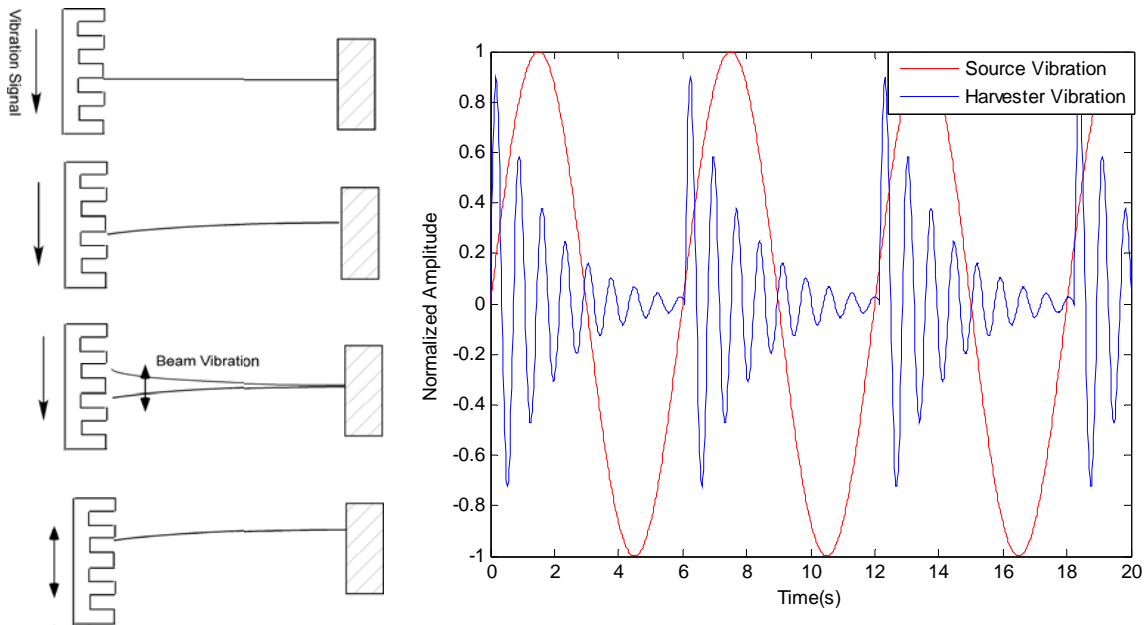
Figure 7.10. Left: Rack exciting a cantilever beam. Right: Motion of source and harvester

7.1.3 Variable modulus beam

By adding mass to the end of a beam, the natural frequency of the beam changes. However this can be a difficult task to accomplish in real time. By being able to change the internal structure of the beam and move some concentrated mass toward the end or base, the frequency can be adjusted. Figure 7.11 shows an example of the concept.
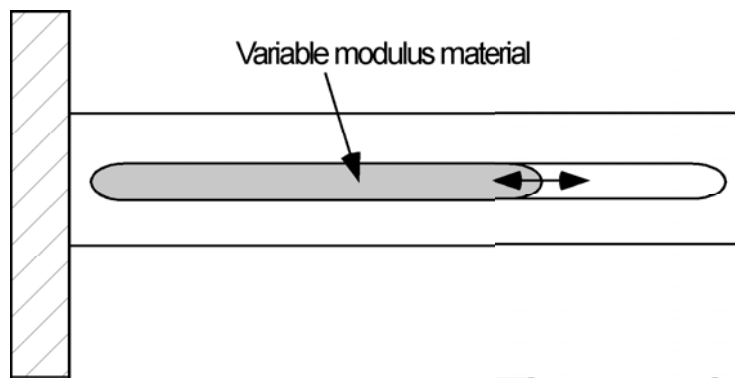
Figure 7.11. Cantilever beam with variable modulus core

If the center of the beam is made of a material that is able to undergo a modulus change when a stimulus is applied, the natural frequency of the beam can be adjusted by applying the stimulus and moving the material to various positions along the beam. If the material is closer to the tip, the beam will be less stiff and the natural frequency will decrease. If the material is close to the base, the beam will be stiffer and the natural frequency will increase.

115

8.0   CONCLUSIONS AND FUTURE WORK

This work investigated the feasibility of using a capacitive shunt method to tune piezoelectric bimorph energy harvesters. A brief history of piezoelectric materials was given, followed by fundamentals of piezoelectric sensors and actuators. Attention was given to cantilever energy harvesters with respect to different modes of operation (33, 31, 15).

A review of research done in the energy harvesting area was performed. This was followed by a presentation of previous research done on methods of storing generated energy from energy harvesters. Research leading up to the capacitive method used in this work was discussed and was followed by other methods of tuning the frequency of energy harvesters.

The capacitive tuning method was presented. The concept was utilized on a multilayer beam with a harvesting layer, tuning layer, and substrate layer. Ratios of the layer thicknesses were varied to determine the optimum configurations for determining the greatest amount of tunability. The greatest tunability occurs when the ratios of substrate to piezoelectric layer thickness are small (less than 2). As long as the neutral axis is not within a piezoelectric layer, this will ensure the maximum amount of energy can be generated in this range as well. It was assumed these findings applied to a multi-layer plate as well.

A binary capacitor array was next introduced for tuning purposes. By properly choosing the values of capacitors in the array, the capacitance could be varied with a certain resolution across a wide range of capacitance using a minimal amount of capacitors.

Mode shapes of beams were determined using Euler-Bernoulli beam theory and the equation to calculate the natural frequency of cantilever beam was derived. Mode shapes of plates were then calculated using a combination of the beam mode shapes. The natural frequency of a plate was derived using the Ritz method.

Analytical energy generation models were performed. This was begun with a static bimorph energy model that calculated the amount of energy generated from a static load using a strain energy method. Using the previously derived mode shapes, a similar method was used to find the energy in a base excited bimorph. Finally, a base excited plate energy model was given.

The capacitive tuning method was experimentally validated. The construction process of the bimorph energy harvesters used in testing was given first and followed by testing procedure and results. It was shown that it takes approximately a four-order magnitude change of the ratio of shunt capacitance to piezoelectric capacitance to change a piezoelectric bimorph from open circuit stiffness to short circuit stiffness. It is theoretically possible to achieve up to 2.94 percent tuning for a bimorph (with all layers approximately the same thickness) if both layers are used for tuning. Around 1.74 percent tuning can be obtained if only one layer is used. Experimentally up to 1.7 percent tuning was obtained using only one layer and 2.32 percent was obtained using both layers.

Effects on power harvesting were also studied. When using the capacitive array on only one layer, effects on the other layer are minimal. It has been shown that the magnitude of the power versus impedance remains relatively constant as the value of the capacitive shunt is increased. Tuning and harvesting from the same layer is also possible. However, as capacitance increases, the amount of power able to be generated decreases. The source impedance also

117

decreases. To harvest off of both layers at the same time a separate rectifier circuit should be used on each layer. Approximately 130 to 160 μW of power could be produced from each layer.

An overview of other possible tuning methods was given. It was shown that in order to harvest from multiple frequencies, the best method is to use a multi-beam array, where each beam in the array is designed to have a slightly different natural frequency and therefore the array spans a certain frequency band. A method to convert a low vibration source into energy using a high frequency harvester was discussed. Finally a variable stiffness beam was presented that could be changed from a high stiffness state to a low stiffness state and vice versa.

8.1   FUTURE WORK

From the experience of this research, several suggestions for future work can be recommended.

- In the energy harvesting model, damping and impedance values were assumed. To more accurately describe the energy models, the damping in the structure can be measured experimentally. Instead of using a load to find the impedance of the bimorphs, an impedance analyzer could be used to find exact values.

- Investigate the possibility of using energy from tuning layer to power a simple controller circuit that could automatically adjust capacitance to keep structure natural frequency matching source.

- Further characterize plate models to account for situations where the plate is not symmetrical.

- It is noted that at higher plate modes, there are stresses in each direction. Charge cancellation could occur when modes are symmetrical. Investigate possibility of

partitioning plates and re-poling the partitions so that the charge adds. Since the percentage of tuning remains the same, higher modes would have a larger tuning range and possibly a significant amount of energy that could be generated.

APPENDIX A

MATLAB CODE FOR AVAILABLE BEAM STIFFNESS

```matlab
%Tunability using only tuning layer for tuning

clear
%Layers:Substrate, Tuneable Layer, Harvesting Layer (case 1)
%Define constants
Eb=70e9;                                    %Substrate elastic modulus
Ep=6.2e10;                                  %Piezoelectric modulus
b=10e-3;                                     %Width of each layer
hp=0:.1:10;                                  %Thickness of piezoelectric layer
hb=0:.1:10;                                  %Thickness of tuning layer
ht=1;                            %Thickness of substrate
ep=3800*8.854e-12;                          %PZT relative permittivity
d31 = -320e-12;                             %PZT strain constant
L=1;

%basic calculations

At=b*ht;                                    %Area of substrate layer

Sp=1/Ep;                                    %PZT compliance
Etshort=Sp^-1;                              %Modulus of short circuited tuning
layer
Etopen=(Sp-d31^2/ep)^-1;                    %Modulus of open circuited tuning
layer
Epopen=(Sp-d31^2/ep)^-1
%Convert beam to entirely substrate material
np=Epopen/Eb;
ntshort=Etshort/Eb;
ntopen=Etopen/Eb;


%Calclulate location of neutral axis for each circuit case
for j=1:length(hp)
    for i=1:length(hb)
        %short circuit
        Ap(j)=b*hp(j);
        Ab(i)=b*hb(i);
```

```
ybarshort(i,j)=(hb(i)/2*Ab(i)+ntshort*At*(hb(i)+ht/2)+np*Ap(j)*(hb(i)+ht+hp(j
)/2))/(Ab(i)+ntshort*At+np*Ap(j));

        Ibshort(i,j)=(b*hb(i)^3)/12+Ab(i)*(ybarshort(i,j)-hb(i)/2)^2;
        Itshort(i,j)=(ntshort*b*ht^3)/12+ntshort*At*(ybarshort(i,j)-
(hb(i)+ht/2))^2;
        Ipshort(i,j)=(np*b*(hp(j))^3)/12+np*Ap(j)*(ybarshort(i,j)-
(hb(i)+ht+hp(j)/2))^2;
        Ishort(i,j)=Ibshort(i,j)+Itshort(i,j)+Ipshort(i,j);

        Ksc(i,j)=3*Eb*Ishort(i,j)/L;

        %open circuit

ybaropen(i,j)=(hb(i)/2*Ab(i)+ntopen*At*(hb(i)+ht/2)+np*Ap(j)*(hb(i)+ht+hp(j)/
2))/(Ab(i)+ntopen*At+np*Ap(j));

        Ibopen(i,j)=(b*hb(i)^3)/12+Ab(i)*(ybaropen(i,j)-hb(i)/2)^2;
        Itopen(i,j)=(ntopen*b*ht^3)/12+ntopen*At*(ybaropen(i,j)-
(hb(i)+ht/2))^2;
        Ipopen(i,j)=(np*b*(hp(j))^3)/12+np*Ap(j)*(ybaropen(i,j)-
(hb(i)+ht+hp(j)/2))^2;
        Iopen(i,j)=Ibopen(i,j)+Itopen(i,j)+Ipopen(i,j);

        Koc(i,j)=3*Eb*Iopen(i,j)/L;

    end
end

hbtratio=(hb/ht);
hptratio=(hp/ht);
figure(2)
mesh(hbtratio,hptratio,Koc./Ksc)
xlabel('hb/ht')
ylabel('hp/ht')
zlabel('Ratio of Effective Stiffness (koc/ksc)')
Title('Stiffness ratios vs layer thickness ratios (Case 1)')
-------------------------------------------------------------------------

%Tunability using both piezoelectric layers for tuning

clear
%Layers:Substrate, Tuneable Layer, Harvesting Layer (Case 1)
%Define constants
Eb=70e9;                                    %Substrate elastic modulus
Ep=6.2e10;                                  %Piezoelectric modulus
b=10e-3;                                    %Width of each layer
hp=0:.1:10;                                 %Thickness of piezoelectric layer
hb=0:.1:10;                                 %Thickness of tuning layer
ht=1;                           %Thickness of substrate
ep=3800*8.854e-12;                          %PZT relative permittivity
d31 = -320e-12;                             %PZT strain constant
L=1;

%basic calculations
```

```matlab
At=b*ht;                                        %Area of substrate layer

Sp=1/Ep;                                        %PZT compliance
Etshort=Sp^-1;                                  %Modulus of short circuited tuning
layer
Etopen=(Sp-d31^2/ep)^-1;                        %Modulus of open circuited tuning
layer
Epopen=(Sp-d31^2/ep)^-1
%Convert beam to entirely substrate material
npshort=Ep/Eb;
npopen=Epopen/Eb;
ntshort=Etshort/Eb;
ntopen=Etopen/Eb;


%Calclulate location of neutral axis for each circuit case
for j=1:length(hp)
    for i=1:length(hb)
        %short circuit
        Ap(j)=b*hp(j);
        Ab(i)=b*hb(i);

ybarshort(i,j)=(hb(i)/2*Ab(i)+ntshort*At*(hb(i)+ht/2)+npshort*Ap(j)*(hb(i)+ht
+hp(j)/2))/(Ab(i)+ntshort*At+npshort*Ap(j));

        Ibshort(i,j)=(b*hb(i)^3)/12+Ab(i)*(ybarshort(i,j)-hb(i)/2)^2;
        Itshort(i,j)=(ntshort*b*ht^3)/12+ntshort*At*(ybarshort(i,j)-
(hb(i)+ht/2))^2;
        Ipshort(i,j)=(npshort*b*(hp(j))^3)/12+npshort*Ap(j)*(ybarshort(i,j)-
(hb(i)+ht+hp(j)/2))^2;
        Ishort(i,j)=Ibshort(i,j)+Itshort(i,j)+Ipshort(i,j);

        Ksc(i,j)=3*Eb*Ishort(i,j)/L;

        %open circuit

ybaropen(i,j)=(hb(i)/2*Ab(i)+ntopen*At*(hb(i)+ht/2)+npopen*Ap(j)*(hb(i)+ht+hp
(j)/2))/(Ab(i)+ntopen*At+npopen*Ap(j));

        Ibopen(i,j)=(b*hb(i)^3)/12+Ab(i)*(ybaropen(i,j)-hb(i)/2)^2;
        Itopen(i,j)=(ntopen*b*ht^3)/12+ntopen*At*(ybaropen(i,j)-
(hb(i)+ht/2))^2;
        Ipopen(i,j)=(npopen*b*(hp(j))^3)/12+npopen*Ap(j)*(ybaropen(i,j)-
(hb(i)+ht+hp(j)/2))^2;
        Iopen(i,j)=Ibopen(i,j)+Itopen(i,j)+Ipopen(i,j);

        Koc(i,j)=3*Eb*Iopen(i,j)/L;

    end
end

hbtratio=(hb/ht);
hptratio=(hp/ht);
figure(2)
mesh(hbtratio,hptratio,Koc./Ksc)
xlabel('hb/ht')
```

```matlab
ylabel('hp/ht')
zlabel('Ratio of Effective Stiffness (koc/ksc)')
Title('Stiffness ratios vs layer thickness ratios (Case 1)')
%--------------------------------------------------------------------------

%Tunability using both piezoelectric layers for tuning

clear
%Layers:Substrate, Harvesting Layer, Tuning Layer (Case 2)
%Define constants
Eb=70e9;                                %Substrate elastic modulus
Ep=6.2e10;                              %Piezoelectric modulus
b=10e-3;                                %Width of each layer
hp=0:.1:10;                             %Thickness of piezoelectric layer
hb=0:.1:10;                             %Thickness of tuning layer
ht=1;                           %Thickness of substrate
ep=3800*8.854e-12;                      %PZT relative permittivity
d31 = -320e-12;                         %PZT strain constant
L=1;


%basic calculations

At=b*ht;                                %Area of substrate layer

Sp=1/Ep;                                %PZT compliance
Etshort=Sp^-1;                          %Modulus of short circuited tuning
layer
Etopen=(Sp-d31^2/ep)^-1;                %Modulus of open circuited tuning
layer
Epopen=(Sp-d31^2/ep)^-1
Epshort=Sp^-1;
%Convert beam to entirely substrate material
npopen=Epopen/Eb;
npshort=Epshort/Eb;
ntshort=Etshort/Eb;
ntopen=Etopen/Eb;


%Calclulate location of neutral axis for each circuit case
for j=1:length(hp)
    for i=1:length(hb)
        %short circuit
        Ap(j)=b*hp(j);
        Ab(i)=b*hb(i);

ybarshort(i,j)=(hb(i)/2*Ab(i)+npshort*Ap(j)*(hb(i)+hp(j)/2)+ntshort*At*(hb(i)
+hp(j)+ht/2))/(Ab(i)+ntshort*At+npshort*Ap(j));
        Ibshort(i,j)=(b*hb(i)^3)/12+Ab(i)*(ybarshort(i,j)-hb(i)/2)^2;
        Ipshort(i,j)=(npshort*b*(hp(j))^3)/12+npshort*Ap(j)*(ybarshort(i,j)-
(hb(i)+hp(j)/2))^2;
        Itshort(i,j)=(ntshort*b*ht^3)/12+ntshort*At*(ybarshort(i,j)-
(hb(i)+hp(j)+ht/2))^2;
        Ishort(i,j)=Ibshort(i,j)+Itshort(i,j)+Ipshort(i,j);

        Ksc(i,j)=3*Eb*Ishort(i,j)/L;

        %open circuit
```

123

```
ybaropen(i,j)=(hb(i)/2*Ab(i)+npopen*Ap(j)*(hb(i)+hp(j)/2)+ntopen*At*(hb(i)+hp
(j)+ht/2))/(Ab(i)+ntopen*At+npopen*Ap(j));
        Ibopen(i,j)=(b*hb(i)^3)/12+Ab(i)*(ybaropen(i,j)-hb(i)/2)^2;
        Ipopen(i,j)=(npopen*b*(hp(j))^3)/12+npopen*Ap(j)*(ybaropen(i,j)-
(hb(i)+hp(j)/2))^2;
        Itopen(i,j)=(ntopen*b*ht^3)/12+ntopen*At*(ybaropen(i,j)-
(hb(i)+hp(j)+ht/2))^2;
        Iopen(i,j)=Ibopen(i,j)+Itopen(i,j)+Ipopen(i,j);

        Koc(i,j)=3*Eb*Iopen(i,j)/L;

    end
end

hbtratio=(hb/ht);
hptratio=(hp/ht);
mesh(hbtratio,hptratio,Koc./Ksc)
xlabel('hb/ht')
ylabel('hp/ht')
zlabel('Ratio of Effective Stiffness (koc/ksc)')
Title('Stiffness ratios vs layer thickness ratios (Case 2)')
-------------------------------------------------------------------------

%Tunability using both piezoelectric layers for tuning

clear
%Layers:Tuning Layer ,Substrate Layer, Harvesting Layer (Case 3)
%Define constants
Eb=70e9;                                 %Substrate elastic modulus
Ep=6.2e10;                               %Piezoelectric modulus
b=10e-3;                                 %Width of each layer
hp=0:.1:10;                              %Thickness of piezoelectric layer
hb=0:.1:10;                              %Thickness of tuning layer
ht=1;                                    %Thickness of substrate
ep=3800*8.854e-12;                       %PZT relative permittivity
d31 = -320e-12;                          %PZT strain constant
L=1;

%basic calculations

At=b*ht;                                 %Area of tuning layer

Sp=1/Ep;                                 %PZT compliance
Etshort=Sp^-1;                           %Modulus of short circuited tuning
layer
Etopen=(Sp-d31^2/ep)^-1;                 %Modulus of open circuited tuning
layer
Epshort=Ep;
Epopen=(Sp-d31^2/ep)^-1
%Convert beam to entirely substrate material
npopen=Epopen/Eb;
npshort=Epshort/Eb;
ntshort=Etshort/Eb;
ntopen=Etopen/Eb;
```

```matlab
%Calclulate location of neutral axis for each circuit case
for j=1:length(hp)
    for i=1:length(hb)
        %short circuit
        Ap(j)=b*hp(j);
        Ab(i)=b*hb(i);

ybarshort(i,j)=(ntshort*ht/2*At+Ab(i)*(ht+hb(i)/2)+npshort*Ap(j)*(ht+hb(i)+hp
(j)/2))/(Ab(i)+ntshort*At+npshort*Ap(j));
        Ibshort(i,j)=(b*hb(i)^3)/12+Ab(i)*(ybarshort(i,j)-(ht+hb(i)/2))^2;
        Ipshort(i,j)=(npshort*b*(hp(j))^3)/12+npshort*Ap(j)*(ybarshort(i,j)-
(ht+hb(i)+hp(j)/2))^2;
        Itshort(i,j)=(ntshort*b*ht^3)/12+ntshort*At*(ybarshort(i,j)-
(ht/2))^2;
        Ishort(i,j)=Ibshort(i,j)+Itshort(i,j)+Ipshort(i,j);

        Ksc(i,j)=3*Eb*Ishort(i,j)/L;

        %open circuit

ybaropen(i,j)=(ntopen*ht/2*At+Ab(i)*(ht+hb(i)/2)+npopen*Ap(j)*(ht+hb(i)+hp(j)
/2))/(Ab(i)+ntopen*At+npopen*Ap(j));
        Ibopen(i,j)=(b*hb(i)^3)/12+Ab(i)*(ybaropen(i,j)-(ht+hb(i)/2))^2;
        Ipopen(i,j)=(npopen*b*(hp(j))^3)/12+npopen*Ap(j)*(ybaropen(i,j)-
(ht+hb(i)+hp(j)/2))^2;
        Itopen(i,j)=(ntopen*b*ht^3)/12+ntopen*At*(ybaropen(i,j)-(ht/2))^2;
        Iopen(i,j)=Ibopen(i,j)+Itopen(i,j)+Ipopen(i,j);

        Koc(i,j)=3*Eb*Iopen(i,j)/L;

    end
end

hbtratio=(hb/ht);
hptratio=(hp/ht);
mesh(hbtratio,hptratio,Koc./Ksc)
xlabel('hb/ht')
ylabel('hp/ht')
zlabel('Ratio of Effective Stiffness (koc/ksc)')
Title('Stiffness ratios vs layer thickness ratios (Case 3)')
-------------------------------------------------------------------------


%Tunability using only tuning layer for tuning

clear
%Layers:Substrate, Harvesting Layer, Tuning Layer (Case 2)
%Define constants
Eb=70e9;                                 %Substrate elastic modulus
Ep=6.2e10;                               %Piezoelectric modulus
b=10e-3;                                 %Width of each layer
hp=0:.1:10;                              %Thickness of piezoelectric layer
hb=0:.1:10;                              %Thickness of tuning layer
ht=1;                          %Thickness of substrate
ep=3800*8.854e-12;                       %PZT relative permittivity
d31 = -320e-12;                          %PZT strain constant
```

```matlab
L=1;

%basic calculations

At=b*ht;                                        %Area of substrate layer

Sp=1/Ep;                                        %PZT compliance
Etshort=Sp^-1;                                  %Modulus of short circuited tuning
layer
Etopen=(Sp-d31^2/ep)^-1;                        %Modulus of open circuited tuning
layer
Epopen=(Sp-d31^2/ep)^-1
%Convert beam to entirely substrate material
np=Epopen/Eb;
ntshort=Etshort/Eb;
ntopen=Etopen/Eb;



%Calclulate location of neutral axis for each circuit case
for j=1:length(hp)
    for i=1:length(hb)
        %short circuit
        Ap(j)=b*hp(j);
        Ab(i)=b*hb(i);

ybarshort(i,j)=(hb(i)/2*Ab(i)+np*Ap(j)*(hb(i)+hp(j)/2)+ntshort*At*(hb(i)+hp(j
)+ht/2))/(Ab(i)+ntshort*At+np*Ap(j));
        Ibshort(i,j)=(b*hb(i)^3)/12+Ab(i)*(ybarshort(i,j)-hb(i)/2)^2;
        Ipshort(i,j)=(np*b*(hp(j))^3)/12+np*Ap(j)*(ybarshort(i,j)-
(hb(i)+hp(j)/2))^2;
        Itshort(i,j)=(ntshort*b*ht^3)/12+ntshort*At*(ybarshort(i,j)-
(hb(i)+hp(j)+ht/2))^2;
        Ishort(i,j)=Ibshort(i,j)+Itshort(i,j)+Ipshort(i,j);

        Ksc(i,j)=3*Eb*Ishort(i,j)/L;

        %open circuit

ybaropen(i,j)=(hb(i)/2*Ab(i)+np*Ap(j)*(hb(i)+hp(j)/2)+ntopen*At*(hb(i)+hp(j)+
ht/2))/(Ab(i)+ntopen*At+np*Ap(j));
        Ibopen(i,j)=(b*hb(i)^3)/12+Ab(i)*(ybaropen(i,j)-hb(i)/2)^2;
        Ipopen(i,j)=(np*b*(hp(j))^3)/12+np*Ap(j)*(ybaropen(i,j)-
(hb(i)+hp(j)/2))^2;
        Itopen(i,j)=(ntopen*b*ht^3)/12+ntopen*At*(ybaropen(i,j)-
(hb(i)+hp(j)+ht/2))^2;
        Iopen(i,j)=Ibopen(i,j)+Itopen(i,j)+Ipopen(i,j);

        Koc(i,j)=3*Eb*Iopen(i,j)/L;

    end
end

hbtratio=(hb/ht);
hptratio=(hp/ht);
mesh(hbtratio,hptratio,Koc./Ksc)
xlabel('hb/ht')
ylabel('hp/ht')
```

```matlab
zlabel('Ratio of Effective Stiffness (koc/ksc)')
Title('Stiffness ratios vs layer thickness ratios (Case 2)')
```

```matlab
%Tunability using only tuning layer for tuning (Case 3)

clear
%Layers:Tuning Layer ,Substrate Layer, Harvesting Layer
%Define constants
Eb=70e9;                                    %Substrate elastic modulus
Ep=6.2e10;                                  %Piezoelectric modulus
b=10e-3;                                     %Width of each layer
hp=0:.1:10;                                  %Thickness of piezoelectric layer
hb=0:.1:10;                                  %Thickness of tuning layer
ht=1;                             %Thickness of substrate
ep=3800*8.854e-12;                          %PZT relative permittivity
d31 = -320e-12;                             %PZT strain constant
L=1;


%basic calculations

At=b*ht;                                    %Area of tuning layer

Sp=1/Ep;                                    %PZT compliance
Etshort=Sp^-1;                              %Modulus of short circuited tuning
layer
Etopen=(Sp-d31^2/ep)^-1;                    %Modulus of open circuited tuning
layer
Epopen=(Sp-d31^2/ep)^-1
%Convert beam to entirely substrate material
np=Epopen/Eb;
ntshort=Etshort/Eb;
ntopen=Etopen/Eb;


%Calclulate location of neutral axis for each circuit case
for j=1:length(hp)
    for i=1:length(hb)
        %short circuit
        Ap(j)=b*hp(j);
        Ab(i)=b*hb(i);

ybarshort(i,j)=(ntshort*ht/2*At+Ab(i)*(ht+hb(i)/2)+np*Ap(j)*(ht+hb(i)+hp(j)/2
))/(Ab(i)+ntshort*At+np*Ap(j));
        Ibshort(i,j)=(b*hb(i)^3)/12+Ab(i)*(ybarshort(i,j)-(ht+hb(i)/2))^2;
        Ipshort(i,j)=(np*b*(hp(j))^3)/12+np*Ap(j)*(ybarshort(i,j)-
(ht+hb(i)+hp(j)/2))^2;
        Itshort(i,j)=(ntshort*b*ht^3)/12+ntshort*At*(ybarshort(i,j)-
(ht/2))^2;
        Ishort(i,j)=Ibshort(i,j)+Itshort(i,j)+Ipshort(i,j);

        Ksc(i,j)=3*Eb*Ishort(i,j)/L;

        %open circuit
```

```
ybaropen(i,j)=(ntopen*ht/2*At+Ab(i)*(ht+hb(i)/2)+np*Ap(j)*(ht+hb(i)+hp(j)/2))
/(Ab(i)+ntopen*At+np*Ap(j));
        Ibopen(i,j)=(b*hb(i)^3)/12+Ab(i)*(ybaropen(i,j)-(ht+hb(i)/2))^2;
        Ipopen(i,j)=(np*b*(hp(j))^3)/12+np*Ap(j)*(ybaropen(i,j)-
(ht+hb(i)+hp(j)/2))^2;
        Itopen(i,j)=(ntopen*b*ht^3)/12+ntopen*At*(ybaropen(i,j)-(ht/2))^2;
        Iopen(i,j)=Ibopen(i,j)+Itopen(i,j)+Ipopen(i,j);

        Koc(i,j)=3*Eb*Iopen(i,j)/L;

    end
end

hbtratio=(hb/ht);
hptratio=(hp/ht);
mesh(hbtratio,hptratio,Koc./Ksc)
xlabel('hb/ht')
ylabel('hp/ht')
zlabel('Ratio of Effective Stiffness (koc/ksc)')
Title('Stiffness ratios vs layer thickness ratios (Case 3)')
```

APPENDIX B

MATLAB CODE FOR BEAM AND PLATE MODE SHAPES

```matlab
%Calculates 1st five mode shapes for a free-free beam, clamped-free beam,
%and a cantilever plate
clear
close all

%values for a clamped-free beam
lamda=[1.8751041 4.6940911 7.8547574 10.9955407 14.1371684];
alpha=[.7340955 1.01846644 .9992245 1.00003355 .99999855];
x=linspace(0,1,100);

%values for a free-free beam
mu=[0 0 4.7300408 7.8532046 10.9956078]
beta=[0 0 0.98250222 1.00077731 .99996645 1.00000145]
y=linspace(0,1,100);

a=1;
b=1;

for i=1:length(lamda)
    for j=1:length(x)
X(i,j)=.5*(cosh(lamda(i)*x(j)/a)-cos(lamda(i)*x(j)/a)-
alpha(i)*[sinh(lamda(i)*x(j)/a)-sin(lamda(i)*x(j)/a)]);
Y(i,j)=.5*(cosh(mu(i)*y(j)/b)+cos(mu(i)*y(j)/a)-
beta(i)*[sinh(mu(i)*y(j)/b)+sin(mu(i)*y(j)/b)]);
    end
end

for j=1:length(y)
    Y(1,j)=1;
    Y(2,j)=sqrt(3)*(1-2*y(j)/b);
end


mode1=X(1,:)'*Y(1,:);
mode2=X(1,:)'*Y(2,:);
mode3=X(2,:)'*Y(1,:);
mode4=X(1,:)'*Y(3,:);
```

129

```
mode5=X(2,:)'*Y(2,:);

figure(1)
mesh(x,y,mode1)
xlabel('x/a')
ylabel('y/b')
title('Normalized mode shape for mode 1')

figure(2)
mesh(x,y,mode2)
xlabel('x/a')
ylabel('y/b')
title('Normalized mode shape for mode 2')

figure(3)
mesh(x,y,mode3)
xlabel('x/a')
ylabel('y/b')
title('Normalized mode shape for mode 3')

figure(4)
mesh(x,y,mode4)
xlabel('x/a')
ylabel('y/b')
title('Normalized mode shape for mode 4')

figure(5)
mesh(x,y,mode5)
xlabel('x/a')
ylabel('y/b')
title('Normalized mode shape for mode 5')

figure(6)
plot(x/a,Y(1,:),'r')
hold
plot(x/a,Y(2,:),'b')
plot(x/a,Y(3,:),'g')
plot(x/a,Y(4,:),'+')
plot(x/a,Y(5,:),'^')
Title('Mode shapes for a free-free beam')
xlabel('x/b')
ylabel('Normalized magnitude')
legend('1st mode','2nd mode','3rd mode','4th mode','5th mode')

figure(7)
plot(x/a,X(1,:),'r')
hold
plot(x/a,X(2,:),'b')
plot(x/a,X(3,:),'g')
plot(x/a,X(4,:),'+')
plot(x/a,X(5,:),'^')
Title('Mode shapes for a clamped-free beam')
xlabel('x/a')
ylabel('Normalized magnitude')
legend('1st mode','2nd mode','3rd mode','4th mode','5th mode')
```

APPENDIX C

MATHCAD CODE FOR STATIC BEAM MODEL

Energy Generation from a Static Input

Calculate neutral axis

$$nt := \frac{Et}{Eb} \qquad np := \frac{Ep}{Eb}$$

$$Ep3 := \frac{Vp}{tp} \qquad Et3 := \frac{Vt}{tp}$$

$$Ap := np \cdot b \cdot tp$$

$$At := nt \cdot b \cdot tp$$

$$Ab := b \cdot tb$$
$$A := Ap + At + Ab$$

$$ybar := \frac{\left[\frac{tp}{2} \cdot Ap - \frac{tb}{2} \cdot Ab - \left(tb + \frac{tp}{2}\right) \cdot At\right]^{\blacksquare}}{A}$$

Find Curvature

$$F \cdot (L - x) = \begin{bmatrix} \displaystyle\int_{-tb}^{0} Eb \cdot \kappa \cdot (y - ybar) \cdot (y - ybar) \cdot b \; dy \; ... \\[2em] + \displaystyle\int_{0}^{tp} Ep \cdot \left[\kappa \cdot (y - ybar) - d31 \cdot Ep3 \right] \cdot (y - ybar) \cdot b \; dy \end{bmatrix} \quad ... \\[3em] + \int_{-tb-tp}^{-tb} Et \cdot \left[\kappa \cdot (y - ybar) - d31 \cdot Et3 \right] \cdot (y - ybar) \cdot b \; dy$$

$$B := b \cdot \left(3 \cdot Eb \cdot tb \cdot ybar^2 + 3 \cdot Ep \cdot ybar^2 \cdot tp + 3 \cdot Et \cdot tb^2 \cdot tp + 3 \cdot Et \cdot tb \cdot tp^2 + Et \cdot tp^3 + 6 \cdot Et \cdot ybar \cdot tb \cdot tp \; ... \right. \\ \left. + 3 \cdot Et \cdot tp^2 \cdot ybar + Eb \cdot tb^3 + 3 \cdot Eb \cdot tb^2 \cdot ybar + 3 \cdot Et \cdot ybar^2 \cdot tp + Ep \cdot tp^3 - 3 \cdot Ep \cdot tp^2 \cdot ybar \right) \blacksquare$$

$$\kappa := \frac{-3}{2} \cdot \frac{-2 \cdot L + 2 \cdot x}{B} \cdot F - \frac{3}{2} \cdot \frac{2 \cdot Et \cdot b \cdot d31 \cdot tb \cdot tp + Et \cdot b \cdot d31 \cdot tp^2 + 2 \cdot Et \cdot b \cdot ybar \cdot d31 \cdot tp}{B} \cdot Et \\[1.5em] + \left(\frac{-3}{2} \cdot \frac{-Ep \cdot b \cdot tp^2 \cdot d31 + 2 \cdot Ep \cdot b \cdot ybar \cdot tp \cdot d31}{B} \cdot Ep3 \right)$$

Define stresses of each layer

$$\sigma t := Et \cdot \left[\kappa \cdot (y - ybar) - d31 \cdot Et3 \right]$$

$$\sigma b := Eb \cdot \left[\kappa \cdot (y - ybar) \right]$$

$$U1 := \int_{0}^{L} \int_{0}^{b} \left(\int_{-tb-tp}^{-tp} dUt \; dy \right) dz \, dx$$

$$\sigma p := Ep \cdot \left[\kappa \cdot (y - ybar) - d31 \cdot Ep3 \right]$$

$$dUp := \frac{1 \cdot \sigma p^2}{2 \cdot Ep} + d31 \cdot Ep3 \cdot \sigma p + \frac{1}{2} \cdot \varepsilon \cdot Ep3^2$$

$$U2 := \int_{0}^{L} \int_{0}^{b} \left(\int_{-tb}^{0} dUb \; dy \right) dz \, dx$$

$$dUt := \frac{1 \cdot \sigma p^2}{2 \cdot Ep} + d31 \cdot Et3 \cdot \sigma p + \frac{1}{2} \cdot \varepsilon \cdot Et3^2$$

$$U3 := \int_{0}^{L} \int_{0}^{b} \left(\int_{0}^{tp} dUp \; dy \right) dz \, dx$$

$$dUb := \frac{1}{2 \cdot Eb} \cdot \sigma b^2$$

132

$$Q1 := \frac{d}{dVp} U1 \qquad Q2 := \frac{d}{dVp} U2 \qquad Q3 := \frac{d}{dVp} U3$$

$$Qgen := \frac{3}{4} \cdot b \cdot L^2 \cdot Ep \cdot \frac{d31}{tp} \cdot F \cdot \frac{\begin{array}{l} 3 \cdot b \cdot Ep \cdot tb \cdot tp^4 + 3 \cdot b \cdot Ep \cdot tp^3 \cdot tb^2 + tb^2 \cdot B - 3 \cdot b \cdot Ep \cdot tp^2 \cdot tb^2 \cdot ybar \ ... \\ + 2 \cdot tb \cdot ybar \cdot B + 2 \cdot tp \cdot tb \cdot B - 2 \cdot b \cdot Ep \cdot tp \cdot tb^3 \cdot ybar + b \cdot Ep \cdot tp^2 \cdot tb^3 \ ... \\ + \left(-6 \cdot b \cdot Ep \cdot tp \cdot tb^2 \cdot ybar^2 \right) - 6 \cdot tb \cdot b \cdot Ep \cdot tp \cdot ybar^3 - 9 \cdot b \cdot Ep \cdot tp^2 \cdot tb \cdot ybar^2 \ ... \\ + 6 \cdot Eb \cdot tb^2 \cdot b \cdot tp \cdot ybar^2 + 3 \cdot Eb \cdot tb^2 \cdot b \cdot tp^2 \cdot ybar + Eb \cdot tb^3 \cdot b \cdot tp^2 \ ... \\ + \left(-6 \cdot Eb \cdot tb \cdot b \cdot tp \cdot ybar^3 \right) + 3 \cdot Eb \cdot tb \cdot b \cdot tp^2 \cdot ybar^2 - 2 \cdot Eb \cdot tb^3 \cdot b \cdot tp \cdot ybar \ ... \\ + \left(-6 \cdot b \cdot Ep \cdot tp^2 \cdot ybar^3 \right) - 5 \cdot b \cdot Ep \cdot tp^4 \cdot ybar + b \cdot Ep \cdot tp^5 + 9 \cdot b \cdot Ep \cdot tp^3 \cdot ybar^2 \end{array}}{B^2}$$

$$Cfree := \frac{d^2}{dVp^2} U1 + \frac{d^2}{dVp^2} U2 + \frac{d^2}{dVp^2} U3$$

$$Cfree := \frac{1}{4} \cdot b \cdot L \cdot \frac{\begin{array}{l} 57 \cdot b^2 \cdot Ep^3 \cdot tp^5 \cdot d31^2 \cdot ybar^2 - 21 \cdot b^2 \cdot Ep^3 \cdot tp^6 \cdot d31^2 \cdot ybar + 36 \cdot b^2 \cdot Ep^3 \cdot tp^3 \cdot d31^2 \cdot ybar^4 \ ... \\ + \left(-72 \cdot b^2 \cdot Ep^3 \cdot tp^4 \cdot d31^2 \cdot ybar^3 \right) + 9 \cdot tb^2 \cdot Ep^3 \cdot d31^2 \cdot b^2 \cdot tp^5 + 9 \cdot tb \cdot Ep^3 \cdot d31^2 \cdot b^2 \cdot tp^6 \ ... \\ + \left(-4 \cdot tp \cdot Ep \cdot d31^2 \cdot B^2 \right) + 4 \cdot tb \cdot Ep \cdot d31^2 \cdot B^2 + 3 \cdot b^2 \cdot Ep^3 \cdot d31^2 \cdot tp^7 + 3 \cdot tb^3 \cdot Ep^3 \cdot d31^2 \cdot b^2 \cdot tp^4 \ ... \\ + 4 \cdot tp \cdot \varepsilon \cdot B^2 + 3 \cdot Eb \cdot tb^3 \cdot b^2 \cdot Ep^2 \cdot d31^2 \cdot tp^4 + 36 \cdot tb \cdot Ep^3 \cdot d31^2 \cdot b^2 \cdot tp^3 \cdot ybar^3 \ ... \\ + \left(-27 \cdot tb \cdot Ep^3 \cdot d31^2 \cdot b^2 \cdot tp^4 \cdot ybar^2 \right) + 36 \cdot tb \cdot Ep^3 \cdot d31^2 \cdot b^2 \cdot tp^2 \cdot ybar^4 \ ... \\ + 12 \cdot tb \cdot Ep^2 \cdot d31^2 \cdot b \cdot tp^3 \cdot B - 27 \cdot tb^2 \cdot Ep^3 \cdot d31^2 \cdot b^2 \cdot tp^4 \cdot ybar \ ... \\ + 12 \cdot tb^3 \cdot Ep^3 \cdot d31^2 \cdot b^2 \cdot tp^2 \cdot ybar^2 - 12 \cdot tb^3 \cdot Ep^3 \cdot d31^2 \cdot b^2 \cdot tp^3 \cdot ybar \ ... \\ + 36 \cdot tb^2 \cdot Ep^3 \cdot d31^2 \cdot b^2 \cdot tp^2 \cdot ybar^3 - 18 \cdot tb \cdot Ep^3 \cdot d31^2 \cdot b^2 \cdot tp^5 \cdot ybar \ ... \\ + 6 \cdot tb^2 \cdot Ep^2 \cdot d31^2 \cdot b \cdot tp^2 \cdot B - 12 \cdot tb^2 \cdot Ep^2 \cdot d31^2 \cdot b \cdot tp \cdot ybar \cdot B - 24 \cdot tb \cdot Ep^2 \cdot d31^2 \cdot b \cdot tp \cdot ybar^2 \cdot B \ ... \\ + \left(-12 \cdot Eb \cdot tb^3 \cdot b^2 \cdot Ep^2 \cdot d31^2 \cdot tp^3 \cdot ybar \right) - 36 \cdot Eb \cdot tb^2 \cdot b^2 \cdot Ep^2 \cdot d31^2 \cdot tp^3 \cdot ybar^2 \ ... \\ + 36 \cdot Eb \cdot tb \cdot b^2 \cdot Ep^2 \cdot d31^2 \cdot tp^2 \cdot ybar^4 + 12 \cdot Eb \cdot tb^3 \cdot b^2 \cdot Ep^2 \cdot d31^2 \cdot tp^2 \cdot ybar^2 \ ... \\ + 9 \cdot Eb \cdot tb \cdot b^2 \cdot Ep^2 \cdot d31^2 \cdot tp^4 \cdot ybar^2 + 36 \cdot Eb \cdot tb^2 \cdot b^2 \cdot Ep^2 \cdot d31^2 \cdot tp^2 \cdot ybar^3 \ ... \\ + \left(-12 \cdot tb \cdot Ep^2 \cdot d31^2 \cdot b \cdot tp^2 \cdot ybar \cdot B \right) - 36 \cdot Eb \cdot tb \cdot b^2 \cdot Ep^2 \cdot d31^2 \cdot tp^3 \cdot ybar^3 \ ... \\ + 9 \cdot Eb \cdot tb^2 \cdot b^2 \cdot Ep^2 \cdot d31^2 \cdot tp^4 \cdot ybar \end{array}}{B^2 \cdot tp^2}$$

$$V_{gen} := \frac{Q_{gen}}{C_{free}}$$

$V_{gen} := 3 \cdot L \cdot d31 \cdot E_p \cdot tp \cdot F \cdot$

$$\frac{\begin{array}{l} 3 \cdot b \cdot E_p \cdot tb \cdot tp^4 + 3 \cdot b \cdot E_p \cdot tp^3 \cdot tb^2 + tb^2 \cdot B - 3 \cdot b \cdot E_p \cdot tp^2 \cdot tb^2 \cdot ybar \ \ldots \\ + 2 \cdot tb \cdot ybar \cdot B + 2 \cdot tp \cdot tb \cdot B - 2 \cdot b \cdot E_p \cdot tp \cdot tb^3 \cdot ybar + b \cdot E_p \cdot tp^2 \cdot tb^3 \ \ldots \\ + \left(-6 \cdot b \cdot E_p \cdot tp \cdot tb^2 \cdot ybar^2\right) - 6 \cdot tb \cdot b \cdot E_p \cdot tp \cdot ybar^3 - 9 \cdot b \cdot E_p \cdot tp^2 \cdot tb \cdot ybar^2 \ \ldots \\ + \left(-6 \cdot Eb \cdot tb^2 \cdot b \cdot tp \cdot ybar^2\right) + 3 \cdot Eb \cdot tb^2 \cdot b \cdot tp^2 \cdot ybar + Eb \cdot tb^3 \cdot b \cdot tp^2 \ \ldots \\ + \left(-6 \cdot Eb \cdot tb \cdot b \cdot tp \cdot ybar^3\right) + 3 \cdot Eb \cdot tb \cdot b \cdot tp^2 \cdot ybar^2 - 2 \cdot Eb \cdot tb^3 \cdot b \cdot tp \cdot ybar \ \ldots \\ + \left(-6 \cdot b \cdot E_p \cdot tp^2 \cdot ybar^3\right) - 5 \cdot b \cdot E_p \cdot tp^4 \cdot ybar + b \cdot E_p \cdot tp^5 + 9 \cdot b \cdot E_p \cdot tp^3 \cdot ybar^2 \end{array}}{\begin{array}{l} 57 \cdot b^2 \cdot E_p^3 \cdot tp^5 \cdot d31^2 \cdot ybar^2 - 21 \cdot b^2 \cdot E_p^3 \cdot tp^6 \cdot d31^2 \cdot ybar \ \ldots \\ + 36 \cdot b^2 \cdot E_p^3 \cdot tp^3 \cdot d31^2 \cdot ybar^4 - 72 \cdot b^2 \cdot E_p^3 \cdot tp^4 \cdot d31^2 \cdot ybar^3 \ \ldots \\ + 9 \cdot tb^2 \cdot E_p^3 \cdot d31^2 \cdot b^2 \cdot tp^5 + 9 \cdot tb \cdot E_p^3 \cdot d31^2 \cdot b^2 \cdot tp^6 - 4 \cdot tp \cdot E_p \cdot d31^2 \cdot B^2 \ \ldots \\ + 4 \cdot tb \cdot E_p \cdot d31^2 \cdot B^2 + 3 \cdot b^2 \cdot E_p^3 \cdot d31^2 \cdot tp^7 + 3 \cdot tb^3 \cdot E_p^3 \cdot d31^2 \cdot b^2 \cdot tp^4 + 4 \cdot tp \cdot \varepsilon \cdot B^2 \ \ldots \\ + 3 \cdot Eb \cdot tb^3 \cdot b^2 \cdot E_p^2 \cdot d31^2 \cdot tp^4 + 36 \cdot tb \cdot E_p^3 \cdot d31^2 \cdot b^2 \cdot tp^3 \cdot ybar^3 \ \ldots \\ + \left(-27 \cdot tb \cdot E_p^3 \cdot d31^2 \cdot b^2 \cdot tp^4 \cdot ybar^2\right) + 36 \cdot tb \cdot E_p^3 \cdot d31^2 \cdot b^2 \cdot tp^2 \cdot ybar^4 \ \ldots \\ + 12 \cdot tb \cdot E_p^2 \cdot d31^2 \cdot b \cdot tp^3 \cdot B - 27 \cdot tb^2 \cdot E_p^3 \cdot d31^2 \cdot b^2 \cdot tp^4 \cdot ybar \ \ldots \\ + 12 \cdot tb^3 \cdot E_p^3 \cdot d31^2 \cdot b^2 \cdot tp^2 \cdot ybar^2 - 12 \cdot tb^3 \cdot E_p^3 \cdot d31^2 \cdot b^2 \cdot tp^3 \cdot ybar \ \ldots \\ + 36 \cdot tb^2 \cdot E_p^3 \cdot d31^2 \cdot b^2 \cdot tp^2 \cdot ybar^3 - 18 \cdot tb \cdot E_p^3 \cdot d31^2 \cdot b^2 \cdot tp^5 \cdot ybar \ \ldots \\ + 6 \cdot tb^2 \cdot E_p^2 \cdot d31^2 \cdot b \cdot tp^2 \cdot B - 12 \cdot tb^2 \cdot E_p^2 \cdot d31^2 \cdot b \cdot tp \cdot ybar \cdot B \ \ldots \\ + \left(-24 \cdot tb \cdot E_p^2 \cdot d31^2 \cdot b \cdot tp \cdot ybar^2 \cdot B\right) - 12 \cdot Eb \cdot tb^3 \cdot b^2 \cdot E_p^2 \cdot d31^2 \cdot tp^3 \cdot ybar \ \ldots \\ + 36 \cdot Eb \cdot tb^2 \cdot b^2 \cdot E_p^2 \cdot d31^2 \cdot tp^3 \cdot ybar^2 + 36 \cdot Eb \cdot tb \cdot b^2 \cdot E_p^2 \cdot d31^2 \cdot tp^2 \cdot ybar^4 \ \ldots \\ + 12 \cdot Eb \cdot tb^3 \cdot b^2 \cdot E_p^2 \cdot d31^2 \cdot tp^2 \cdot ybar^2 + 9 \cdot Eb \cdot tb \cdot b^2 \cdot E_p^2 \cdot d31^2 \cdot tp^4 \cdot ybar^2 \ \ldots \\ + 36 \cdot Eb \cdot tb^2 \cdot b^2 \cdot E_p^2 \cdot d31^2 \cdot tp^2 \cdot ybar^3 - 12 \cdot tb \cdot E_p^2 \cdot d31^2 \cdot b \cdot tp^2 \cdot ybar \cdot B \ \ldots \\ + \left(-36 \cdot Eb \cdot tb \cdot b^2 \cdot E_p^2 \cdot d31^2 \cdot tp^3 \cdot ybar^3\right) + 9 \cdot Eb \cdot tb^2 \cdot b^2 \cdot E_p^2 \cdot d31^2 \cdot tp^4 \cdot ybar \end{array}}$$

$$\text{Ugen} := \frac{1}{2} \cdot \text{Cfree} \cdot \text{Vgen}^2$$

$$\text{Ugen} := \frac{9 \cdot b \cdot F^2 \cdot Ep^2 \cdot d31^2 \cdot L^3}{8 \cdot B^2} \cdot \frac{\left(\begin{array}{l} 3 \cdot b \cdot Ep \cdot tb \cdot tp^4 + 3 \cdot b \cdot Ep \cdot tp^3 \cdot tb^2 + tb^2 \cdot B - 3 \cdot b \cdot Ep \cdot tp^2 \cdot tb^2 \cdot ybar \ldots \\ + 2 \cdot tb \cdot ybar \cdot B + 2 \cdot tp \cdot tb \cdot B - 2 \cdot b \cdot Ep \cdot tp \cdot tb^3 \cdot ybar + b \cdot Ep \cdot tp^2 \cdot tb^3 \ldots \\ + -6 \cdot b \cdot Ep \cdot tp \cdot tb^2 \cdot ybar^2 - 6 \cdot tb \cdot b \cdot Ep \cdot tp \cdot ybar^3 \ldots \\ + 9 \cdot b \cdot Ep \cdot tp^2 \cdot tb \cdot ybar^2 - 6 \cdot Eb \cdot tb^2 \cdot b \cdot tp \cdot ybar^2 + 3 \cdot Eb \cdot tb^2 \cdot b \cdot tp^2 \cdot ybar \ldots \\ + Eb \cdot tb^3 \cdot b \cdot tp^2 - 6 \cdot Eb \cdot tb \cdot b \cdot tp \cdot ybar^3 + 3 \cdot Eb \cdot tb \cdot b \cdot tp^2 \cdot ybar^2 \ldots \\ + 2 \cdot Eb \cdot tb^3 \cdot b \cdot tp \cdot ybar - 6 \cdot b \cdot Ep \cdot tp^2 \cdot ybar^3 - 5 \cdot b \cdot Ep \cdot tp^4 \cdot ybar + b \cdot Ep \cdot tp^5 \ldots \\ + 9 \cdot b \cdot Ep \cdot tp^3 \cdot ybar^2 \end{array} \right)^2}{\begin{array}{l} 57 \cdot b^2 \cdot Ep^3 \cdot tp^5 \cdot d31^2 \cdot ybar^2 - 21 \cdot b^2 \cdot Ep^3 \cdot tp^6 \cdot d31^2 \cdot ybar \ldots \\ + 36 \cdot b^2 \cdot Ep^3 \cdot tp^3 \cdot d31^2 \cdot ybar^4 - 72 \cdot b^2 \cdot Ep^3 \cdot tp^4 \cdot d31^2 \cdot ybar^3 \ldots \\ + 9 \cdot tb^2 \cdot Ep^3 \cdot d31^2 \cdot b^2 \cdot tp^5 + 9 \cdot tb \cdot Ep^3 \cdot d31^2 \cdot b^2 \cdot tp^6 - 4 \cdot tp \cdot Ep \cdot d31^2 \cdot B^2 \ldots \\ + 4 \cdot tb \cdot Ep \cdot d31^2 \cdot B^2 + 3 \cdot b^2 \cdot Ep^3 \cdot d31^2 \cdot tp^7 + 3 \cdot tb^3 \cdot Ep^3 \cdot d31^2 \cdot b^2 \cdot tp^4 \ldots \\ + 4 \cdot tp \cdot \varepsilon \cdot B^2 + 3 \cdot Eb \cdot tb^3 \cdot b^2 \cdot Ep^2 \cdot d31^2 \cdot tp^4 + 36 \cdot tb \cdot Ep^3 \cdot d31^2 \cdot b^2 \cdot tp^3 \cdot ybar^3 \ldots \\ + \left(-27 \cdot tb \cdot Ep^3 \cdot d31^2 \cdot b^2 \cdot tp^4 \cdot ybar^2 \right) + 36 \cdot tb \cdot Ep^3 \cdot d31^2 \cdot b^2 \cdot tp^2 \cdot ybar^4 \ldots \\ + 12 \cdot tb \cdot Ep^2 \cdot d31^2 \cdot b \cdot tp^3 \cdot B - 27 \cdot tb^2 \cdot Ep^3 \cdot d31^2 \cdot b^2 \cdot tp^4 \cdot ybar \ldots \\ + 12 \cdot tb^3 \cdot Ep^3 \cdot d31^2 \cdot b^2 \cdot tp^2 \cdot ybar^2 - 12 \cdot tb^3 \cdot Ep^3 \cdot d31^2 \cdot b^2 \cdot tp^3 \cdot ybar \ldots \\ + 36 \cdot tb^2 \cdot Ep^3 \cdot d31^2 \cdot b^2 \cdot tp^2 \cdot ybar^3 - 18 \cdot tb \cdot Ep^3 \cdot d31^2 \cdot b^2 \cdot tp^5 \cdot ybar \ldots \\ + 6 \cdot tb^2 \cdot Ep^2 \cdot d31^2 \cdot b \cdot tp^2 \cdot B - 12 \cdot tb^2 \cdot Ep^2 \cdot d31^2 \cdot b \cdot tp \cdot ybar \cdot B \ldots \\ + \left(-24 \cdot tb \cdot Ep^2 \cdot d31^2 \cdot b \cdot tp \cdot ybar^2 \cdot B \right) - 12 \cdot Eb \cdot tb^3 \cdot b^2 \cdot Ep^2 \cdot d31^2 \cdot tp^3 \cdot ybar \ldots \\ + \left(-36 \cdot Eb \cdot tb^2 \cdot b^2 \cdot Ep^2 \cdot d31^2 \cdot tp^3 \cdot ybar^2 \right) + 36 \cdot Eb \cdot tb \cdot b^2 \cdot Ep^2 \cdot d31^2 \cdot tp^2 \cdot ybar^4 \ldots \\ + 12 \cdot Eb \cdot tb^3 \cdot b^2 \cdot Ep^2 \cdot d31^2 \cdot tp^2 \cdot ybar^2 + 9 \cdot Eb \cdot tb \cdot b^2 \cdot Ep^2 \cdot d31^2 \cdot tp^4 \cdot ybar^2 \ldots \\ + 36 \cdot Eb \cdot tb^2 \cdot b^2 \cdot Ep^2 \cdot d31^2 \cdot tp^2 \cdot ybar^3 - 12 \cdot tb \cdot Ep^2 \cdot d31^2 \cdot b \cdot tp^2 \cdot ybar \cdot B \ldots \\ + \left(-36 \cdot Eb \cdot tb \cdot b^2 \cdot Ep^2 \cdot d31^2 \cdot tp^3 \cdot ybar^3 \right) + 9 \cdot Eb \cdot tb^2 \cdot b^2 \cdot Ep^2 \cdot d31^2 \cdot tp^4 \cdot ybar \end{array}}$$

APPENDIX D

MATHCAD CODE FOR DYNAMIC BEAM MODEL

Energy Generation from a Dynamic Input

Calculate neutral axis

$$nt := \frac{Et}{Eb} \qquad np := \frac{Ep}{Eb}$$

$$Ap := np \cdot b \cdot tp$$

$$Ep3 := \frac{Vp}{tp} \qquad Et3 := \frac{Vt}{tp}$$

$$At := nt \cdot b \cdot tp$$

$$Ab := b \cdot tb$$

$$M(x) := \frac{d}{dx} dw(x)$$

$$A := Ap + At + Ab$$

$$ybar := \frac{\left[\frac{tp}{2} \cdot Ap - \frac{tb}{2} \cdot Ab - \left(tb + \frac{tp}{2} \right) \cdot At \right]^{\blacksquare}}{A}$$

$$M(x) = \int_{-tb}^{0} Eb \cdot \kappa \cdot (y - ybar) \cdot (y - ybar) \cdot b \, dy + \int_{0}^{tp} Ep \cdot \left[\kappa \cdot (y - ybar) - d31 \cdot Ep3 \right] \cdot (y - ybar) \cdot b \, dy \ldots$$

$$+ \int_{-tb-tp}^{-tb} Et \cdot \left[\kappa \cdot (y - ybar) - d31 \cdot Et3 \right] \cdot (y - ybar) \cdot b \, dy$$

$$B := b \cdot \left(\begin{array}{l} Eb \cdot tb^3 + 3 \cdot Eb \cdot tb^2 \cdot ybar + 3 \cdot Eb \cdot tb \cdot ybar^2 + Ep \cdot tp^3 - 3 \cdot Ep \cdot tp^2 \cdot ybar + 3 \cdot Ep \cdot ybar^2 \cdot tp \ldots \\ + 3 \cdot Et \cdot tb^2 \cdot tp + 3 \cdot Et \cdot tb \cdot tp^2 + Et \cdot tp^3 + 6 \cdot Et \cdot ybar \cdot tb \cdot tp + 3 \cdot Et \cdot tp^2 \cdot ybar + 3 \cdot Et \cdot ybar^2 \cdot tp \end{array} \right)^{\blacksquare}$$

$$\kappa := \frac{-3}{2} \cdot \frac{2 \cdot Et \cdot b \cdot d31 \cdot tb \cdot tp + Et \cdot b \cdot d31 \cdot tp^2 + 2 \cdot Et \cdot b \cdot ybar \cdot d31 \cdot tp}{B} \cdot Et3 \ldots$$

$$+ \left(\frac{-3}{2} \cdot \frac{-Ep \cdot b \cdot tp^2 \cdot d31 + 2 \cdot Ep \cdot b \cdot ybar \cdot tp \cdot d31}{B} \cdot Ep3 \right) + 3 \cdot \frac{\frac{d}{dx} dw(x)}{B}$$

Define stresses of each layer

$$\sigma t := Et \cdot \left[\kappa \cdot (y - ybar) - d31 \cdot Et3 \right]$$

$$\sigma b := Eb \cdot \left[\kappa \cdot (y - ybar) \right]$$

$$\sigma p := Ep \cdot \left[\kappa \cdot (y - ybar) - d31 \cdot Ep3 \right]$$

$$dUp := \frac{1 \cdot \sigma p^2}{2 \cdot Ep} + d31 \cdot Ep3 \cdot \sigma p + \frac{1}{2} \cdot \varepsilon \cdot Ep3^2$$

$$dUt := \frac{1 \cdot \sigma p^2}{2 \cdot Ep} + d31 \cdot Et3 \cdot \sigma p + \frac{1}{2} \cdot \varepsilon \cdot Et3^2$$

$$dUb := \frac{1}{2 \cdot Eb} \cdot \sigma b^2$$

$$U1 := \int_0^L \int_0^b \left(\int_{-tb-tp}^{-tp} dUt \, dy \right) dz \, dx$$

$$U2 := \int_0^L \int_0^b \left(\int_{-tb}^{0} dUb \, dy \right) dz \, dx$$

$$U3 := \int_0^L \int_0^b \left(\int_0^{tp} dUp \, dy \right) dz \, dx$$

137

$$Q1 := \frac{d}{dVp}U1 \qquad Q2 := \frac{d}{dVp}U2 \qquad Q3 := \frac{d}{dVp}U3$$

$$Qgen := \frac{-3}{2} \cdot b \cdot Ep \cdot \frac{d31}{tp} \cdot dw(L) \cdot \frac{\begin{aligned}& 6 \cdot b \cdot ybar^2 \cdot Ep \cdot tb^2 \cdot tp - tb^2 \cdot B - 2 \cdot tb \cdot ybar \cdot B \ldots \\ & + (-2 \cdot tb \cdot tp \cdot B) + 3 \cdot b \cdot ybar \cdot Ep \cdot tb^2 \cdot tp^2 + 2 \cdot b \cdot ybar \cdot Ep \cdot tb^3 \cdot tp \ldots \\ & + 9 \cdot b \cdot ybar^2 \cdot Ep \cdot tb \cdot tp^2 - 3 \cdot b \cdot Ep \cdot tp^3 \cdot tb^2 - b \cdot Ep \cdot tp^2 \cdot tb^3 \ldots \\ & + 6 \cdot tb \cdot b \cdot ybar^3 \cdot tp \cdot Ep - 3 \cdot b \cdot Ep \cdot tp^4 \cdot tb + 6 \cdot Eb \cdot tb \cdot b \cdot tp \cdot ybar^3 \ldots \\ & + 2 \cdot Eb \cdot tb^3 \cdot b \cdot tp \cdot ybar - 3 \cdot Eb \cdot tb \cdot b \cdot tp^2 \cdot ybar^2 + 6 \cdot Eb \cdot tb^2 \cdot b \cdot tp \cdot ybar^2 \ldots \\ & + \left(-Eb \cdot tb^3 \cdot b \cdot tp^2\right) - 3 \cdot Eb \cdot tb^2 \cdot b \cdot tp^2 \cdot ybar + 5 \cdot b \cdot Ep \cdot tp^4 \cdot ybar - b \cdot Ep \cdot tp^5 \ldots \\ & + 6 \cdot b \cdot ybar^3 \cdot tp^2 \cdot Ep - 9 \cdot b \cdot ybar^2 \cdot Ep \cdot tp^3 \end{aligned}}{B^2}$$

$$Cfree := \frac{d^2}{dVp^2}U1 + \frac{d^2}{dVp^2}U2 + \frac{d^2}{dVp^2}U3$$

$$Cfree := \frac{1}{4} \cdot b \cdot L \cdot \frac{\begin{aligned}& 4 \cdot tp \cdot \varepsilon \cdot B^2 + 3 \cdot Eb \cdot tb^3 \cdot b^2 \cdot Ep^2 \cdot d31^2 \cdot tp^4 + 36 \cdot Eb \cdot tb^2 \cdot b^2 \cdot Ep^2 \cdot d31^2 \cdot tp^2 \cdot ybar^3 \ldots \\ & + \left(-36 \cdot Eb \cdot tb^2 \cdot b^2 \cdot Ep^2 \cdot d31^2 \cdot tp^3 \cdot ybar^2\right) - 12 \cdot tb^3 \cdot Ep^3 \cdot d31^2 \cdot b^2 \cdot ybar \cdot tp^3 \ldots \\ & + \left(-12 \cdot tb^2 \cdot Ep^2 \cdot d31^2 \cdot b \cdot ybar \cdot tp \cdot B\right) + 4 \cdot tb \cdot Ep \cdot d31^2 \cdot B^2 + 12 \cdot tb \cdot Ep^2 \cdot d31^2 \cdot b \cdot tp^3 \cdot B \ldots \\ & + 36 \cdot tb^2 \cdot Ep^3 \cdot d31^2 \cdot b^2 \cdot ybar^3 \cdot tp^2 + 9 \cdot tb \cdot Ep^3 \cdot d31^2 \cdot b^2 \cdot tp^6 \ldots \\ & + \left(-24 \cdot tb \cdot Ep^2 \cdot d31^2 \cdot b \cdot ybar^2 \cdot tp \cdot B\right) - 27 \cdot tb^2 \cdot Ep^3 \cdot d31^2 \cdot b^2 \cdot ybar \cdot tp^4 \ldots \\ & + \left(-21 \cdot b^2 \cdot ybar \cdot tp^6 \cdot d31^2 \cdot Ep^3\right) - 18 \cdot tb \cdot Ep^3 \cdot d31^2 \cdot b^2 \cdot ybar \cdot tp^5 \ldots \\ & + 57 \cdot b^2 \cdot ybar^2 \cdot Ep^3 \cdot d31^2 \cdot tp^5 - 27 \cdot tb \cdot Ep^3 \cdot d31^2 \cdot b^2 \cdot ybar^2 \cdot tp^4 \ldots \\ & + 12 \cdot tb \cdot Ep^2 \cdot d31^2 \cdot b \cdot ybar \cdot tp^2 \cdot B + 6 \cdot tb^2 \cdot Ep^2 \cdot d31^2 \cdot b \cdot tp^2 \cdot B + 3 \cdot tb^3 \cdot Ep^3 \cdot d31^2 \cdot b^2 \cdot tp^4 \ldots \\ & + 36 \cdot tb \cdot Ep^3 \cdot d31^2 \cdot b^2 \cdot ybar^3 \cdot tp^3 + 36 \cdot tb \cdot Ep^3 \cdot d31^2 \cdot b^2 \cdot ybar^4 \cdot tp^2 + 9 \cdot tb^2 \cdot Ep^3 \cdot d31^2 \cdot b^2 \cdot tp^5 \ldots \\ & + 12 \cdot tb^3 \cdot Ep^3 \cdot d31^2 \cdot b^2 \cdot ybar^2 \cdot tp^2 - 72 \cdot b^2 \cdot ybar^3 \cdot tp^4 \cdot d31^2 \cdot Ep^3 \ldots \\ & + 36 \cdot b^2 \cdot ybar^4 \cdot tp^3 \cdot d31^2 \cdot Ep^3 + 9 \cdot Eb \cdot tb^2 \cdot b^2 \cdot Ep^2 \cdot d31^2 \cdot tp^4 \cdot ybar \ldots \\ & + \left(-36 \cdot Eb \cdot tb \cdot b^2 \cdot Ep^2 \cdot d31^2 \cdot tp^3 \cdot ybar^3\right) - 12 \cdot Eb \cdot tb^3 \cdot b^2 \cdot Ep^2 \cdot d31^2 \cdot tp^3 \cdot ybar \ldots \\ & + 12 \cdot Eb \cdot tb^3 \cdot b^2 \cdot Ep^2 \cdot d31^2 \cdot tp^2 \cdot ybar^2 + 3 \cdot b^2 \cdot Ep^3 \cdot d31^2 \cdot tp^7 \ldots \\ & + 36 \cdot Eb \cdot tb \cdot b^2 \cdot Ep^2 \cdot d31^2 \cdot tp^2 \cdot ybar^4 - 4 \cdot tp \cdot Ep \cdot d31^2 \cdot B^2 + 9 \cdot Eb \cdot tb \cdot b^2 \cdot Ep^2 \cdot d31^2 \cdot tp^4 \cdot ybar^2 \end{aligned}}{B^2 \cdot tp^2}$$

$$\text{Vgen} := \frac{\text{Qgen}}{\text{Cfree}}$$

$$\text{Vgen} := -6 \cdot Ep \cdot d31 \cdot tp \cdot \frac{dw(L)}{L} \cdot \left[\frac{N}{D} \right]$$

where the numerator N is:

$6 \cdot b \cdot ybar^2 \cdot Ep \cdot tb^2 \cdot tp - tb^2 \cdot B - 2 \cdot tb \cdot ybar \cdot B - 2 \cdot tb \cdot tp \cdot B \ldots$

$+ 3 \cdot b \cdot ybar \cdot Ep \cdot tb^2 \cdot tp^2 + 2 \cdot b \cdot ybar \cdot Ep \cdot tb^3 \cdot tp + 9 \cdot b \cdot ybar^2 \cdot Ep \cdot tb \cdot tp^2 \ldots$

$+ \left(-3 \cdot b \cdot Ep \cdot tp^3 \cdot tb^2 \right) - b \cdot Ep \cdot tp^2 \cdot tb^3 + 6 \cdot tb \cdot b \cdot ybar^3 \cdot tp \cdot Ep - 3 \cdot b \cdot Ep \cdot tp^4 \cdot tb \ldots$

$+ 6 \cdot Eb \cdot tb \cdot b \cdot tp \cdot ybar^3 + 2 \cdot Eb \cdot tb^3 \cdot b \cdot tp \cdot ybar - 3 \cdot Eb \cdot tb \cdot b \cdot tp^2 \cdot ybar^2 \ldots$

$+ 6 \cdot Eb \cdot tb^2 \cdot b \cdot tp \cdot ybar^2 - Eb \cdot tb^3 \cdot b \cdot tp^2 - 3 \cdot Eb \cdot tb^2 \cdot b \cdot tp^2 \cdot ybar \ldots$

$+ 5 \cdot b \cdot Ep \cdot tp^4 \cdot ybar - b \cdot Ep \cdot tp^5 + 6 \cdot b \cdot ybar^3 \cdot tp^2 \cdot Ep - 9 \cdot b \cdot ybar^2 \cdot Ep \cdot tp^3$

and the denominator D is:

$4 \cdot tp \cdot \varepsilon \cdot B^2 + 3 \cdot Eb \cdot tb^3 \cdot b^2 \cdot Ep^2 \cdot d31^2 \cdot tp^4 \ldots$

$+ 36 \cdot Eb \cdot tb^2 \cdot b^2 \cdot Ep^2 \cdot d31^2 \cdot tp^2 \cdot ybar^3 \ldots$

$+ \left(-36 \cdot Eb \cdot tb^2 \cdot b^2 \cdot Ep^2 \cdot d31^2 \cdot tp^3 \cdot ybar^2 \right) - 12 \cdot tb^3 \cdot Ep^3 \cdot d31^2 \cdot b^2 \cdot ybar \cdot tp^3 \ldots$

$+ \left(-12 \cdot tb^2 \cdot Ep^2 \cdot d31^2 \cdot b \cdot ybar \cdot tp \cdot B \right) + 4 \cdot tb \cdot Ep \cdot d31^2 \cdot B^2 \ldots$

$+ 12 \cdot tb \cdot Ep^2 \cdot d31^2 \cdot b \cdot tp^3 \cdot B + 36 \cdot tb^2 \cdot Ep^3 \cdot d31^2 \cdot b^2 \cdot ybar^3 \cdot tp^2 \ldots$

$+ 9 \cdot tb \cdot Ep^3 \cdot d31^2 \cdot b^2 \cdot tp^6 - 24 \cdot tb \cdot Ep^2 \cdot d31^2 \cdot b \cdot ybar^2 \cdot tp \cdot B \ldots$

$+ \left(-27 \cdot tb^2 \cdot Ep^3 \cdot d31^2 \cdot b^2 \cdot ybar \cdot tp^4 \right) - 21 \cdot b^2 \cdot ybar \cdot tp^6 \cdot d31^2 \cdot Ep^3 \ldots$

$+ \left(-18 \cdot tb \cdot Ep^3 \cdot d31^2 \cdot b^2 \cdot ybar \cdot tp^5 \right) + 57 \cdot b^2 \cdot ybar^2 \cdot Ep^3 \cdot d31^2 \cdot tp^5 \ldots$

$+ 27 \cdot tb \cdot Ep^3 \cdot d31^2 \cdot b^2 \cdot ybar^2 \cdot tp^4 - 12 \cdot tb \cdot Ep^2 \cdot d31^2 \cdot b \cdot ybar \cdot tp^2 \cdot B \ldots$

$+ 6 \cdot tb^2 \cdot Ep^2 \cdot d31^2 \cdot b \cdot tp^2 \cdot B + 3 \cdot tb^3 \cdot Ep^3 \cdot d31^2 \cdot b^2 \cdot tp^4 \ldots$

$+ 36 \cdot tb \cdot Ep^3 \cdot d31^2 \cdot b^2 \cdot ybar^3 \cdot tp^3 + 36 \cdot tb \cdot Ep^3 \cdot d31^2 \cdot b^2 \cdot ybar^4 \cdot tp^2 \ldots$

$+ 9 \cdot tb^2 \cdot Ep^3 \cdot d31^2 \cdot b^2 \cdot tp^5 + 12 \cdot tb^3 \cdot Ep^3 \cdot d31^2 \cdot b^2 \cdot ybar^2 \cdot tp^2 \ldots$

$+ \left(-72 \cdot b^2 \cdot ybar^3 \cdot tp^4 \cdot d31^2 \cdot Ep^3 \right) + 36 \cdot b^2 \cdot ybar^4 \cdot tp^3 \cdot d31^2 \cdot Ep^3 \ldots$

$+ 9 \cdot Eb \cdot tb^2 \cdot b^2 \cdot Ep^2 \cdot d31^2 \cdot tp^4 \cdot ybar - 36 \cdot Eb \cdot tb \cdot b^2 \cdot Ep^2 \cdot d31^2 \cdot tp^3 \cdot ybar^3 \ldots$

$+ -12 \cdot Eb \cdot tb^3 \cdot b^2 \cdot Ep^2 \cdot d31^2 \cdot tp^3 \cdot ybar \ldots$

$+ 12 \cdot Eb \cdot tb^3 \cdot b^2 \cdot Ep^2 \cdot d31^2 \cdot tp^2 \cdot ybar^2 + 3 \cdot b^2 \cdot Ep^3 \cdot d31^2 \cdot tp^7 \ldots$

$+ 36 \cdot Eb \cdot tb \cdot b^2 \cdot Ep^2 \cdot d31^2 \cdot tp^2 \cdot ybar^4 - 4 \cdot tp \cdot Ep \cdot d31^2 \cdot B^2 \ldots$

$+ 9 \cdot Eb \cdot tb \cdot b^2 \cdot Ep^2 \cdot d31^2 \cdot tp^4 \cdot ybar^2$

$$Ugen := \frac{1}{2} \cdot Cfree \cdot Vgen^2$$

$$Ugen := \frac{9 \cdot b \cdot Ep^2 \cdot d31^2 \cdot dw(L)^2}{2 \cdot L \cdot B^2} \cdot \frac{\left[\begin{matrix} 3 \cdot b \cdot Ep \cdot tb \cdot tp^4 + 3 \cdot b \cdot Ep \cdot tp^3 \cdot tb^2 + tb^2 \cdot B - 3 \cdot b \cdot Ep \cdot tp^2 \cdot tb^2 \cdot ybar \ ... \\ + 2 \cdot tb \cdot ybar \cdot B + 2 \cdot tp \cdot tb \cdot B - 2 \cdot b \cdot Ep \cdot tp \cdot tb^3 \cdot ybar + b \cdot Ep \cdot tp^2 \cdot tb^3 \ ... \\ + \left(-6 \cdot b \cdot Ep \cdot tp \cdot tb^2 \cdot ybar^2\right) - 6 \cdot tb \cdot b \cdot Ep \cdot tp \cdot ybar^3 \ ... \\ + \left(-9 \cdot b \cdot Ep \cdot tp^2 \cdot tb \cdot ybar^2\right) - 6 \cdot Eb \cdot tb^2 \cdot b \cdot tp \cdot ybar^2 \ ... \\ + 3 \cdot Eb \cdot tb^2 \cdot b \cdot tp^2 \cdot ybar + Eb \cdot tb^3 \cdot b \cdot tp^2 - 6 \cdot Eb \cdot tb \cdot b \cdot tp \cdot ybar^3 \ ... \\ + 3 \cdot Eb \cdot tb \cdot b \cdot tp^2 \cdot ybar^2 - 2 \cdot Eb \cdot tb^3 \cdot b \cdot tp \cdot ybar - 6 \cdot b \cdot Ep \cdot tp^2 \cdot ybar^3 \ ... \\ + \left(-5 \cdot b \cdot Ep \cdot tp^4 \cdot ybar\right) + b \cdot Ep \cdot tp^5 + 9 \cdot b \cdot Ep \cdot tp^3 \cdot ybar^2 \end{matrix}\right]^2}{\left[\begin{matrix} 57 \cdot b^2 \cdot Ep^3 \cdot tp^5 \cdot d31^2 \cdot ybar^2 - 21 \cdot b^2 \cdot Ep^3 \cdot tp^6 \cdot d31^2 \cdot ybar \ ... \\ + 36 \cdot b^2 \cdot Ep^3 \cdot tp^3 \cdot d31^2 \cdot ybar^4 - 72 \cdot b^2 \cdot Ep^3 \cdot tp^4 \cdot d31^2 \cdot ybar^3 \ ... \\ + 9 \cdot tb^2 \cdot Ep^3 \cdot d31^2 \cdot b^2 \cdot tp^5 + 9 \cdot tb \cdot Ep^3 \cdot d31^2 \cdot b^2 \cdot tp^6 - 4 \cdot tp \cdot Ep \cdot d31^2 \cdot B^2 \ ... \\ + 4 \cdot tb \cdot Ep \cdot d31^2 \cdot B^2 + 3 \cdot b^2 \cdot Ep^3 \cdot d31^2 \cdot tp^7 + 3 \cdot tb^3 \cdot Ep^3 \cdot d31^2 \cdot b^2 \cdot tp^4 \ ... \\ + 4 \cdot tp \cdot \varepsilon \cdot B^2 + 3 \cdot Eb \cdot tb^3 \cdot b^2 \cdot Ep^2 \cdot d31^2 \cdot tp^4 \ ... \\ + 36 \cdot tb \cdot Ep^3 \cdot d31^2 \cdot b^2 \cdot tp^3 \cdot ybar^3 - 27 \cdot tb \cdot Ep^3 \cdot d31^2 \cdot b^2 \cdot tp^4 \cdot ybar^2 \ ... \\ + 36 \cdot tb \cdot Ep^3 \cdot d31^2 \cdot b^2 \cdot tp^2 \cdot ybar^4 + 12 \cdot tb \cdot Ep^2 \cdot d31^2 \cdot b \cdot tp^3 \cdot B \ ... \\ + \left(-27 \cdot tb^2 \cdot Ep^3 \cdot d31^2 \cdot b^2 \cdot tp^4 \cdot ybar\right) + 12 \cdot tb^3 \cdot Ep^3 \cdot d31^2 \cdot b^2 \cdot tp^2 \cdot ybar^2 \ ... \\ + \left(-12 \cdot tb^3 \cdot Ep^3 \cdot d31^2 \cdot b^2 \cdot tp^3 \cdot ybar\right) + 36 \cdot tb^2 \cdot Ep^3 \cdot d31^2 \cdot b^2 \cdot tp^2 \cdot ybar^3 \ ... \\ + \left(-18 \cdot tb \cdot Ep^3 \cdot d31^2 \cdot b^2 \cdot tp^5 \cdot ybar\right) + 6 \cdot tb^2 \cdot Ep^2 \cdot d31^2 \cdot b \cdot tp^2 \cdot B \ ... \\ + \left(-12 \cdot tb^2 \cdot Ep^2 \cdot d31^2 \cdot b \cdot tp \cdot ybar \cdot B\right) - 24 \cdot tb \cdot Ep^2 \cdot d31^2 \cdot b \cdot tp \cdot ybar^2 \cdot B \ ... \\ + \left(-12 \cdot Eb \cdot tb^3 \cdot b^2 \cdot Ep^2 \cdot d31^2 \cdot tp^3 \cdot ybar\right) \ ... \\ + -36 \cdot Eb \cdot tb^2 \cdot b^2 \cdot Ep^2 \cdot d31^2 \cdot tp^3 \cdot ybar^2 \ ... \\ + 36 \cdot Eb \cdot tb \cdot b^2 \cdot Ep^2 \cdot d31^2 \cdot tp^2 \cdot ybar^4 + 12 \cdot Eb \cdot tb^3 \cdot b^2 \cdot Ep^2 \cdot d31^2 \cdot tp^2 \cdot ybar^2 \ ... \\ + 9 \cdot Eb \cdot tb \cdot b^2 \cdot Ep^2 \cdot d31^2 \cdot tp^4 \cdot ybar^2 + 36 \cdot Eb \cdot tb^2 \cdot b^2 \cdot Ep^2 \cdot d31^2 \cdot tp^2 \cdot ybar^3 \ ... \\ + \left(-12 \cdot tb \cdot Ep^2 \cdot d31^2 \cdot b \cdot tp^2 \cdot ybar \cdot B\right) - 36 \cdot Eb \cdot tb \cdot b^2 \cdot Ep^2 \cdot d31^2 \cdot tp^3 \cdot ybar^3 \ ... \\ + 9 \cdot Eb \cdot tb^2 \cdot b^2 \cdot Ep^2 \cdot d31^2 \cdot tp^4 \cdot ybar \end{matrix}\right]}$$

APPENDIX E

MATLAB CODE FOR EXTRACTING FREQUENCY DATA FROM SIGLAB

```
close all
clear all


for i=100:199
filename= ['Beam' num2str(i) '.vna'];

load (filename, '-mat');

[X,I]=max(20*log10(abs(SLm.xcmeas(1,2).xfer)));
F(i-99)=SLm.fdxvec(I);

end

B=[100 300 630 1200 2530 5030 10000 20000 40000 80000 166000 330000 640000
1330000];

for j=0:16383
    binary=dec2bin(j,14);
    for i=1:14
        decimal(i)=bin2dec(binary(i));
    end
    decimal=fliplr(decimal);
    C(j+1)=B*decimal';
end

Ccap(1)=C(1);

k=[11:10:601 701:100:3101 4101:1000:16101];
for i=2:length(k)+1
    Ccap(i)=C(k(i-1));
end

Ccap(100)=10000000;

semilogx(Ccap/100000,F)



load Beam1sweepoc.vna -mat
```

141

```
figure(1);
plot(SLm.fdxvec, 20*log10(abs(SLm.xcmeas(1,2).xfer)), 'r');


title('5 kHz Random Signal Sweep of Beam 1');
xlabel('Freq. (Hz)'), ylabel('Mag (dB)');
```

BIBLIOGRAPHY

Chandrashekhara, K., and Bangera, K. M., 1993, "Vibration of Symmetrically Laminated Clamped-Free Beam With a Mass At The Free End," *Journal of Sound and Vibration,* **160**(1), 93-101.

Clark, W.W., 2000, "Vibration Control with State-Switched Piezoelectric Materials," *Journal of Intelligent Material Systems and Structures,* 11, 402-407.

Davis, C. L. and G.A. Lesieutre, 1998, "An Actively-Tuned Solid State Piezoelectric Vibration Absorber," *Proceedings of the SPIE Symposium on Smart Structures and Materials, Passive Damping and Isolation,* L.P. Davis, Ed., 169-182

Dmuchoski, M., 2000, "Design Issues In Electromechanical Filters With Piezoelectric Transducers," Masters Thesis, University of Pittsburgh, PA.

Eggborn, Timothy, 2003, "Analytical Models to Predict Power Harvesting with Piezoelectric Materials," Masters Thesis, Virginia Polytechnic Institute and State University, VA

Frederick, A. A., Clark, W. W., and Hu, H., 2005, "Analysis of a Tunable Piezoelectric Resonator Using Interdigitated Electrodes," *Proceedings from IMECE Symposium on Dynamics and Control of Micro and Nanosystems,* November 5-11, 2005 Orlando, Fl.

Goldfarb, M., and Jones, L. D., 1999, "On the efficiency of Electric Power Generation with Piezoelectric Ceramic," *ASME Journal of Dynamic Systems, Measurement, and Control,* Vol. 121, 566-571.

Hagood, N. H. and A. von Flotow, 1991, "Damping of Structural Vibrations with Piezoelectric Materials and Passive Electrical Networks," *Journal of Sound and Vibration,* Vol. 146, No. 2, 243-268.

Hausler, E. and Stein, E. 1984. "Implantable Physiological Power Supply with PVDF Film," *Ferroelectrics*, 60:277-282.

IEEE standard 176. *IEEE Standard on Piezoelectricity,* The Institute of Electrical and Electronics Engineers, 1978.

Inman, Daniel J. *Engineering Vibration.* Prentice Hall: Upper Saddle River, NJ. 2001

Kasyap, A., Lim, J., Johnson, D., Horowitz, S., Nishida, T., Ngo, K., Sheplak, M., and Cattafesta, L., 2002, "Energy Reclamation from a Vibrating Piezoceramic Composite Beam," *Proceedings of 9th International Congress on Sound and Vibration,* Orlando, FL, Paper No. 271.

Kim, S., 2002 "Low Power Energy Harvesting with Piezoelectric Generators," Ph.D. Dissertation, University of Pittsburgh, Pittsburgh, PA

Kymissis, J., Kendall, C., Paradiso, J., and Gershenfeld, N., 1998, "Parasitic Power Harvesting in Shoes," *Proceedings of the 2nd IEEE International Symposium on Wearable Computers*, October 19-20, Pittsburgh, PA, 132-139.

Leland, E. S., and Wright, W. K., 2006, "Resonance tuning of piezoelectric vibration energy scavenging generators using compressive axial preload," *Smart Materials and Structures,* **15**, 1413-1420.

Leissa, Arthur, W. *Vibration of Plates.* U.S. Government Printing Office: Washington, D.C. 1969

Lesieutre, G. A., and Davis, C. L., 1997, "Can a coupling coefficient of a piezoelectric actuator be higher than those of its active material?," *Journal of Intelligient Material Systems and Structures. 8, 859-67*

Lu, F., Lee, H. P., and Lim, S. P., 2004, "Modeling and Analysis of Micro Piezoelectric Power Generators for Micro-electromechanical-systems applications," *Smart Materials and Structures*, Vol 13, 57-63.

Mo, C., Sunghwan, K., Clark, W. W., 2005, "Analysis of Power Generating Performance For Unimorph Cantilever Piezoelectric Beams With The Interdigitated Electrode," *Proceedings of the ASME International Design Engineering Technical Conference*, Sept. 24-28, Long Beach, CA

Muriuki, M. G., 2004, "An Investigation into the Design and Control of Tunable Piezoelectric Resonators," Ph.D. Dissertation, University of Pittsburgh, PA.

Ottman, G.K., Hoffman, H., Bhatt, C.A. and Lesieutre, G.A. 2002. "Adaptive Piezoelectric Energy Harvesting Circuit for Wireless, Remote Power Supply," *IEEE Transactions on Power Electronics,* 17(5):1-8.

Priya, S., Chen, C. Fye, D. and Zahnd, J. 2005. "Piezoelectric Windmill: A Novel Solution to Remote Sensing," *Japanese Journal of Applied Physics.* Vol. 44, No. 3, L104-L107.

Ramsay, M. J., and Clark W. W., "Piezoelectric Energy Harvesting for Bio MEMS Applications," *Proceedings of the SPIE 8th Annual Smart Materials and Structures Conference*, Newport Beach, CA, Vol. 4332-2001, 429-438

Riley, W. F., Sturges, L. D., and Morris, D. H. 2002. *Statics and Mechanics of Materials: An Integrated Approach.* John Wiley & Sons: NY.

Roundy, Shad, Wright, P.K., and Rabaey, J., 2003, "A Study of Low Level Vibrations As A Power Source For Wireless Sensor Nodes," *Computer Communications*, Vol. 26, 1131-1144.

Shahruz, S. M., 2006, "Design of Mechanical Band-Pass Filters for Energy Scavenging," *Journal of Sound and Vibration*, 292, 987-998

Shu, Y. C. and Lien, I. C., 2006, "Analysis of Power Output for Piezoelectric Energy Harvesting Systems," *Smart Materials and Structures,* Vol. 15, 1499-1512.

Smits, J.G., and Dalke, S. I., and Cooney, T. K., 1991, "The consitituent equations of piezoelectric bimorphs," Sensors and Actuators A, **A28**, pp.41-61

Sodano, H.A., Magliula, E. A., Park, G., and Inman, D. J., 2002, "Electric Power Generation from Piezoelectric Materials," *Proceedings of the 13th International Conference on Adaptive Structures and Technologies,* October 7-9, Potsdam/Berlin, Germany.

Sodano, H.A, Park, G., and Inman, D.J., 2004a. "Estimation of Electric Charge Output for Piezoelectric Energy Harvesting," *Strain*. Vol 40, 49-58

Sodano, H.A., Inman, D.J., and Park, G., 2004. "Generation and Storage of Electricity from Power Harvesting Devices," *Journal of Intelligent Material Systems and Structures,* 16(1), 67-75

Sodano, H.A., Inman, D.J., and Park, G., 2005. "Comparison of Piezoelectric Energy Harvesting Devices for Recharging Batteries," *Journal of Intelligient Material Systems and Structures,* Vol. 16, October 2005.

Sood, R, Jeon, Y.B, Jeong, J.-h., and Kim, S.G. 2005. "Piezoelectric Micro Power Generator For Energy Harvesting" Sensors and Actuators A, **A122**, pp.16-22

Starner, T. "Human Powered Wearable Computing," *IBM Systems Journal,* Vol. 35 No. 3-4, 618-628.

Tieck, R. M., Carman, G. P., and Enoch Lee, D. G. "Electrical Energy Harvesting Using a Mechanical Rectification Approach," Proceedings *from IMECE 2006, November 5-10, 2006, Chicago, IL*

Ugural, Ansel C., *Stresses in Plates and Shells*. McGraw Hill: Boston, MA, 1999.

Umeda, M., Nakamura, K., and Ueha, S., 1996, "Analysis of Transformation of Mechanical Impact Energy to Electrical Energy Using a Piezoelectric Vibrator," *Japanese Journal of Applied Physics,* Vol. 35, Part 1, No. 5B, 3273.

Umeda, M., Nakamura, K. and Ueha, S. 1997. "Energy Storage Characteristics of a Piezo-Generator Using Impact Induced Vibration," *Japanese Journal of Applied Physics, Part 1,* 35(5B); 3146-3151

Wang, K. W., J.S. Lai and W.K. Yu, 1996, "An Energy-Based Parametric Control Approach for Structural Vibration Suppression via Semi-Active Piezoelectric Networks," *Journal of Vibration and Acoustics*, Vol. 118, 505-509.

Wang, W. and Du, X., 1999, "Electromechanical Coupling and Output Efficiency of Piezoelectric Bending Actuators," *IEEE Transactions On Ultrasonics, Ferroelectrics, and Frequency Control*, Vol. 46, No. 3

Wang, Q. and Cross, E. L., 1999, "Constitutive Equations of Symmetrical Triple Layer Piezoelectric Benders," *IEEE Transactions On Ultrasonics, Ferroelectrics, and Frequency Control*, Vol. 46, No. 6

Williams, C. B, and Yates, R. B., 1996 "Analysis of a micro-electric generator for Microsystems, *Sensors and Actuators* A, Vol. 52, 8-11.

Young, Dana, 1950. "Vibration of Rectangular Plates by the Ritz Method,' *Journal of Applied Mechanics*, December 1950, 448-453.